**Surface Functionalization and Enhancement of Properties of Biomaterials through Atomic Layer Deposition**

By

**Sarah Hashemi Astaneh**
B.S. in Polymer Engineering, Amirkabir University of Technology, Iran 2008
M.S. in Polymer Engineering, Amirkabir University of Technology, Iran 2010

THESIS

Submitted as partial fulfillment of the requirements
For the degree of Doctor of Philosophy in Chemical Engineering
In the Graduate College of the
University of Illinois at Chicago, 2021

Chicago, Illinois

Defense Committee:

Christos G. Takoudis, Chair and Advisor
Cortino Sukotjo, College of Dentistry
Vikas Berry, Chemical Engineering
Alan Feinerman, Electrical and Computer Engineering
Gregory Jursich, Chemistry Department and Bioengineering

To my parents, Ashraf Norouzi and Morteza Hashemi Astaneh
To my brothers, Amirhossein and Amirhesam

& to my love Mohammadreza Yaghoobi

# ACKNOWLEDGEMENTS

Doing this dissertation would be impossible without the help and support of the people I now wish to acknowledge.

In particular, I would like to thank my family for their continuous love and support, My mom and dad, and dearest brothers Amirhossein and Amirhesam. I have been blessed with a family who gave me a strong foundation. Also, my dearest friends Mahsa Keshavarzi, Yassaman Behbahani, Mohammad Mehdizadeh, Nasim Azimi, and Neshat Mohammadi for all the in-person/virtual times that we have spent together.

And last but definitely not least, I would like to thank my husband, Mohammadreza, for his genuine love and partnership. Without his patience, we could not work through the challenges of a long-distance relationship and we could not navigate our longer-term goals, adventures and hopes.

Thanks, سپاسگزارم

Sarah Hashemi Astaneh
November 2020

# CONTRIBUTION OF AUTHORS

Section 1 of this dissertation is accepted in Acta Biomaterial as a review paper, Dr. Takoudis helped with correcting the manuscript, and Dr. Sukotjo helped with section 1.1, the methodology. Section 2.1 was published in Applied Surface Science where I am the first author, Dr. Jursich and Soumya Saha did the XANES data acquisition in Argonne National Lab, Dr. Jursich contributed to data interpretation. Section 2.2 is adapted from my published paper, where I am the first author, the idea of this work was initiated by Dr. Feinerman and he contributed to helpful correction and review of the manuscript as well. Sungjoon Kim and Ngoc Hoang Lan Nguyen from Dr. Berry's lab helped with AFM. Section 2.3 is prepared to submit. Cell culture test was done by Dr. Sukotjo. Section 2.4 is prepared to submit, Harshdeep Bhatia conducted the RGA and helped with RGA data interpretations and Dr. Valentim Barão and Bruna Egumi Nagay helped with the bacteria test.

As the first author, I conducted all other experiments and wrote the manuscripts. Dr. Takoudis and Dr. Sukotjo helped with project planning, supervising, discussions, correction, and review of the manuscripts.

# TABLE OF CONTENTS

# TABLE OF CONTENTS (Continued)

# LIST OF TABLES

# LIST OF FIGURES

# SUMMARY

Atomic layer deposition was introduced in 1960s as a method for thin film deposition in semiconductor industry. Several precursors were synthesized and different types of ALD reactors were developed to fabricate metal oxide and metal thin films. Uniformity and conformality at nanometer and Angstrom scale are the major advantages over other thin film deposition methods. Gradually, ALD expanded its application into surface functionalization of materials in other field of engineering and science. Biomaterials with complex, 3D, and porous micro/nanostructures were one essential group of materials which have taken advantage of ALD functionalization.

Surface functionalization is indeed an increasingly promising approach for property enhancement of engineered materials, including biomaterials. Due to the importance of the interface region in biological environments, surface modification has several advantages over bulk functionalization. The interface of this biomaterial and the biological environment has a major role in the effectiveness of the biomaterial. Therefore, instead of mixing nanomaterial with the matrix that eventually yields to random distribution of nanomaterial on the interface of biomaterial and biological environment, focusing on the surface modification can result in an efficient distribution of the functionalizing agents at that interface. There are several chemical nanofabrication techniques (alone or combination of them) used for biomaterial fabrication and modification: (i) anodic oxidation (anodization), (ii) acid treatment, (iii) alkali treatment, (iv) chemical etching with hydrogen peroxide, (v) sol-gel treatment, (vi) chemical vapor deposition (CVD), and (vii) atomic layer deposition (ALD) [1].

The focus of this thesis is on development, optimization of ALD processing conditions and fabrication ALD thin films on materials which has application mostly in dental industry. Several surface characterizations were done to study the metal and metaloxide ALD films, and

## SUMMARY (Continued)

different invitro and invivo tests were done to evaluate the potential applications of these materials for in body environment.

Polydimethylsiloxane (PDMS) is widely being used in medical applications due to its mechanical properties and inertness. Surface functionalization of an inert surface is challenging and has not fundamentally studied. In this study, atomic layer deposition (ALD) of $TiO_2$ on polydimethylsiloxane (PDMS) is investigated at the early stages of nucleation and growth of $TiO_2$ on both $O_2$-plasma treated and non-plasma treated PDMS. X-ray absorption near edge structure (XANES), scanning electron microscopy/energy dispersive X-ray spectroscopy (SEM/EDS), and X-ray photoelectron spectroscopy (XPS) are used for material characterization. Results indicate that ALD-like surface growth of $TiO_2$ takes place on plasma-treated PDMS; for non-plasma treated pristine PDMS, apparent favorable diffusion/infiltration of $TiO_2$ into the subsurface of the polymer is obtained, without noticeable external surface deposition for at least the first 25 ALD cycles.

A simple physical masking method is presented for selective ALD. Iron powder and a magnet are used as a masking pair. This method is easy and efficient for depositing patterned thin films with feature sizes estimated 0.3 mm or larger on any substrate. In this work, using iron powder held in place by a magnet would mask part of the silicon wafer substrate, while no iron powder is on the unmasked part. A silver particulated thin film was deposited on the masked Si wafer. X-ray photoelectron spectroscopy, atomic force microscopy, and scanning electron microscopy were used for silver characterization on the masked and unmasked parts of the sample. Results indicated that an ALD-like surface growth of a silver thin film occurred on the unmasked Si wafer, and no growth was detected on the masked portion of the Si wafer.

# SUMMARY (Continued)

For the first time, thermal atomic layer deposition (ALD) of silver was carried out on commercially available collagen membrane to improve the bioactivity of collagen. The aim of this research is to study the chemical and morphological changes of the collagen membrane and investigate the bioactivity of collagen after its functionalization with silver. For two groups of samples, the role of metaloxide interlayer in the silver ALD was also investigated. All thin film depositions were done via ALD. Four different sample groups were investigated: pristine collagen, silver-coated collagen (Ag/Collagen), and two groups of silver ALD (650 cycles and 1300 cycles) on top of ALD $TiO_2$-coated collagen (Ag/$TiO_2$/Collagen).

XPS and SEM were used to characterize the chemical and morphological changes of the collagen membrane after silver ALD. XPS of the silver-coated collagen showed the corresponding double peaks of Ag 3d and Ag 3p. Particulated silver thin film appeared on collagen fibrils with an average diameter of ~16 nm. Comparison of gingival cells cultured on pristine collagen, silver-coated collagen, and silver-coated samples with an interlayer of $TiO_2$ demonstrated that the silver nanoparticle size and concentration are below the toxicity level of silver in an oral environment. This novel material can be used in surgeries as bone grafting agent with improved antibacterial properties.

# 1. INTRODUCTION

There are different ways to categorize dental materials, the main three ways being: (1) based on the nature of the dental material; (2) based on their interaction with the body, i.e., either they are bioinert when they are implanted in the body or they are bioactive; and (3) based on the shape and form of the dental materials [1]. There are reports in the literature on the failure of conventional dental materials earlier than expected which increase the risk of second surgeries, and significantly higher costs for the patients. Also, simple dental materials cannot meet all clinical expectations. Studies in dental materials are actively proceeding in different aspects such as design, material and technique so that we come up with more suitable effective materials [2, 3]. Therefore, there are several studies either on fabricating new materials or enhancing the properties of available dental materials. Property enhancement of current materials can be performed with known modification methods such as microstructural modification, conventional functionalization methods, e.g., adding nanoscopic fillers to dental material compounds [4-6] or performing novel functionalization techniques, e.g., surface functionalization [7-9].

Surface functionalization is indeed an increasingly promising approach for property enhancement of dental materials [10]. Due to the importance of the interface region in biological environments, surface modification has several advantages over bulk functionalization. The interface of the biomaterial and the biological environment has a major role in the effectiveness of the biomaterial. Therefore, instead of mixing nanomaterial with the matrix that eventually

yields to random distribution of nanomaterial on the interface, focusing on the surface modification can result in an efficient distribution of the functionalizing agents at the interface. There are several chemical nanofabrication techniques (alone or combination of them) used for dental material fabrication and modification: (i) anodic oxidation (anodization), (ii) acid treatment, (iii) alkali treatment, (iv) chemical etching with hydrogen peroxide, (v) sol-gel treatment, (vi) chemical vapor deposition (CVD), and (vii) atomic layer deposition (ALD) [11-17].

ALD has several advantages over other thin film deposition methods [18, 19]. CVD and ALD are both vapor phase thin film deposition techniques. In CVD both precursors are introduced into the reactor at the same time while in ALD precursors are sequentially introduced to the reactor each followed by an inert gas purge. This sequential process is a key difference between CVD and ALD, which consequently makes ALD a self-limiting reaction without gas phase reactions and gives unique characteristics to this method [20]. A detailed comparison of ALD and other thin film deposition methods is discussed in Ovirah et. al [21]. Outstanding advantages of ALD thin films over those from other techniques incliude high quality, high density, excellent reproducibility of the results, and control over the thickness down to sub-nm length scale.

The motivation of the current work originated in part from the shape and microstructure complexity of dental materials. Most of the modern dental materials are porous and/or have complex physical shapes. Also, at a smaller scale, these materials show 3D microstructure, which makes it hard to get them conformally coated and functionalized with other techniques. Other dental materials are resorbable in solutions, which makes it impossible to functionalize them via methods which include solvents (acid treatment, sol-gel treatment, chemical etching

with hydrogen peroxide, or anodic oxidation). ALD is a unique and powerful approach for surface functionalization of substrates which results in uniform and conformal thin films, especially for surfaces with high aspect ratios, porous surfaces, and complex microstructures [17]. Further, processing conditions of ALD are tunable for the functionalization of materials with low degradation temperature.

ALD consists of sequential cycles. Each cycle typically consists of four consecutive steps with designated time durations, under vacuum, i) precursor pulse, ii) precursor purge, iii) oxidizer (or co-reactant) pulse, iv) oxidizer (or co-reactant) purge:

(i)     **precursor pulse** into the reactor to react/interact with the substrate surface,

(ii)    unreacted **precursor** molecules **purge** out of the reactor with only one monolayer of precursor covering the substrate surface,

(iii)   **oxidizer (or co-reactant) pulse** into the reactor to react with the monolayer of the precursor,

(iv)    **oxidizer (or co-reactant) purge** to remove the unreacted co-reactant and byproducts

Once the oxidizer (or co-reactant) is pulsed into the reactor, reaction between chemisorbed precursor molecules and pulsed oxidizer molecules takes place. One cycle of a typical ALD is illustrated in Figure 1.

On the other hand, limitations of ALD are the slow deposition rate, sometimes expensive precursors, and the ALD of many metals and metal compounds have not yet been studied and developed well. Yet, the slow ALD rate has been increasingly addressed effectively with "Spatial ALD (SALD) systems in which precursors are continuously supplied in different locations and kept apart by an inert gas region or zone. Film growth is achieved by exposing the substrate to the locations containing the different precursors. Because the purge step is

3

eliminated, the process becomes faster, being indeed compatible with fast-throughput techniques such as roll-to-roll, and much more versatile, easier and cheap to scale up" [22].

Precursors play a key role in the ALD reaction. Precursors must be volatile, chemisorb on the surface, and be thermally stable [23]. Precursors are mostly commercially available. An inert gas like nitrogen ($N_2$) or Argon (Ar) can be used as carrier and purging gas [17].



i) precursor pulse

ii) precursor purge

iv) oxidizer & by-products purge

iii) oxidizer pulse

v) reaction between chemisorbed
precursor molecules and oxidizer
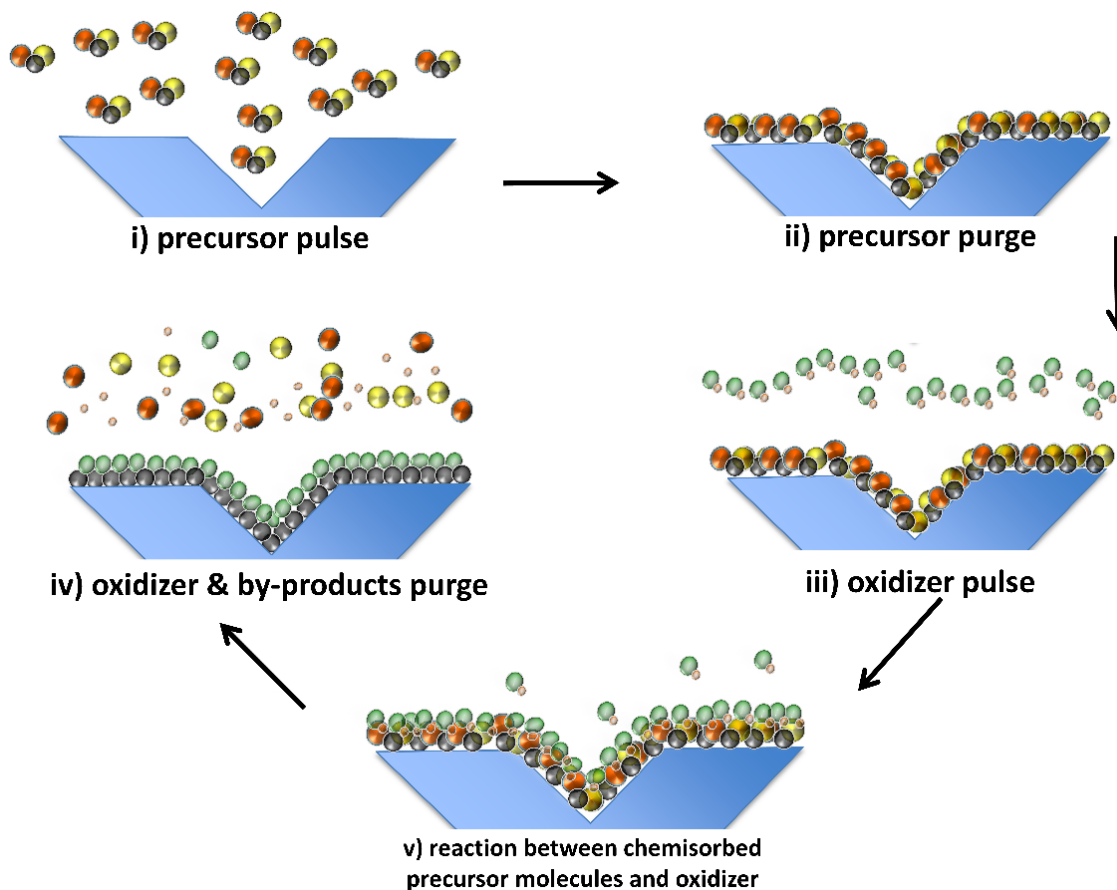
Figure 1: Schematic of one cycle of an ALD process: a) precursor pulse, b) precursor purge, c) oxidizer/co-reactant pulse, d) chemisorbed reaction moment, e) co-reactant & by-products purge & thin film formation after an ALD cycle.

By adjusting the number of cycles, one can tune the final thickness of the thin film. Each cycle of ALD includes chemisorption and self-limiting reaction, which means the entire surface gets exposed to the flow of the pulsed materials and therefore at the end of each cycle

(depending on the growth rate), the entire surface can be covered with the targeted thin film. That is why ALD results in uniform, pinhole free, and conformal thin films, which are important advantages of this technique over other vapor phase thin film deposition methods. The final thin film is in the nanometer length scale and allows control over the thickness down to a few Ångström. The invention and introduction of the first ALD dated back to 1960 [24]. It was first used in the microelectronic and semiconductor industry. For each ALD process there is a temperature window, where the growth rate is constant and saturated [19]. For the fabrication of semiconductor devices via thermal ALD, this temperature window is wide and not suitable for heat sensitive polymeric and biological materials.

However after the discovery of processes and precursors for thin film deposition below 100 °C, ALD has been increasingly used in the field of biomedical-advanced materials [25-27]. Biosensors, biomedical implants, and biomaterials are some of the examples that make use of ALD in the biomedical industry [25, 28]. The present work provides a detailed overview of dental materials, which have been functionalized with ALD so far.

## 1.1 <u>Methodology</u>

For this literature review, an electronic search was conducted for papers in the databases Google Scholar, Pubmed, Scopus, Web of Science and SciFinder, using the keywords: atomic layer deposition, dental material, and dentistry. The notable published researches in the area of ALD on dental materials were reviewed first. Next, the search was expanded to their relevant references and citations. Among those references and citations, in the case of any relevant work, again its references and citations were checked. This process continued until all relevant research was covered. Inclusion criteria were: no time limit of publication, only in the English language, and relationships between ALD and dental materials, through clinical, animal, and in vitro investigations. Figure 2 includes number of records found on different search engines, time

evolution of number of publications, studies per country on application of atomic layer deposition in dentistry, and most productive continents.
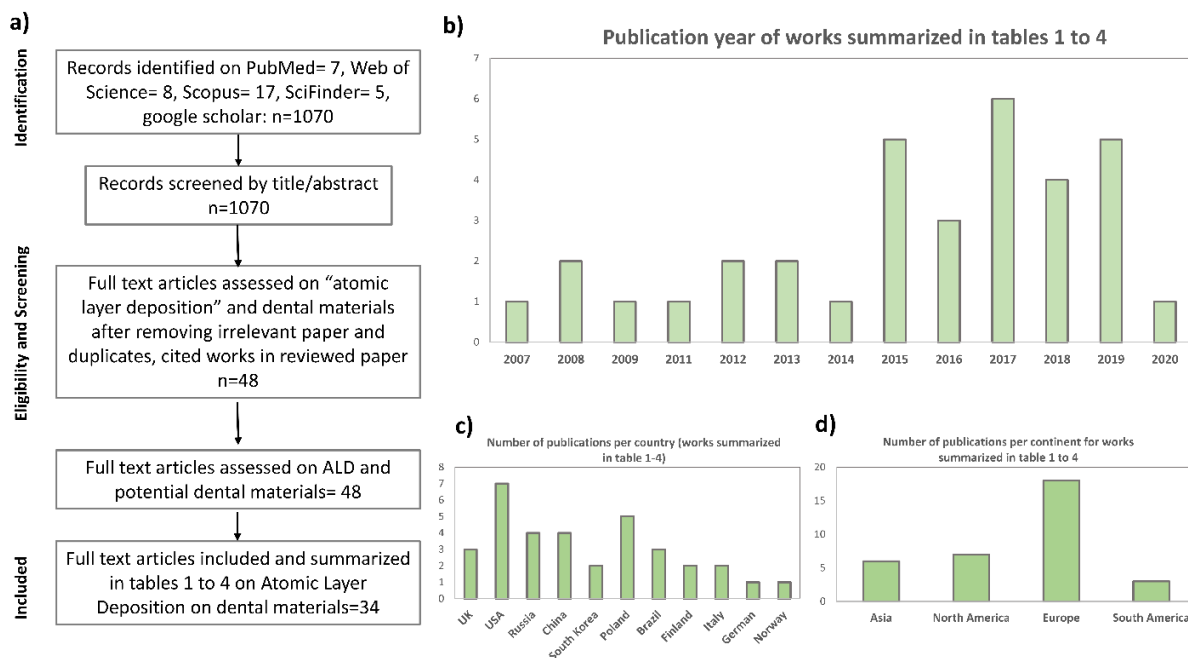


Figure 2: a) Number of records found on different search engines, b) time evolution of number of publications, c) studies per country on application of atomic layer deposition in dentistry, and d) most productive continents.

## 1.2   ALD in dental materials

### 1.2.1   ALD of metal oxides on metal and metal alloys dental materials

One of the challenges handling restorative dental materials is the unpredictable adherence of those materials to the instruments used in clinical work upon pull out from the cavity. Therefore, development of non-stick dental restorative instruments can be an answer to this challenge. Doped diamond like carbon coating (DLC) and Polytetrafluoroethylene (PTFE) coatings are two of the conventional methods to solve such unpredictable adherence problems. Leppaniemi et al. compared these two hydrophobic coatings with proposed novel superhydrophobic coating. The new coating was developed via ALD on dental restorative instruments [29] and consists of 3 different layers: 1) 5 nm $Al_2O_3$, 2) 2 nm $TiO_2$, 3) organosilicon

self-assembled monolayer (SAM). Results showed that the non-stick performance of the superhydrophobic coating improved by 40% on pull out force and 90% on the adherent material to the instrument. This novel coating provides a possible solution for suppressing unwanted adherence of dental materials to the metal instruments [29].

In orthodontics, NiTi shape memory alloys are being used as orthodontic wire. There is a chance of Ni release in the oral environment, which can cause serious problems. Lin et al [30] used ALD to deposit thin film of $Al_2O_3$ on NiTi alloy. Results showed that $Al_2O_3$-coated NiTi, was more effectively resistant to Ni release in simulated bio fluid (SBF) solution (Figure 3). It was also reported that the adhesion between $Al_2O_3$ and NiTi was sustainable upon deformation.
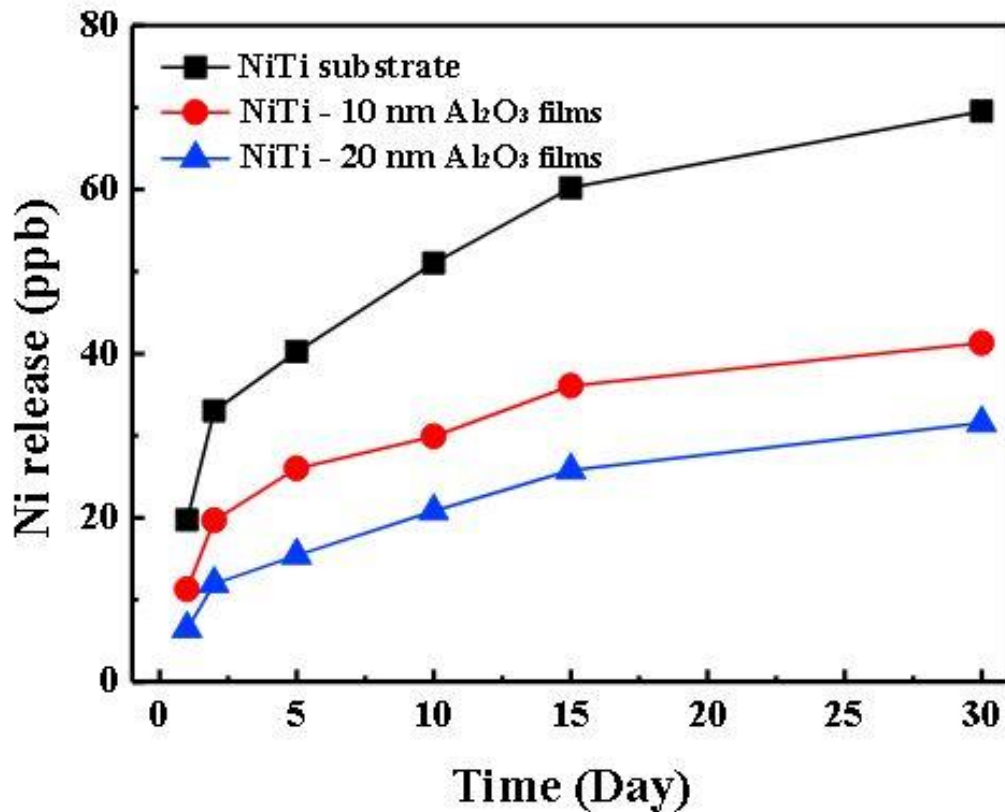


Figure 3: The Ni ion release of NiTi alloy and 10 nm and 20-nm thick $Al_2O_3$ coated NiTi alloys in SBF (from [30] with permission).

The most important advantage of ALD compared to other functionalization methods is its ability to coat an ultra thin film in nanometer or Ångström length level on a targeted substrate uniformly and conformally. These characteristics can be especially useful in functionalization of highly porous materials and materials with 3D shapes [31, 32]. In the dental industry, materials with 3D shape and porous surfaces are widely used. The mechanical strength and biocompatibility of titanium make it the first choice for metal implants and restorative castings [33]. It has been widely reported that metal oxides on metal surfaces has a significant effect on the biocompatibility and bio-corrosion resistance of metal implants [34, 35]. However, the metaloxide which may spontaneously form on the metallic alloys implant (e.g., Ti-6Al-4V) surface is not protective enough, especially in harsh and corrosive dental environments [36]. Therefore, one approach to enhance the biocompatibility of metal implants is functionalizing them with metal oxides. For instance, Dobrzański et al. studied the efficiency of ALD in coating porous Ti and Ti alloy with potential bone or dental scaffold applications [37-39]. The fabrication method of porous Ti was selective laser sintering. Their scanning electron microscopy (SEM) results showed outstanding uniformity across the porous titanium scaffold; the deviation between thicknesses measurements of different spots across the area were not greater than 2.0 nm which is only achievable with ALD. The minimum thickness tolerance occurred at 1050 cycles for samples which were deposited at 300 °C. They extended this study to an in vitro test [38] and showed that the presence of $TiO_2$ thin film has no negative effect on the viability of osteoblast cells; however, it did not show a considerable effect on cell growth and proliferation.

Ti is commonly used as bio implant due to its inertness. Therefore, the main considerations and standards are not very different for dental and orthopedic implants. Although this review

mainly focused on the applications and studies on dental implants, due to similarities between orthopedic and dental implants, studies of ALD on orthopedic implant modification are also included.

Two years after Dobrzański et al., Liu et al. [40] used TDMATi/$H_2O$ (as precursor/oxidizer) to deposit $TiO_2$ on Ti implants for orthopedic applications. ~100 nm-thick $TiO_2$ corresponding to 2500 ALD cycles at three different temperatures (120, 160, and 190 ˚C) were deposited on Alfa Aesar 99.5% Ti foils. A comprehensive study on antibacterial properties, protein adsorption, cell adhesion and proliferation, were reported by Liu et al [40]. Three bacteria cell lines were studied: S. Aureus (ATCC 25923), E. Coli (ATCC 25922), and MRSA (ATCC 43300). $TiO_2$ deposited at 160 ˚C showed the best results in adhesion inhibition and growth (exceeding 80%) of all three bacteria lines when compared to pristine Ti which could be related to increased protein adsorption of $TiO_2$-coated Ti. Further analyses with fluorescent microscopy confirmed that $TiO_2$ has also the potential to kill bacteria to some extent. Fibroblast (after 4 hours and after 24 hours) and osteoblast (after 4 hours and after 5 days) cell culture results showed that ~100 nm-thick $TiO_2$ (deposited at 160 ˚C) selectively promoted osteoblast growth while suppressed fibroblast growth. This phenomenon is preferable and controls the formation of undesirable fibrous tissue around the implant (Figure 4). Among osteoblast, fibroblast, and microbial agents, to achieve reasonable osteointegration, osteoblasts must win the race for the surface.
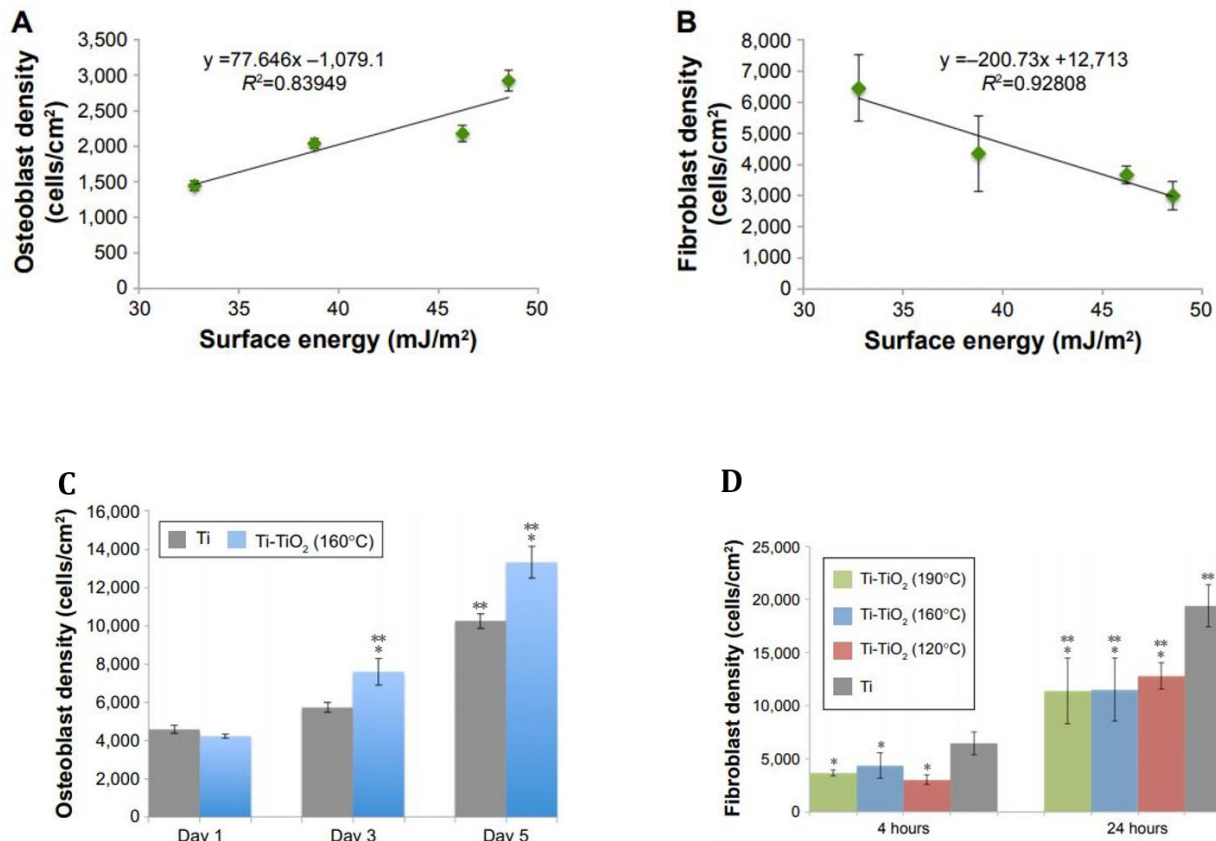
Figure 4: (**A**) Osteoblast and (**B**) fibroblast cell density (after 4 hours of culture) was directly proportional to the surface energy on Ti controls and Ti-TiO$_2$ samples. Error bars represent SD, C) Osteoblast proliferation on Ti and Ti-TiO$_2$ (160°C) samples. Data represent mean ± SD. N=3. **p,0.05 compared with Ti at the same period, **p,0.05 compared with the same sample (Day 1), D) Fibroblast adhesion and growth on Ti and Ti-TiO$_2$ samples. Data represent mean ± SD. *p,0.05 compared with Ti control at the same time period, **p,0.05 compared with the same sample (4 hours) (from [40] with permission).

Nazarov et al. [36] studied the effect of ~20 nm-thick TiO$_2$ ALD deposited by a "Nanoserf" ALD system at 250 °C on two different 3D structures of Ti, sponge and coral, with different surface roughnesses. The fabricated films had anatase crystalline form. Osteoblast MG-63 cell culture test showed more improved adhesion on samples with ~20 nm-thick TiO$_2$ when compared to uncoated Ti surfaces. Similar results on the role of anatase form were reported by Grigal et al. [41]. Anatase TiO$_2$ (samples with > 300 ALD cycles of TiO$_2$) has been reported to prepare an interesting condition for hydroxyapatite (HA) growth from simulated body fluid

(SBF), while results of the amorphous TiO$_2$ showed no HA growth upon immersion in SBF.

Figure 5 Shows the quality and differences of HA which were grown on amorphous and anatase

TiO$_2$ deposited with ALD.
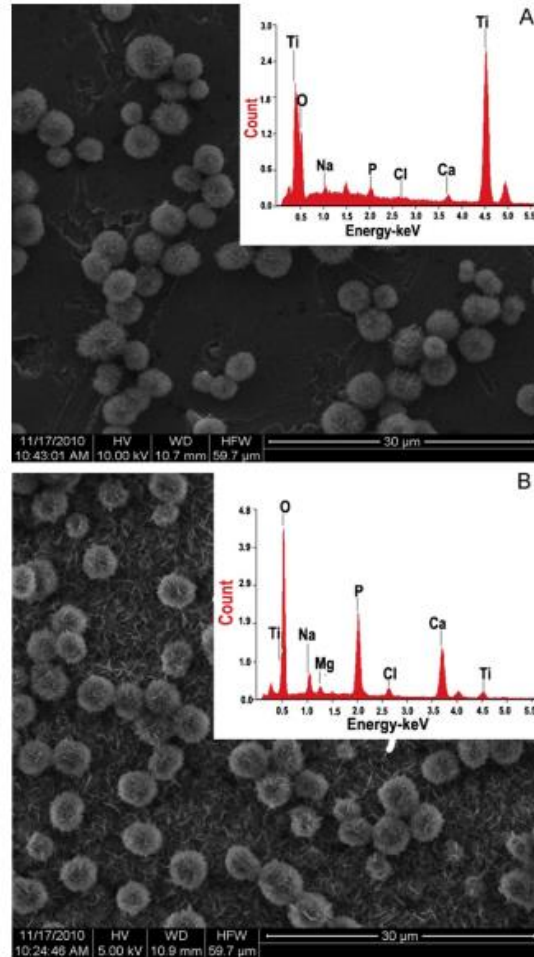


Figure 5: SEM image and electron probe of A) amorphous (100 cycles) B) anatase (300 cycles) TiO$_2$ ALD coating on Ti grade 4, after immersion in SBF, The presence of Mg$^{2+}$ and Na$^+$ on the analyzed surface is confirmed by the presence of Na and Mg peaks in EPMA spectra which resulted in continuous HA growth (figure B)  (from [41] with permission). For 100 ALD cycles of TiO$_2$ on Ti, only ball like HA growth can be seen, while on 300 ALD cycles TiO$_2$, a continuous HA formed with needle like morphology after immersion in SBF.

A plausible scenario that Grigal et al. suggested is: due to the negative charge formation on

anatase TiO$_2$, Ca ions from the SBF can favorably be attracted to TiO$_2$ thin film and

consequently absorb PO$_4$ and improve HA formation on the surface [41].

Another interesting feature of anatase over other crystalline forms of $TiO_2$ is its ability to enhance osteoblast adhesion, spreading, and proliferation [42, 43]. To elucidate the role of anatase and rutile crystalline form on bioactivity of dental implants, Solovyev et al. [42] used 500 cycles of $TiO_2$ on grade 4 Ti. The anatase form was deposited at higher than 300 ˚C, and the rutile form was achieved after rapid thermal annealing at 650 ˚C. Results of soaked $TiO_2$ coated samples in SBF for both crystalline forms showed uniform growth of hydroxyapatite. However comparing the mass gain of rutile and anatase samples after 3, 6, 9 and 12 days of soaking in the SBF solution showed that bone tissue growth on anatase was 18±5 % greater than on rutile (Figure 6).
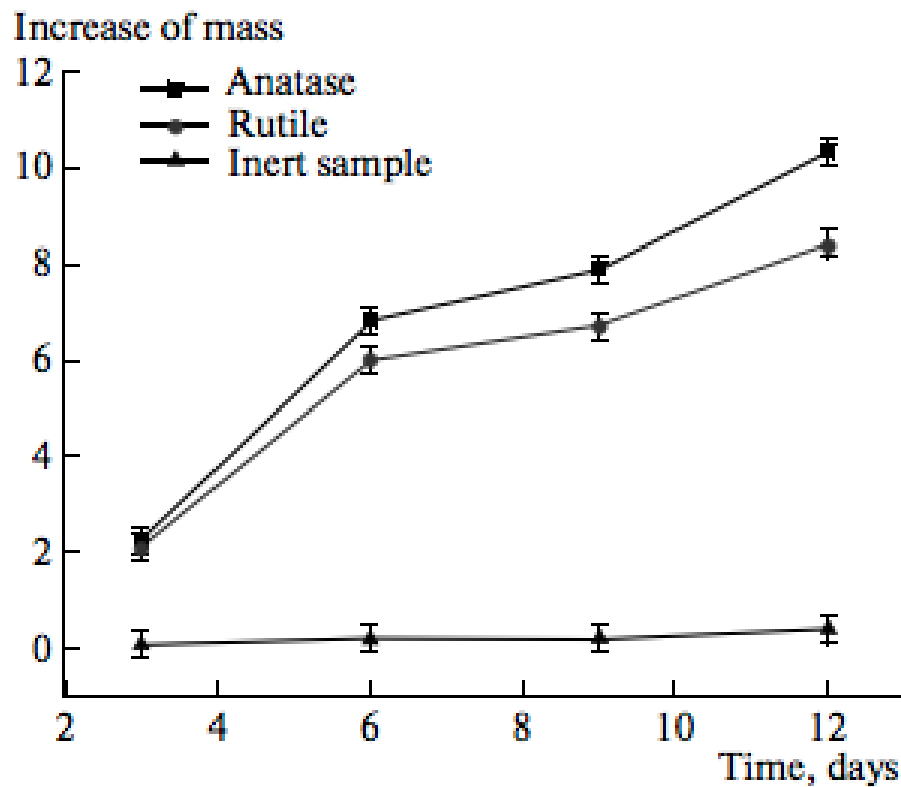


Figure 6: Mass change of ALD $TiO_2$ samples with anatase (square), rutile (circle) and un-coated Ti (triangle) after soaked in simulated body fluid after 3, 6, 9, and 12 days (from [42] with permission).

The anchorage of dental implant into the jawbone is an ultimate target of every surface modification in the context of osseointegration. Hydroxyapatite is an essential component of bone regeneration. Therefore, pre-deposition of a thin layer of such essential osseoconductive coating on the implant surface can improve and accelerate the osseointegration process [44]. Following this idea, Radtke et al. [45] first deposited titania nanotubes (TNT) on Ti6Al4V via electrochemical deposition and then deposited a very thin film (~5 nm) of $CaCO_3$ via ALD on the surface of titania nanotubes and converted them into HA in a separate wet treatment step. The wet treatment step can also be substituted with another ALD step to deposit the final HA layer [46]. The key to this promising Ti treatment is the deposition of a very thin layer of $CaCO_3$. Thicker HA coatings (> 100 μm), which were deposited via electrodeposition, were reported to reduce the mechanical properties of Ti. Thicker HA films were also reported to delaminate easier [45]. Here, ALD provided a unique way to deposit a very thin film of HA without having adverse effects on the mechanical properties of the substrate. These nanoporous TNTs provided excellent adhesion between the Ti and HA, and hindered the delamination of the HA layer [45]. Fibroblast formation and anti-bacterial properties of the novel HA coated samples (combination of the TNT and ALD HA), when compared to pristine samples and samples without TNT, showed favorable properties (Figure 7).

a)

b)
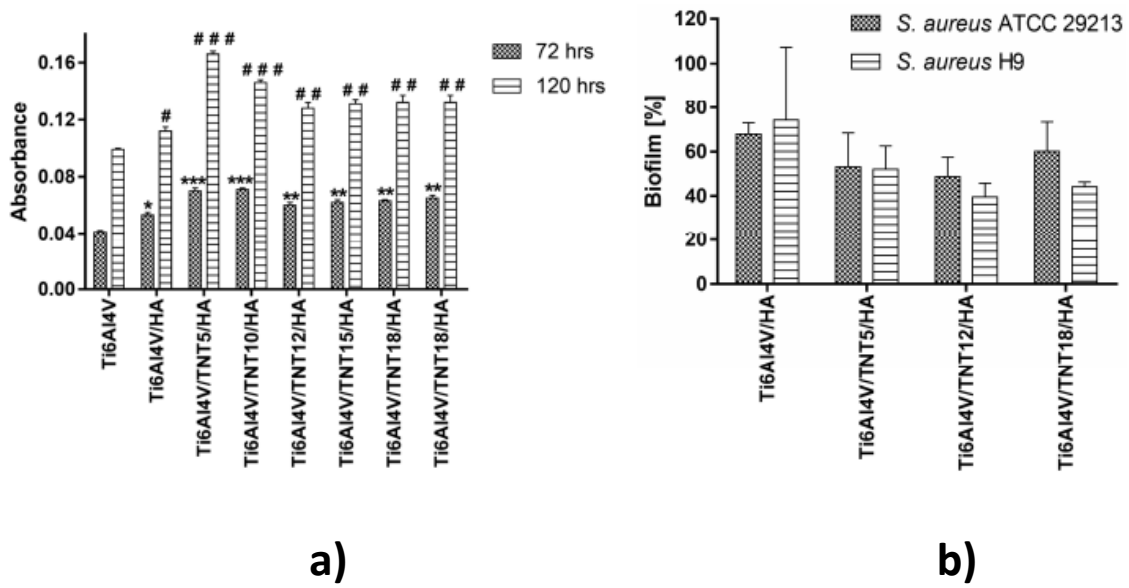
Figure 7: a) L929 murine fibroblasts proliferation (measured after 72 h and 120 h) on the surface of Ti6Al4V, Ti6Al4V/HA and Ti6Al4V/TNT(different voltage for electrochemical deposition)/HA detected by the MTT assay. b) S. aureus ATCC 29213 and S. aureus H9 biofilms (24 h old) on the surfaces of Ti6Al4V/HA and Ti6Al4V/TNT(different voltage for electrochemical deposition)/HA (from [45] with permission).

Surface characteristics such as surface wettability and microstructure of the substrate is another factor that must be considered in the fabrication of thin films on dental materials. It is reported that surface wettability controls osteoblast lineage cells response [47-49]. Upon $TiO_2$ ALD on Ti alloys, Basiaga et al. reported no significant change in wettability [50]. However, Patel et al. [51] proposed a systematic cleaning preparation procedure to minimize the organic/inorganic contamination prior to loading the sample into the ALD chamber. The proposed protocol for Ti-II and Ti-V has 5-steps: 1- wash with DI water for 30 s and $N_2$ drying, 2- 15 min of methanol 99% sonication, 3- 10 nm $TiO_2$ ALD, 4- 30 sec DI water wash followed by 5- $N_2$ drying. Their results showed that following these steps water contact angle of Ti-II and Ti-V with initial values of 30° and 54°, respectively, were decreased to < 10° which is more favorable for cell adhesion.

14

In 2011, Kang et al. [52] studied thermal ALD of $TiO_2$ on stainless steel, which could be tailored to fabricate self-cleaning stainless steel [52]. TDMAT and $H_2O$ were used as precursor and oxidizer, respectively, and resulted in 2.2 Å/cycle growth rate. Depending on the deposition temperature, $TiO_2$ thin film could have different microstructural characteristics; for example, at lower temperature, e.g., 200 °C, it was amorphous, at ~300 °C the microstructure was anatase-dominant, and at the highest temperature (400 °C), the rutile phase was dominant. Their results showed that the optimum thickness to achieve photocatalytic properties for $TiO_2$ on stainless steel is ~120 nm and among all microstructures anatase phases showed better photocatalytic activity. They did not discuss how this optimum photocatalytic effect could harness in dental industry; however, Pantaroto et al. [53] in another study showed that anatase and mixture of anatase-rutile showed better photocatalytic activity compared to pure rutile microstructure. Although the $TiO_2$ thin films they deposited were via magnetron sputtering (not via ALD), this result could be generalized to ALD $TiO_2$ films. It was shown that due to its electron hole separation and type II alignment, mixtures of anatase-rutile have the most antibacterial activity [53], which yielded formation of more reactive oxygen species (ROS). The results showed a direct relation between photocatalytic activity percentage (above 7%) and the achievement of a significant antibacterial effect and showed that rutile $TiO_2$ has no antibacterial activity [53].

Risk of delamination of these thin films under mechanical stresses is an important issue that needs to be considered when designing ALD-coated dental materials. For example, Marin et al. studied the adhesion properties of $TiO_2$, $Al_2O_3$, and multilayer $Al_2O_3/TiO_2$ ALD thin films on AISI 316. Results showed that multilayer configuration had better adhesion to the substrate compared to a single layer. In addition, thinner single layer showed reduction in delamination compared with thicker ALD films of each [54]. Another report in the literature which addressed

that suggests an optimum thickness at which the maximum adhesion between the $TiO_2$ ALD thin film and both Ti4Al6V and Ti4Al7Nb alloys can be achieved. Thin films deposited with 500 and 2500 cycles showed lower adhesion to the Ti alloys substrates compared to $TiO_2$ thin films which were deposited for 1250 cycles [50].

### 1.2.1.1 <u>ALD thin films on metal and metal alloy substrates and their interactions with the biological surroundings</u>

The interaction of different ALD thin films with biological environments is discussed next.

### 1.2.1.1.1 <u>Ti and Ti alloys</u>

There are concerns on the corrosion behavior and long-term release of metallic ions in oral environment. Studies reported that Ti alloys coated with $TiO_2$ via ALD showed improvement in corrosion and electrochemical properties [50, 55]. For example, there is a risk of toxic aluminum and vanadium release from Ti-6Al-4V permanent implants in the body. Presence of ALD thin films of $TiO_2$, $Al_2O_3$ and nanolaminates of $TiO_2/Al_2O_3$ on Ti-6Al-4V showed improvement in tribocorrosion resistance of Ti-6Al-4V against the Ringer solution (NaCl–8.6 g/l, KCl–0.3 g/l, $CaCl_2$-$6H_2O$–0.48 g/l) and showed lower friction coefficient when compared to uncoated Ti-6Al-4V [55]. These results suggested that ALD thin films of $TiO_2$, $Al_2O_3$ and nanolaminates of $TiO_2/AL_2O_3$ can be considered as coatings with corrosion protection properties. Basiaga et al. [50] studied the corrosion resistance of either Ti4Al6V or Ti4Al7Nb alloys coated with $TiO_2$ for different numbers of $TiO_2$ ALD cycles. Results indicated that 2500 cycles of $TiO_2$ (~120 nm-thick) showed the best corrosion resistance properties in the aggressive corrosion environment of the Ringer solution when compared to uncoated Ti alloys. These corrosion resistance improvements due to $TiO_2$ ALD could be generalized to harsh and corrosive oral environments.

16

### 1.2.1.1.2  Cobalt- Chromium alloys

Another class of metal-based implants is cobalt-chromium (Co-Cr) alloys, which are mostly used in prosthetic dentistry, e.g., crown or bridge [56]. Alloys of Co with Cr at concentrations more than 25% Cr were reported to be reliable alloys in dentistry applications [37]. This alloy showed reasonable mechanical properties, corrosion resistance and biocompatibility, and controlled dosage of Cr (below 50 mg/kg body mass) is crucial for human metabolism so that this alloy is benign to the human body [57]. However, suppressing metal release from implants is important and the need for the development of a novel barrier layer is of great interest. It was reported that ALD thin films of $TiO_2$ (20 to 300 nm-thick) on Co-Cr acted as a barrier layer preventing diffusion of Co and Cr toward bone tissue due to the reduction of Co-Cr corrosion in biological environments (Figure 8) [35].
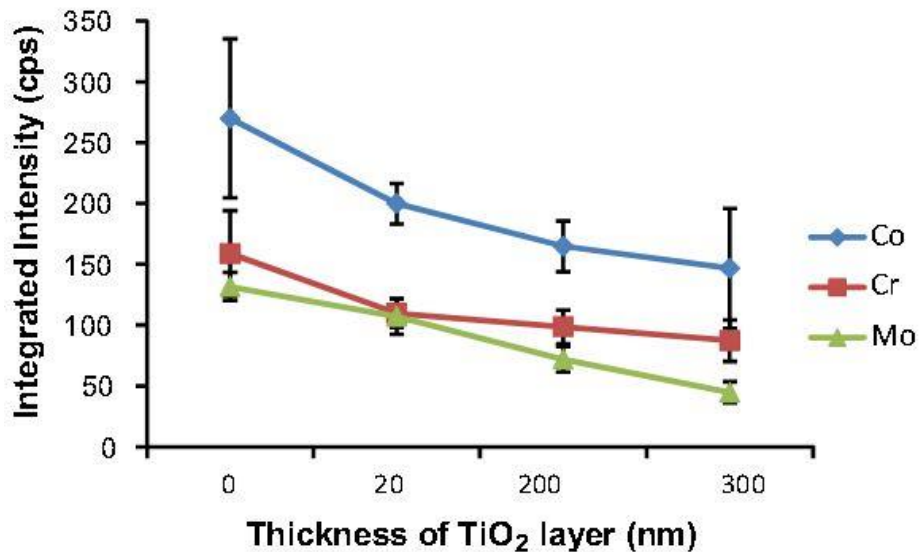


Figure 8: Intensity of released Co, Cr, and Mo at 600 μm far from the implant edge for different thicknesses of $TiO_2$ on Co-Cr implant (from [35] with permission).

Another metal oxide which was studied in order to improve the corrosion property of Co-Cr was $ZrO_2$ which was deposited via ALD. Ziebowicz et al. [58] studied two different samples

of cobalt alloys: a conventional casted Co-Cr and Direct Metal Laser Sintered Co-Cr samples. In the samples, which were prepared by the casting method, the ratio of Co/Cr was reported as 59/25 and in the Direct Metal Laser Sintering sample this ratio was 63.8/24.7. Atomic force microscopy results of both casted and sintered samples showed decrease in roughness upon $ZrO_2$ ALD. It was also determined that the wettability of samples treated with $ZrO_2$ thin film on top was reduced. Corrosion resistance of both samples were determined by potentiodynamic polarization and it was found that $ZrO_2$ deposition improved pitting corrosion resistance of the samples.

### 1.2.1.1.3  <u>Stainless Steel</u>

Surgical grade stainless steel is another metal used in dental implants. This grade of stainless steel is known for its good mechanical properties and ductility; however it is reported that stainless steel can show some biocompatibility challenges due to its lower corrosion resistance compared to other metal implants [59]. This makes pristine stainless steel mostly suitable for temporary implants in the body [60]. Functionalization of its surface with biocompatible material is a way to fabricate stainless steel, with longer-term applications into the body. For example, Shan et al.'s [61] study indicated that 50 nm-thick $TiO_2$ ALD on stainless steel improved the corrosion resistance of stainless steel in NaCl solution. Marin et al. studied the role of $Al_2O_3$ and $TiO_2$ deposited by ALD on corrosion protection of AISI 316 stainless steel. Their results showed that the alternately deposited multilayer of $Al_2O_3/TiO_2$ was more effective than single layer of each [54]. The Vickers indentation was used to evaluate the mechanical/adhesion properties of the ALD thin films on the AISI 316. Results showed that multilayer configuration had better adhesion to the substrate compared to single layers. In addition, thinner single layers showed reduction in delamination [54].

### 1.2.1.1.4  Magnesium-Strontium alloys

Similar improvement in corrosion resistance was reported by Yang et al. [62] for the $ZrO_2$ ALD thin films deposited on magnesium-strontium (Mg-Sr). The Mg-Sr alloy recently attracted interest as a biomaterial of choice for temporary implants; in vitro results of Yang et al. [62] indicated that cell and tissue growth was also enhanced due to the biocompatibility of $ZrO_2$ thin films. Table I summarizes the ALD thin film/substrate material system, precursors, and ALD processing conditions for the metal oxides thin films on metallic dental materials.

**Table I: Atomic layer deposition of metal oxides on metallic materials**

| Substrate / ALD thin film | Precursor / Co − reactant | Processing conditions | Stage of translation | Type of study | Inferences | Ref |
|---|---|---|---|---|---|---|
| *Porous Ti* / $TiO_2$ | $TiCl_4$ / $H_2O$ | 200- 400 ˚C<br>TiCl₄ pulse/purge time: 0.1/4.0 sec<br>H₂O pulse/purge time: 0.1/4.0 sec<br>No. of cycles: 550-1550 | 1-2 | microstructure | Conformality in the range < 2 nm all over the porous Ti scaffolds. TiO₂ had no negative effect on osteoblast viability. | [37, 38] |
| *Ti* / $TiO_2$ | *TDMATi* / $H_2O$ | 120 ˚C, 160 ˚C, 190 ˚C<br>TDMATi pulse/purge time: 0.1/6.0 sec<br>H₂O pulse/purge time: 0.1/6.0 sec<br>No. of cycles: 2500 | 2 | In vitro | Great antibacterial properties. Enhancement in osteoblast growth. Suppressed fibroblast growth. | [40] |
| *Ti(iv)* / $TiO_2$ | *Titanium ethoxide* / $H_2O$ | 300 ˚C<br>Ti ethoxide pulse/purge time: 0.1/4.0 sec<br>H₂O pulse/purge time: 0.2/4.0 sec<br>No. of cycles: 100 to 2000 | 2 | In vitro | Amorphous TiO₂ showed no bioactivity Anatase TiO₂ achieved at higher number of cycles (>300) HA growth enhancement on anatase TiO₂. | [41] |
| *PorousTi* / $TiO_2$ | *Ti isopropoxide* / $H_2O$ | 250 ˚C<br>Ti isopropoxide pulse/purge time: 0.02/5.0 sec<br>H₂O pulse/purge time: 0.5/5.0 sec<br>Another 20 sec purge<br>No. of cycles: 400 | 2 | In vitro | ~20 nm TiO₂ coated Ti showed improved osteoblast adhesion and spreading. | [36] |
| *Ti* / $TiO_2$ | *TDEAT* / *DI water* | 250 ˚C<br>H₂O pulse time: 0.05 sec<br>No. of cycles: 100 | 1 | Microstructure Surface properties | Proposed systematic cleaning followed by ALD of TiO₂ to achieve super hydrophilic Ti (II) and Ti (V) | [51] |
| *TNT* / $CaCO_3$ | $Ca(thd)_2$ / $O_3$ | 250 ˚C<br>No. of cycles: 100 | 2 | In vitro | With the aid of ALD extremely thin CaCO₃ was deposited on TiO₂ nanotubes. The final nanocomposite showed the best osteoblast adhesion, proliferation and at the same time good antibacterial activity. | [45] |
| *Grade 4 Ti* / $TiO_2$ | $Ti(OCH_3)_4$ / $H_2O$ | 300 ˚C<br>Ti(OCH₃)₄ pulse/purge time: 0.2/4.0 | 2 | In vitro | Enhanced HA formation from SBF on the anatase | [43] |

| | | sec<br>$H_2O$ pulse/purge time: 0.1/4.0 sec<br>No. of cycles: 100-1500 | | | $TiO_2$ regardless of the number of cycles & crystallite size of $TiO_2$ ALD | |
|---|---|---|---|---|---|---|
| $\dfrac{Grade\ 4\ Ti}{TiO_2}$ | $\dfrac{Ti(OC_2H_5)_4}{H_2O}$ | 300 ˚C<br>$Ti(OC_2H_5)_4$ pulse/purge time: 0.1/4.0 s<br>$H_2O$ pulse/purge time: 0.1/4.0 s<br>No. of cycles: 500 | 1 | In vitro | Comparing anatase & rutile, HA formation on anatase is ~18% faster on anatase | [42] |
| $\dfrac{Ti4Al6V}{TiO_2/Al_2O_3}$ | $\dfrac{TMA}{H_2O}$<br>$\dfrac{TTIP}{H_2O}$ | 250 ˚C<br>TMA pulse/purge time: 0.15/0.75 sec<br>$H_2O$ pulse/purge time: 0.15/0.75 sec<br>TTIP pulse/purge time: 0.5/1.0 sec<br>$H_2O$ pulse/purge time: 0.15/0.75 sec<br>Each supercycle: 90 cycles of $TiO_2$ and 1 cycle of $Al_2O_3$<br>Total number of supercycles: 30 | 1 | Tribocorrosion | Enhancement in corrosion resistance of ALD coated samples in compare with bare Ti.<br>Friction coefficient reduction for samples with thin film on Ti alloy. | [55, 63] |
| $\dfrac{Ti4Al6V}{TiO_2}$ | $\dfrac{TiCl_4}{H_2O}$ | 200 ˚C<br>No. of cycles: 500, 1250, 2500 | 1 | Tribocorrosion<br>Water contact angle | 120 nm $TiO_2$ coated Ti alloys became corrosion resistance.<br>No significant change in wettability after $TiO_2$ deposition. | [50] |
| $\dfrac{Ti}{ZnO}$ | $\dfrac{DEZ}{H_2O}$ | (Deposited ZnO as a seed layer for ZnO nanotubes & polydopamine (PDA))<br>100 ˚C<br>DEZ pulse/purge time: 0.1/20 sec<br>$H_2O$ pulse/purge time: 0.1/20 sec<br>No. of cycles: 300 | 3 | In vitro<br>In vivo | ZnO ALD was used as seed layer for RGDC nanorods and other functionalizing agents.<br>ZnO/PDA/RGDC functionalized Ti showed balanced antibacterial and osteoblast growth. | [64] |
| $\dfrac{Ti}{ZnO}$ | $\dfrac{DEZ}{H_2O}$ | TDMAZ pulse/purge time:0.03/10 sec<br>$H_2O$ pulse/purge time: 0.03/10 sec<br>No. of cycles: 30, 100,300 | 2 | In vitro | ZnO ALD was used as the top layer on the CNT/Chitosan hybrid on the Ti implants.<br>Presence of ZnO showed improved antibacterial activity against (E.coli and S.aureus) and enhanced osteoblast growth. | [65] |
| $\dfrac{Co-Cr}{ZrO_2}$ | $\dfrac{TEMAZr}{H_2O}$ | 200 ˚C | 1 | Corrosion<br>Surface properties | Upon $ZrO_2$ deposition, roughness of Co-Cr decreased<br>WCA decreased for $ZrO_2$ coated samples.<br>Pitting corrosion of $ZrO_2$ samples improved in compare to uncoated Co-Cr alloy. | [58] |
| $\dfrac{Mg-Sr}{ZrO_2}$ | $\dfrac{TDMAZ}{H_2O}$ | 250 ˚C<br>TDMAZ pulse/purge time:0.03/10 sec<br>$H_2O$ pulse/purge time: 0.15/10 sec<br>No. of cycles: 100,200,300,400 | 2 | Corrosion<br>In vitro | Corrosion resistance of Mg-Sr improved.<br>Cell growth improved on $ZrO_2$-coated samples | [62] |
| $\dfrac{Co-Cr}{TiO_2}$ | $\dfrac{TDMAT}{H_2O}$ | 90 ˚C<br>Thickness: 20- 300 nm | 2 | Metal diffusion from alloy into bone tissue | Significant decrease in metal release for samples with $TiO_2$ barrier layer into the bone tissue.<br>Enhancement in corrosion resistance for samples with $TiO_2$ layer. | [35] |
| $\dfrac{Stainless\ Steel}{TiO_2}$ | $\dfrac{TTIP}{H_2O}$ | 150 ˚C<br>TTIP pulse/purge time: 0.015/3.0 sec<br>$H_2O$ pulse/purge time: 0.015/3.0 sec<br>No. of cycles: 1500 | 1 | Corrosion | ~50 nm $TiO_2$ enhance the corrosion resistance of stainless Steel in NaCl solution. | [61] |
| $\dfrac{Stainless\ Steel}{TiO_2}$ | $\dfrac{TDMAT}{H_2O}$ | 200 C, 300 C, 400 ˚C<br>TDMAT pulse/purge time: 1.5/5.0 sec<br>$H_2O$ pulse/purge time: 3.0/5.0 sec<br>No. of cycles: 500 | 1 | Photocatalytic properties | Anatase $TiO_2$ showed photocatalytic properties.<br>~120 nm $TiO_2$ is the ideal thickness for best photocatalytic property. | [52] |

| | $\begin{array}{c} TiCl_4 \\ \hline H_2O \\ Al(CH_3)_3 \\ \hline H_2O \end{array}$ | Single layer of TiO$_2$ and Al$_2$O$_3$ and multilayer<br>Both deposited at 120 ˚C<br>Thicknesses: 300 nm, 100 nm, 30 nm, 10 nm | 1 | Microstructure<br>Corrosion<br>Adhesion | Improved corrosion resistance.<br>Better adhesion for multilayer ALD films than single layers. | [54] |
|---|---|---|---|---|---|---|
| $\dfrac{Stainless\ Steel}{TiO_2/Al_2O_3}$ | | | | | | |

### 1.2.2   ALD of metals on metal-based dental material

There are only few studies on the influence of thin metallic films on metal-based dental related materials. Delvin-Mullin et al. [66] comprehensively studied the Ag ALD coated Ti implants for orthopedic applications. As mentioned earlier in the current review paper, due to the quite similar concept of dental and orthopedic implants, orthopedic related researches are also discussed here when needed. For 3D structure implants, ALD offers the most conformal, uniform and at the same time thin enough to minimize cytotoxicity concerns. In vitro results showed that Ti implants coated with Ag suppressed the growth of osteolytic pathogen (S. Epidermitis) by 2-log fold. Also, Ag did not have any negative effect on newly regenerated bone after 12 weeks in rat tibia, which means efficiency of bone regeneration on silver coated and uncoated porous Ti implant was similar [66]. In another work, in vivo studies for the same material system were done and this nontoxic behavior of silver was attributed to biotransformation of silver. Biotransformation mechanism means Ag nanoparticles on the surface colonized with sulfur atoms from the newly bone cells and forms silver sulfide which is less toxic compared to silver ions [67]. Table II summarizes the ALD thin film/substrate, precursor system, and ALD processing conditions for metal thin films on metallic materials with potential use in the dental industry.

**Table II: Atomic layer deposition of metal on metallic materials**

| Substrate ALD thin film | Precursor Co−reactant | Processing conditions | Stage of translation | Type of study | Inferences | Ref |
|---|---|---|---|---|---|---|
| $\frac{Ti}{Ag}$ | $\frac{(hfac)Ag(1,5-COD)}{propan-1-ol}$ | Liquid injection ALD 125 ˚C (hfac)Ag(1,5-COD) pulse/purge time: 4.0/8.0 sec Propan-1-ol pulse/purge time: 4.0/8.0 sec No. of cycles: 500 | 3 | In vitro In vivo | Ag coated Ti has significant effect on osteolytic pathogen reduction. No negative effect on bone regeneration for Ti with Ag ALD. | [66] |
| $\frac{Ti}{Ag}$ | $\frac{(hfac)Ag(1,5-COD)}{propan-1-ol}$ | Liquid injection ALD 125 ˚C (hfac)Ag(1,5-COD) pulse/purge time: 4.0/8.0 sec Propan-1-ol pulse/purge time: 4.0/8.0 sec No. of cycles: 500 | 3 | In vitro In vivo | Biotransformation of Ag to $Ag_2S$ within the newly formed bone, reduced the chance of toxicity of Ag ALD. | [67] |

### 1.2.3   ALD on Organic-based dental materials

Among different acrylic resin materials**,** PMMA is a low-cost polymer and due to its biocompatibility, it is widely being used as removable denture in the dentistry industry. However, it has some drawbacks, which need improvements. For example due to its polymer backbone chemical composition, PMMA is hydrophobic in nature [68] and chemically compatible for adhesion of Candida Albicans on its surface. Considering this along with the porous surface of PMMA, plaque/biofilm formation is the main challenge with PMMA based dentures. As discussed before in this work, $TiO_2$ is a well-established nanomaterial with antimicrobial properties. A conventional way to modify PMMA resin with $TiO_2$ is to add and mix $TiO_2$ nanoparticles (mostly in the size range of 20-30 nm) to the formulation of PMMA resin [69]. However, considering the potential micron size pores on the PMMA dentures, a novel approach for improvement of its antibacterial properties is to coat the surface of PMMA with a thin layer of $TiO_2$. Thanks to ALD technique, uniform and conformal thin films of $TiO_2$ are achievable for such porous materials. Feasibility of coating PMMA with $TiO_2$ via ALD was studied and successfully done by Kemell et al. [70]. No further analysis and discussion were done by Kemell

et al. on the physical, mechanical, and biological properties of this material. In another study, Paul et al [71] deposited thin film of $TiO_2$ on PMMA and investigated the antireflection, adhesion and durability against the environment; all these properties were improved after the ALD $TiO_2$ thin film.

In fabricating a novel PMMA as a denture material, Darwish et al. [68] studied the feasibility of coating PMMA with low temperature $TiO_2$ ALD. Comparison between the results of uncoated and $TiO_2$-coated (~30 nm) polished PMMA, showed that hydrophobicity of PMMA significantly changed and decreased to 5° due to the presence of $TiO_2$ on PMMA. Results also showed that flexural strength of the samples remained unchanged. A 6000 cycles brushing test demonstrated that presence of ~30 nm $TiO_2$ could significantly increase the wear resistance of PMMA samples and control the roughening of its top surface upon usage in an oral environment over time. Antimicrobial activity of the samples was tested with C. Albicans attachment test. Results showed that biofilm formation and adherence of C. Albicans decreased by 56% and 63% for the $TiO_2$-coated PMMA sample, respectively. Furthermore, surface characterizations before and after brushing and polydent sonication confirmed good adhesion between PMMA and $TiO_2$ thin film.

Other than $TiO_2$, ALD of other metal oxides were also studied on PMMA. Napari et al. [72] deposited ZnO on PMMA at 35 ˚C. This low temperature ALD was done on two different types of PMMA, bulk and spin coated PMMA. The growth of ZnO on these substrates showed different growth mechanism. On the bulk PMMA growth of ZnO started from the subsurface while for the spin coated PMMA this was not the case. The deposited ZnO imposed hydrophilicity upon UV exposure independently of PMMA type and ZnO crystal form. ZnO ALD thin films have been reported to have antibacterial properties in other studies [73-76].

However, in that work [72], no further tests and discussion were done on the potential applications of this ZnO-coated PMMA in the dental industry. Based on reported antibacterial properties of ZnO [73, 74], ZnO coated PMMA can be considered as a candidate for modified denture applications, while it needs further study.

As mentioned before, PMMA as substrate and ZnO and $TiO_2$ as ALD thin films were reported to have antibacterial activity and photocatalytic activity. Therefore, combination of these outstanding properties has the potential for the fabrication of new dental materials. However, in vitro and in vivo tests along with mechanical tests are essential before making them commercial and answering the concerns about side effects of zinc ion release in clinical use. For example Choi et al. studied the effect of the sustained release of Zn ions from ZnO ALD thin film [77] on bone matrix and abnormal bone environment. Their invitro and in vivo results showed that on the one hand released Zn ions had Anti-Osteosarcoma effect and on the other hand it showed inflammatory bone resorption. This suggests that the toxicity threshold of these thin films needs to be precisely designed before moving forward and using them in clinical applications.

Another polymer, which is being used in the dental industry, is polydimethylsiloxane (PDMS). PDMS is of interest in biomedical devices like cochlear implants and maxillofacial prostheses. It is inert, flexible and heat resistant [78]. In the field of dental industry, it is mostly being used as an extraoral prosthesis. This kind of prostheses has a couple of limitations. Upon exposure to gradients of temperature, moisture, and sunlight, pigmented PDMS shows color change, which results in the discoloration and degradation of the prostheses on the outside surface. From inside, exposure of the PDMS surface to dark and humid environment between skin and PDMS surface has potential for microbe and bacteria growth and propagation resulting

in biofilm formation and fungal infection adherence on the PDMS surface. Pessoa et al. [79] deposited different thicknesses of $TiO_2$ ALD on PDMS and photocatalytic tests showed that in comparison to pristine PDMS, $TiO_2$-coated samples showed up to 59% increase in antimicrobial activity after exposure to UV. The possible scenario for such improvement in C. Albicans growth suppression was attributed to the higher content of Cl (from the $TiCl_4$ precursor) in $TiO_2$-coated PDMS; however, the proposed mechanism for such improvement cannot be generalized to other precursor/co-reactant systems. Goldfinger et al. [80] also showed that PDMS coated with ALD $TiO_2$ (10-40 nm-thick) showed bacteria-resistant properties.

Bishal et al. [81] deposited 16 nm thick $TiO_2$ thin film via ALD on PDMS. The idea was to investigate whether a thin layer of $TiO_2$ can absorb and scatter UV light and protect PDMS from color deterioration and postpone its replacement. After comparing pristine PDMS and $TiO_2$-coated PDMS, they demonstrated that ~16 nm thick $TiO_2$ ALD had successfully protected PDMS from the potential color change which was induced by artificial aging. Any resulting color change (DE=1.4±0.6) was significantly below the acceptability threshold (DE=3.0). Their results also indicated that the thin film of $TiO_2$ can be resistant to artificial aging [81].

One of the key materials in oral implantology is membranes such as collagen, chitosan, and polyesters. The role of these membranes is to make a guided path for regeneration of osteoblasts. The main advantage of these membranes over other membranes is their bioresorbability, which does not need second surgery for their removal. Collagen, by its nature, is biocompatible; however, work can still be done to minimize the risk of infection and improve bone regeneration properties. Bishal et al. [82] deposited $TiO_2$ ALD on collagen membrane. To minimize the risk of thermal degradation, the deposition was carried out at room temperature. The idea was to improve the bioactivity of collagen while maintaining its unique fibrous structure by taking

advantage of coating collagen with ALD. As the number of cycles increased, the diameter of the collagen fibers increased which corroborated the conformal growth.

In another study, Bishal et al. [83] investigated the role of $TiO_2$ ALD on promoting the bone regeneration process of collagen membrane (Figure 9). In vitro results of osteoblast cell culture tests and MMT assay demonstrated that $TiO_2$-coated collagen showed improvement in cell growth when compared to pristine collagen. All effective parameters of bone regeneration were comprehensively studied in the presence of $TiO_2$ ALD on the collagen membrane [83]. The major parameter that plays role in bone regeneration is capability of $TiO_2$ surface to host the necessary chemical elements from the SBF solution, e.g., calcium (Ca) and phosphorus (P) [84-86]. Absorption of Ca and P on the $TiO_2$ coated surface, yielded the formation of calcium phosphate nucleus, which stimulated the bone regeneration process. Uncoated collagen showed no Ca absorption even after 7 days. Hydrophilicity, nano roughening, and negative charge of the $TiO_2$ surface were other surface features, which made $TiO_2$-coated collagen preferable for osteoblast growth and proliferation. From the mechanical properties point of view, results showed that the elastic moduli of $TiO_2$-coated samples were not affected negatively.
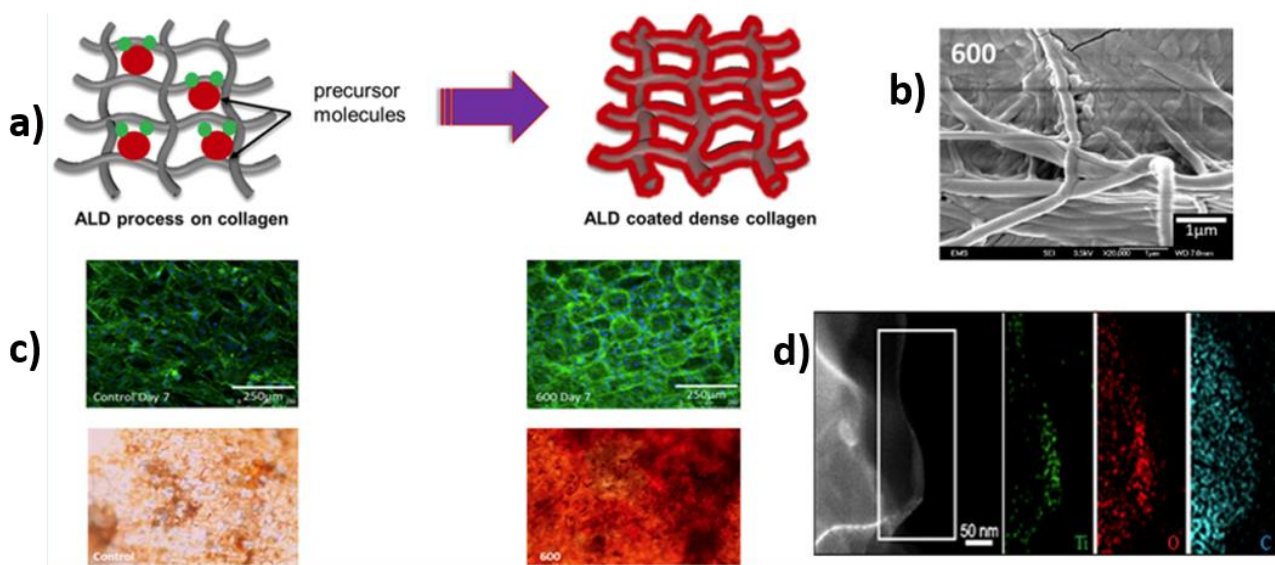
Figure 9: a) Schematic representation of the ALD process on the collagen fibrous substrate. Gray core represents the collagen fiber, and red shell represents the thin ALD coating of $TiO_2$, b) SEM of 600 cycles $TiO_2$ on collagen membrane, c) Fluorescence images of MG63 cells seeded on control collagen (left side) and 600 cycles $TiO_2$ on collagen (right side) for day 7 (green images), Images of the mineralized collagen samples control (left side) and 600 cycles $TiO_2$ on collagen in SBF for 7 days and stained in Alizarin Red S stain, d) energy dispersive X-ray spectroscopy (EDS) mapping of Ti, O, and C elements on 600 cycles $TiO_2$ on collagen (from [83] with permission).

Chitin and chitosan are another group of inorganic materials with wide potential applications in oral surgery, endodontics, periodontology, orthodontic, and conservative dentistry [87]. Choy et al. [88] studied the effect of $TiO_2$ ALD on chitin nanofiber (ChNM) properties. Mechanical properties of $TiO_2$-coated chitin membranes showed excellent toughness along with improvement in tensile strength (which rarely happen together). This improvement in mechanical properties enhanced the resistance to biodegradation of ChNM. Their in vitro results showed no cytotoxicity. Biocompatibility tests showed that bone growth rate ratio for ChNM/400$TiO_2$ was increased to ~0.72, while it was ~0.52 for pristine ChNM. Also, ChNM/$TiO_2$ samples demonstrated enhanced proliferation of MC3T3-E1 preosteoblasts. In vitro proliferation of NIH3T3 fibroblast showed enhancement even on amorphous $TiO_2$ of ChNM/400$TiO_2$ samples. There are contrary results for amorphous $TiO_2$ in the literature: other studies reported

enhancement in osteoblast growth/proliferation only when $TiO_2$ was in the anatase crystalline form [41].

The dental industry always seeks better materials; Polyether Ether Ketone (PEEK) is one of the latest materials, which has attracted interest. According to the recent review of Bathala et al. on 85 research papers on PEEK, 30.6% related to PEEK were as implant, 38.9% were on different prosthodontic applications of PEEK, 10.6% were on other fields of dentistry like, orthodontic, endodontic, oral and maxillofacial surgeries, and 20% was on the properties of PEEK [89]. Therefore, modification of PEEK with ALD has great potential in the field of dentistry. $TiO_2$ ALD on PEEK was successfully done by Kemell et al. [70]. The binding strength of $TiO_2$ thin film on PEEK was tested with the Scotch tape test and showed good adhesion. But no further analyses were performed to evaluate this novel material for its potential use in the dental industry.

In the literature there are several studies on using ALD on organic substrates like PMMA, PDMS, polyurethane, which are being used as dental materials. Most of these works showed the targeted thin films like $TiO_2$, ZnO, $ZrO_2$ have been successfully deposited on substrates [78, 90, 91]. However further analyses and discussions are needed on in vivo and in vitro tests before these materials are implemented in dental applications. Table III summarizes the ALD thin film/substrate, precursor system, and ALD processing conditions for organic materials with potential uses as dental materials.

**Table III: Atomic layer deposition of metal oxides on organic dental substrates**

| Substrate / ALD thin film | Precursor / Co−reactant | Processing conditions | Stage of translation | Type of study | Inferences | Ref |
|---|---|---|---|---|---|---|
| $\frac{PMMA}{TiO_2}$ | $\frac{TiCl_4}{H_2O}$ | 100 ˚C<br>TiCl$_4$ pulse/purge time: 0.2/30 sec<br>H$_2$O pulse/purge time: 0.2/30 sec<br>No. of cycles: 700 | 1 | - | TiO$_2$ successfully deposited on PMMA | [70] |
| $\frac{PMMA}{TiO_2}$ | $\frac{TMA}{O_2}$ | Plasma ALD<br>60 ˚C<br>TMA pulse/purge time: 1.5/7.0 sec<br>O$_2$ pulse/purge time: 6.0/5.0 sec | 1 | Climate test<br>Adhesion test | Conformal TiO$_2$ successfully deposited on PMMA.<br>TiO$_2$ thin films showed good environmental stability.<br>TiO$_2$ on bare PMMA delaminates easily, while precoated PMMA with thermal ALD of Al$_2$O$_3$ showed no delamination. | [71] |
| $\frac{PMMA}{TiO_2}$ | $\frac{TDMAT}{O_3}$ | 65 ˚C<br>TDMAT pulse/purge time: 0.5/10 sec<br>O$_3$ pulse/purge time: 1.0/15 sec<br>No. of cycles: 300 | 2 | Brushing<br>In vitro | ~30 nm TiO$_2$ enhance wear resistance of PMMA against brushing.<br>Decrease of biofilm formation and C. albican adhesion to TiO$_2$ coated PMMA. | [68] |
| $\frac{PMMA}{ZnO}$ | $\frac{diethylzinc}{H_2O}$ | 35 ˚C<br>diethylzinc pulse/purge time 0.3/30 & 0.15/30 sec<br>H$_2$O pulse/purge time: 0.3/30 & 0.15/30 sec<br>No. of cycles: 100-800, 1600 | 1 | Surface properties | ZnO successfully deposited on PMMA with hydrophilic properties after UV. | [72] |
| $\frac{PDMS}{TiO_2}$ | $\frac{TDMAT}{O_3}$ | 70 ˚C<br>No. of cycles: 300 | 1 | color change due to aging | TiO$_2$ protected PDMS from color change upon artificial aging and ALD TiO$_2$ was resistant to artificial aging. | [81] |
| $\frac{PDMS}{TiO_2}$ | $\frac{TiCl_4}{H_2O}$ | 80 ˚C<br>TiCl$_4$ pulse/purge time: 0.25/2.0 sec<br>H$_2$O pulse/purge time: 0.25/2.0 sec<br>No. of cycles: 500-1000-1500-2000 | 2 | In vitro | 59% improvement in antimicrobial activity against C. albican upon UV exposure. | [79] |
| $\frac{Collagen}{TiO_2}$ | $\frac{TDMAT}{O_3}$ | 25 ˚C<br>No. of cycles: 150, 300, 600 | 2 | In vitro | Successful room temperature ALD.<br>600 cycles TiO$_2$ ALD promotes osteoblast growth and proliferation.<br>TiO$_2$ thin film accelerated Ca adhesion to the collagen surface. | [83] |
| $\frac{ChNM}{TiO_2}$ | $\frac{TIP}{H_2O}$ | 70 ˚C<br>TIP pulse/exposure/purge time: 1/40/60 sec<br>H$_2$O pulse/exposure/purge time: 1/40/60 sec<br>No. of cycles: 50, 100, 200, 400 | 2 | In vitro | Improvement in tensile strength & toughness at the same time.<br>Enhancement in pre-osteoblast and fibroblast proliferation.<br>No cytotoxicity. | [88] |
| $\frac{PEEK}{TiO_2}$ | $\frac{TMA}{H_2O}$<br>$\frac{TiCl_4}{H_2O}$ | 150 ˚C<br>TMA pulse/purge time: 0.2/6.0 sec<br>H$_2$O pulse/purge time: 0.2/6.0 sec<br>No. of cycles: 200<br>------------------<br>Temperature: 200 ˚C<br>TiCl$_4$ pulse/purge time: 0.2/10.0 sec<br>H$_2$O pulse/purge time: 0.2/10.0 sec<br>No. of cycles: 1000 | 1 | adhesion | Good adhesion between PEEK & TiO$_2$. | [70] |

### 1.2.4 ALD on Ceramic-based dental materials

One of the drawbacks of using titanium-based implants is their grey color. Especially in surgeries with anterior bone loss, grey implants of Ti imposes appearance problems for the patient [92]. In addressing this problem, ceramics like ZrO$_2$ were proposed as alternative

materials. However biological inertness of $ZrO_2$ causes the main problem, which is the hindrance of osseointegration on the surface of this implant. To improve osteogenesis and suppress bacterial infection of the implant, Zinc Oxide (ZnO) deposition on $ZrO_2$ was studied by Yao et al. [93]. Four groups of $ZrO_2$ samples were prepared and studied: pristine $ZrO_2$, ZnO ALD on $ZrO_2$, sand blasted/ acid washed $ZrO_2$, and ZnO deposited on san blasted/acid washed $ZrO_2$. Sand blasting followed by acid etching formed micro-roughened surface. In vitro results showed that the deposited ZnO had significant effect on S. Aureus, E. Coil, and P. Gingivalis bacteria deaths (Figure 10), increased MC3T3-E1 cells adhesion, and improved osteo differentiation. It also showed that sand blasted-acid etched ZnO coated $ZrO_2$ can be a good candidate in dental applications. Comparing the results of Yao et al. [93] and Choi et al. [77], in designing ZnO thin film-coated dental materials, the optimal thickness should be carefully determined to suppress the chance of release of toxic metals in clinical use.
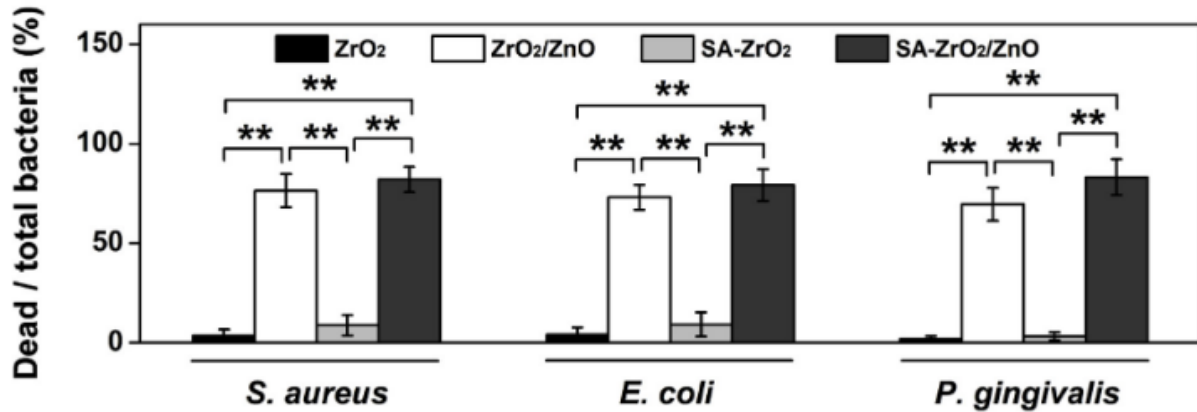


Figure 10: Quantitative statics of dead/total bacteria extracted from fluorescence images for S. aureus, E. coli, and P. gingivalis (from [93] with permission).

Alumina ($Al_2O_3$) is another ceramic material with wide applications in dentistry such as implants, filler for dental composites and bone cement materials, core material for fixed prostheses and orthodontic brackets [94]. Narayan et al. [95] studied the role of $TiO_2$ ALD thin

film porous alumina membranes with different pore sizes (20 nm and 100 nm diameter pore size). The in vitro results on epidermal keratinocyte showed no significant viability change for $TiO_2$-coated alumina compared to uncoated samples. However, results of antibacterial tests showed significant antibacterial activity for alumina with 20 nm pore size coated with $TiO_2$, while for $TiO_2$ coated alumina with 100 nm pore size no antibacterial activity was observed.

Conventional amalgam has very different color in comparison to natural tooth. Therefore, dental composites that have similar color to the color of natural tooth are highly sought-after. These composites mostly consist of light/UV curable resin and ceramic fillers like $SiO_2$. Weimer et al. [96] patented the novel nanofillers of $SiO_2$ coated with ALD of $TiO_2$, $ZrO_2$ or both, with predetermined refractive index, which can be tailored to match the color of the natural tooth enamel.

### 1.2.4.1 Effect of ALD thin films on corrosion properties of ceramic substrates

Highly porous $TiO_2$ ceramic foams are sensitive to intergranular corrosion. This corrosion results into significant mechanical properties loss. Muller et al. [97] deposited ~24 nm-thick $TiO_2$ on highly porous $TiO_2$ scaffold to investigate the corrosion behavior in 1 mM HCl. Both anatase and amorphous $TiO_2$-coated samples after 7 days and 28 days immersion in HCl, did not show any significant reduction in compressive strength compared to pristine $TiO_2$ scaffolds while the non-coated $TiO_2$ underwent reduction in compressive strength after 7 and 28 days of being immersed in 1nM HCl (Figure 11).
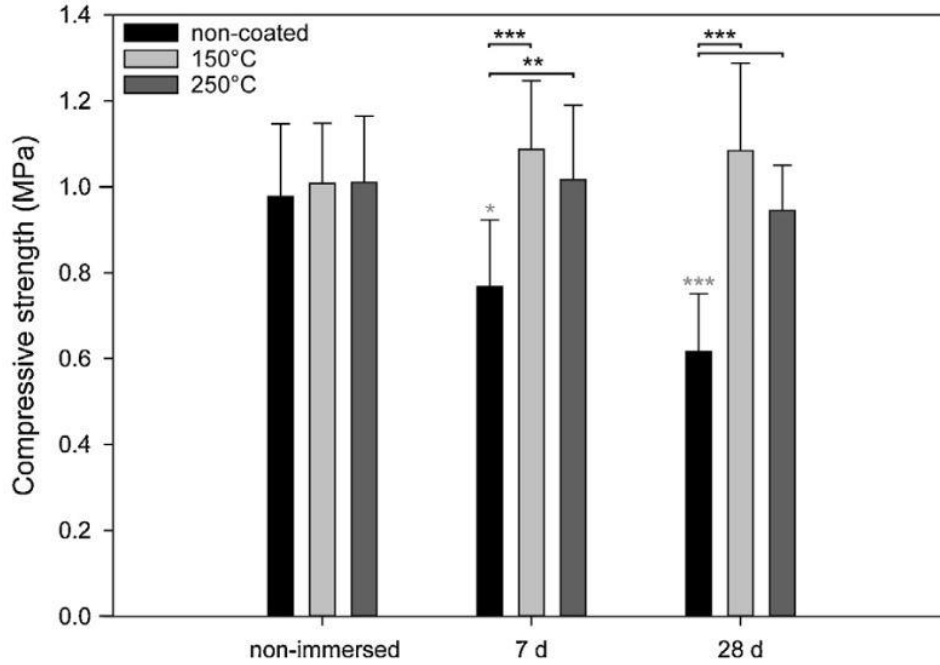
Figure 11: Effect of immersion in 1mM HCl solution on compressive strength of non-coated $TiO_2$ scaffold and atomic layer deposited scaffolds with two different microstructures (deposited at 150 ˚C (mixture of amorphous and some $TiO_2$ crystals), and deposited at 250 ˚C (anatase crystal structure)) after 7 days and 28 days (from [97] with permission).

Table IV summarizes the ALD thin film/substrate, precursor material system, and the ALD processing conditions for ALD on potential dental materials.

**Table IV: Atomic layer deposition of metal oxides on ceramic dental substrates**

| Substrate ALD thin film | Precursor Co − reactant | Processing conditions | Stage of translation | Type of study | Inferences | Ref |
|---|---|---|---|---|---|---|
| $\frac{ZrO_2}{ZnO}$ | $\frac{Diethylzinc}{ddH_2O}$ | 250 ˚C<br>Diethylzinc pulse/exposure/purge time: 0.03/4/10 sec<br>$ddH_2O$ pulse/exposure/purge time: 0.03/4/10 sec<br>No. of cycles: 10- 30- 50 | 2 | In virto | ZnO coated $ZrO_2$ showed enhanced antibacterial activity. Enhancement in cell adhesion, migration, proliferation & osteogenic differentiation for ZnO coated $ZrO_2$. | [93] |
| $\frac{TiO_2}{TiO_2}$ | $\frac{TiCl_4}{H_2O}$ | 120 ˚C- 250 ˚C<br>$TiCl_4$ pulse/exposure/purge time: 1/5/2 sec<br>$H_2O$ pulse/exposure/purge time: 1.5/5/3 sec<br>No. of cycles: 500 | 1 | Corrosion in HCl | ~24 nm $TiO_2$ improved corrosion resistance of $TiO_2$ porous scaffold. | [97] |
| $\frac{Al_2O_3}{TiO_2}$ | $\frac{TiCl_4}{H_2O}$ | 300 ˚C | 2 | In vitro | 7.6 to 9.2 nm of $TiO_2$ ALD, showed great photocatalytic activity for alumina with 20 nm pore size. No meaningful change in cell viability. | [95] |
| $\frac{SiO_2}{TiO_2}$ $\frac{SiO_2}{ZrO_2}$ | $\frac{TiCl_4}{H_2O}$ $\frac{ZrCl_4}{H_2O}$ | In the patent no specific data was given about the processing conditions, only wide range of conditions were presented. | 1 | Appearance | Easy color matching of dental composites with the color of the natural tooth enamel | [96] |

## 1.3  Conclusion

The current work covers how the promising ALD method can be used in the functionalization of dental material surfaces including metal and ceramic implants, dentures, maxillofacial prostheses, and orthodontic materials. The majority of works were done on $TiO_2$ ALD; however, studies on the ALD of Ag, ZnO, $ZrO_2$, $Al_2O_3$, and $CaCO_3$ have also been reported. For removable dental materials, like dentures, challenges are easier: physical and mechanical tests have shown improvement in corrosion resistance, brushing resistance and antibacterial improvement upon $TiO_2$ and ZnO ALD functionalization.

For permanent dental implants, current and future challenges are more serious. In the complex oral environment, there is a tough competition between biological molecules like blood, osteoblast, bacteria, fibroblast, and biofluid reaching the surface of the foreign dental material. Studies at the laboratory level showed that with the bottom up layer by layer thin film ALD, dealing with these challenges becomes easier. At the laboratory level, deposition of $TiO_2$, ZnO, $ZrO_2$ and $CaCO_3$ showed enhancement in osteoblast growth, proliferation and antibacterial activity on specific bacteria lines that were tested. Aside from the osseointegration, longevity of the dental materials in the corrosive oral environment is another challenge. ALD is a suitable method to address corrosion problems in materials. Yet all these biological responses must be studied and addressed prior to human tests. The lack of human tests in this field is making this topic wide open for future projects.

# 2. RESULTS AND DISCUSSION

## 2.1 Surface and Subsurface film growth of titanium dioxide on polydimethylsiloxane by atomic layer deposition

(Chapter 2.1 was previously published as Hashemi Astaneh, S., Jursich, G., Sukotjo, Takoudis, C.G., (2019) Surface and subsurface film growth of titanium dioxide on polydimethylsiloxane by atomic layer deposition, Applied Surface Science, 493, 779-786.)

### 2.1.1 Introduction

Polydimethylsiloxane (PDMS) is nontoxic and widely used in medical applications [98]. PDMS is chemically and physiologically inert which makes it a good choice for long-term implants in the body such as cardiac pacemakers, mammary implants, maxillofacial, voice, and finger joint prostheses, drainage tubes, and catheters [99]. It has also been used in the fabrication of soft contact lenses [100] and has numerous applications in microfluidic devices [101]. Although its chemical inertness makes this polymer very attractive for biomedical applications, the lack of functional groups along its backbone imposes limitations on its applications [102].

$TiO_2$ is well known for its photocatalytic, antibacterial and antifungal properties [103-105]. Further, $TiO_2$ has hydrophilic properties that lead to protein adsorption and make it a well-established material for biomedical applications. Several processing methods such as chemical vapor deposition (CVD), spray pyrolysis, magnetron sputtering, radio frequency sputtering, and atomic layer deposition (ALD) have been implemented for the synthesis and deposition of metal oxides (e.g, $TiO_2$, $Al_2O_3$) on solid surfaces like silicon, glass, and fluorine doped tin oxide coated glass [106-108]. Among these vacuum deposition techniques, ALD results in outstanding features of deposited films in electronic applications [109]. ALD is a unique method for low temperature vapor phase thin film deposition. This deposition method is a cyclic process, where each cycle includes precursor pulse, precursor purge, oxidizer pulse, and oxidizer purge. Ideally, at the end of

each cycle, one atomic layer of desired thin film is deposited [17]. By varying the number of cycles, one can control the thickness of the thin film according to the final application. Another interesting feature of ALD is uniform thin film coverage on the substrate surface; therefore, deposition of the film would be conformal onto irregular surfaces. This feature makes ALD ideal for coating complex morphologies and microstructures of polymers [110]. Despite the limitation of precursor volatility and thermal stability, many metals and metal oxides have been deposited with conventional ALD where these materials exhibit outstanding features in their intended applications. In this study, the focus is the early stages of the deposition of $TiO_2$ on PDMS.

The biocompatibility of PDMS along with the bioactivity of $TiO_2$ makes their combination ideal for biomedical applications. Previous studies have investigated depositing thin films of metal oxide on PDMS. For example, Boudot et al. [99] deposited $TiO_2$ on PDMS surface via a vacuum arc plasma technique. They showed that 150 nm thick $TiO_2$ on top of PDMS resulted in stable surface properties of PDMS over time in water and under sterilization methods such as gamma irradiation (radiation dose 25 kGy) and ethylene oxide (45 °C, 5 h, 680 mg/L, aeration time 80 h). Furthermore, it did not impose any toxicity to the PDMS and was reported to improve cell adhesion to the surface by 260 – 380 % for 7 out of 10 samples which makes it a good candidate for biomedical applications. Pessoa *et al.* investigated [79] the effect of ALD grown films of $TiO_2$ on polyurethane (PU) and PDMS substrates as a means of improving anti-yeast properties. Thin films of $TiO_2$ were deposited on PDMS (growth rate: 0.10-0.11 nm/cycle) and demonstrated the effect of $TiO_2$ ALD films on the inactivation of Candida Albicans yeast. Their results show that $TiO_2$ on PDMS decreased the colony forming unit (CFU) by 59.5%. This study shows promising clinical applications for $TiO_2$ coated organic substrates; however, no discussion was presented on the formation and growth characteristics of $TiO_2$ on the PDMS.

After any surface modification, hydrophobic recovery of PDMS is one of the drawbacks that has been reported in several studies regardless of the method of surface modification [111-113], including ALD [114]. Spagnola *et al.* [114] coated both native PDMS and ultraviolet/$O_3$ treated PDMS with $Al_2O_3$ via ALD. For both substrate types, hydrophilicity of the surface increased significantly right after exposure to less than 100 cycles of ALD; however, after 48 hours, the water contact angle for both samples increased upon air exposure. This effect had been observed by other researchers and correlated with out-diffusion of organic species (e.g., oligomers, low molecular weight chains) [114, 115] and/or hydrocarbon adsorption from lab ambient atmosphere onto the surface [116]. To limit this drawback and make the hydrophilic property of the ALD treated surface more stable, Gong *et al.* used metalorganic infiltration process to suppress the apparent hydrophobic recovery [116]. That is, enough time was given to the metalorganic precursors to infiltrate/diffuse below the surface resulting in subsurface reaction and nucleation. The steps of metalorganic precursor infiltration were as follows: first exposure to metalorganic precursor (trimethylaluminum) for 5 hours followed by argon purge for 30 min and then exposure to water vapor for another 30 min. After the infiltration treatment, PDMS was exposed to typical ALD cycles where trimethylaluminum (TMA) precursor was pulsed/purged for 1 s/30 s and oxidizer (water) was pulsed/purged for 1 s/ 30 s at reactor temperatures of 60-120 °C and reactor pressure of 1 torr. Infiltration of precursor followed by ALD cycles is believed to create an organic/inorganic hybrid interface which may provide a pathway to address the hydrophobic recovery problem of PDMS [116]. Water contact angle of the coated PDMS showed that the hydrophilicity of the $Al_2O_3$ coated PDMS lasted considerably longer, up to 200 hours, demonstrating significant impediment to the hydrophobic–recovery of PDMS [116]. In 2015, Yu *et al.* [117] also deposited $AlO_x$ via ALD onto PDMS; In their work, PDMS was

exposed to sequential infiltration of precursor, which effectively extended the precursor pulsing time. Their results showed that by increasing the TMA pulse time, deep infiltration of the Al precursor took place due to good solubility of TMA in PDMS and it was concentrated within the top ~3 μm region.

ALD overall is a relatively slow vapor phase deposition method, except for some of its modified versions, like spatial ALD (S-ALD) [118]. Therefore, adding another time consuming step, like metalorganic vapor infiltration would make this overall method even slower. However, PDMS is an important polymer in many biomedical applications and modification of its surface with ALD is a challenging issue; there are still unanswered questions about the early (nucleation and growth) stages of metal oxide ALD on its surface as well as within the polymer matrix. More specifically, the apparent mechanism of nucleation and consequent ALD of $TIO_2$ in the absence of functional groups on PDMS has yet to be understood [119]. In this work, the objective is to study the early stages of $TiO_2$ nucleation and growth on PDMS substrates with different surface properties. Both X-ray photoelectron (XPS) and X-ray absorption near edge structure (XANES) spectroscopies are used to further investigate the formation of $TiO_2$ films on such polymeric substrates. XPS probes only the top (external) surface while XANES extends analysis deep within the (interior) subsurface of the material structure. This is the first study on the early stages of ALD film formation on thermoset elastomers like PDMS. These two techniques are then complemented with scanning electron microscopy coupled with energy dispersive X-ray spectroscopy (SEM/EDX) to provide a more complete characterization of ALD $TiO_2$ nucleation and growth on plasma and non-plasma treated PDMS.

## 2.1.2  Materials and Methods

Platinum-catalyzed, vinyl-terminated poly (dimethyl siloxane) elastomer (Factor II, Inc.,

A-2000) combined with functional intrinsic pigments (Factor II, Inc., FI-SK: Functional Intrinsic Skin Colors – Silicone Coloring System) were used as a maxillofacial prosthetic substrate material for deposition in this study. During preparation, the monomer was combined with a polymethyl hydrogen siloxane cross-linking agent at a 1:1 ratio by weight. The molds were placed in a convection oven and held at 98°C for 1 hour to achieve complete polymerization. The molds were removed and polymerized PDMS was allowed to cool to room temperature [81].

Tetrakis(dimethylamido)titanium(IV) (TDMAT™) was used as the titanium precursor. It was purchased from Sigma Aldrich and maintained at 70 °C in the bubbler during all depositions. Ultra-high purity $N_2$ was used as a carrier gas as well as purging gas. $O_3$ was used as an oxidizer for this ALD reaction and it was prepared using a UV-ozone generator placed immediately upstream of the deposition chamber to minimize ozone decomposition in the delivery line as described in our previous studies [120]. Small cut-outs of silicon (approx. 1.5 cm X 1.5 cm) were used as control samples for optical thickness measurements. The silicon substrates used had a 525±25 μm thickness and were purchased from WAFERPRO (item number: C04007). Prior to deposition these silicon cut-outs were rinsed with deionized water from a Barnstead™ Nanopure Infinity lab water system (catalog id: D8961) and then dried with $N_2$ (Praxair NI 4.8-T, purity: 99.998%).

PDMS samples were degassed prior to ALD at <180 mtorr for 6 hours at 190 °C so that any potential non-reacted monomers or other volatile impurities could be removed. Next, PDMS substrates were rinsed with deionized water (> 17.5 MΩ), dried with $N_2$, and cut into 2 cm X 1 cm pieces (the time elapsed in-between degassing and ALD was less than two days). The ALD of $TiO_2$ on PDMS was done in a commercial ALD reactor, ALD-150LE™ from Kurt J. Lesker Company®. Deposition pressure and temperature was 970 mtorr and 120 °C, respectively. The

thermal stability of the PDMS was studied with thermogravimetric analysis (TGA; TA Instruments, Model Q5000) under $N_2$ atmosphere using a 10 °C/min temperature ramp from room temperature to 700 °C [79].
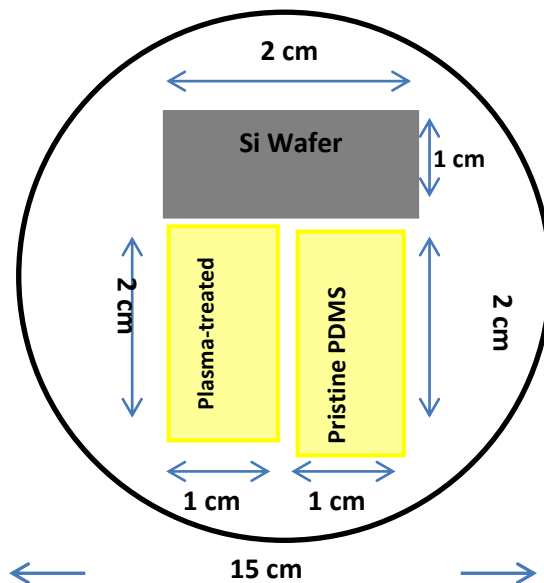


Figure 12: Schematic top view of the inside of the Kurt J. Lesker reactor and sample loading

For each deposition, two pieces of PDMS were loaded into the reactor, one pristine PDMS and one PDMS pretreated with $O_2$ plasma along with a Si wafer reference sample. Surface modification of each PDMS sample was done in a Plasma Etch machine (model: PE-50) for 2 min at 200 mtorr pure oxygen at room temperature. The water contact angle of plasma treated PDMS samples were measured using Ramè-hart C.A. goniometer (model No.: 100-00). Spectral Ellipsometry (J. A. Woollam Co., Model: M-44) was used to measure the thin film thickness on each corresponding Si wafer sample which was loaded as a control sample simultaneously with the pristine PDMS and plasma-treated PDMS. Figure 12 shows details of sample loading in each run of this study although further experiments have shown that interchanging the position of samples in the reactor did not have any effect on the results. $TiO_2$

deposition was carried out at 120 °C with 25-500 ALD cycles. Each cycle of the ALD reaction consisted of 1.7 s/25 s of precursor pulse/purge, respectively, and 1.5 s/20 s of oxidizer pulse/purge, respectively.

The growth and composition of the film on PDMS samples were analyzed with Kratos AXIS-165 XPS equipped with monochromatic Al Kα X-ray source. Samples were attached to the sample holder by means of double sided carbon tape. During XPS, pressure of the chamber was maintained at $10^{-8}$ torr. The Ti K-edge XANES of the deposited $TiO_2$ was performed at the BMD Sector 5 of the Advanced Photo Source facility in Argonne National Laboratory using X-ray fluorescence detection. In these measurements, the PDMS samples were placed at a small incidence angle of about 2-3 degrees with two Vortex ME4 Silicon Drift Detectors positioned orthogonal to X-ray beam direction near the sample and gas chamber ionization detectors centered along the X-ray beam to monitor relative beam intensity so that the fluorescence signal can be normalized to beam intensity throughout the spectral energy scan and provide guidance in aligning samples in the beam. Special precautions were taken to assure linearity of the intensity-normalized fluorescence to the Ti content. First, each sample was carefully aligned within the X-ray beam so that the entire beam irradiated the sample surface. In this configuration, the small angle of incidence allows the beam to spread out over most of the surface to achieve good representation of Ti over the entire sample whereas an additional gas ionization chamber placed after the sample provides a means to center the sample within the beam in its entirety. Second, the fluorescence detectors were placed close enough to the sample to allow good dynamic range of the detection electronics system at our APS Sector yet not too close so as to avoid photon counting dead time errors. And lastly, to assure no significant fluorescence self-absorption was occurring, the low energy onset of XANES fluorescence spectral profile was carefully compared

for all samples having varying $TiO_2$ depositions from 25 to 500 ALD cycles. In all cases, no differences in XANES fluorescence spectral profile were observed when spectra were normalized to an edge-step of 1 which assures no significant contribution of fluorescence self-absorption occurs in these measurements. Collectively, these precautions allow meaningful comparisons of the magnitude of edge-step XANES fluorescence from the different samples to roughly assess relative Ti content in the different samples.

A Hitachi S-3000N VPSEM with Thermo Noran XEDS was also used; prior to SEM/EDX, 6 nm of AuPd was sputter-coated on to the samples. The SEM coating unit E5100 from Polaron Instruments Inc. was used for this purpose.

### 2.1.3   Results and Discussion

TGA of this material under inert $N_2$ atmosphere showed two different degradation temperatures, 475 °C and 650 °C (Figure 13); both are much higher than the ALD temperature (120 °C), and therefore no significant thermal degradation is anticipated during deposition.
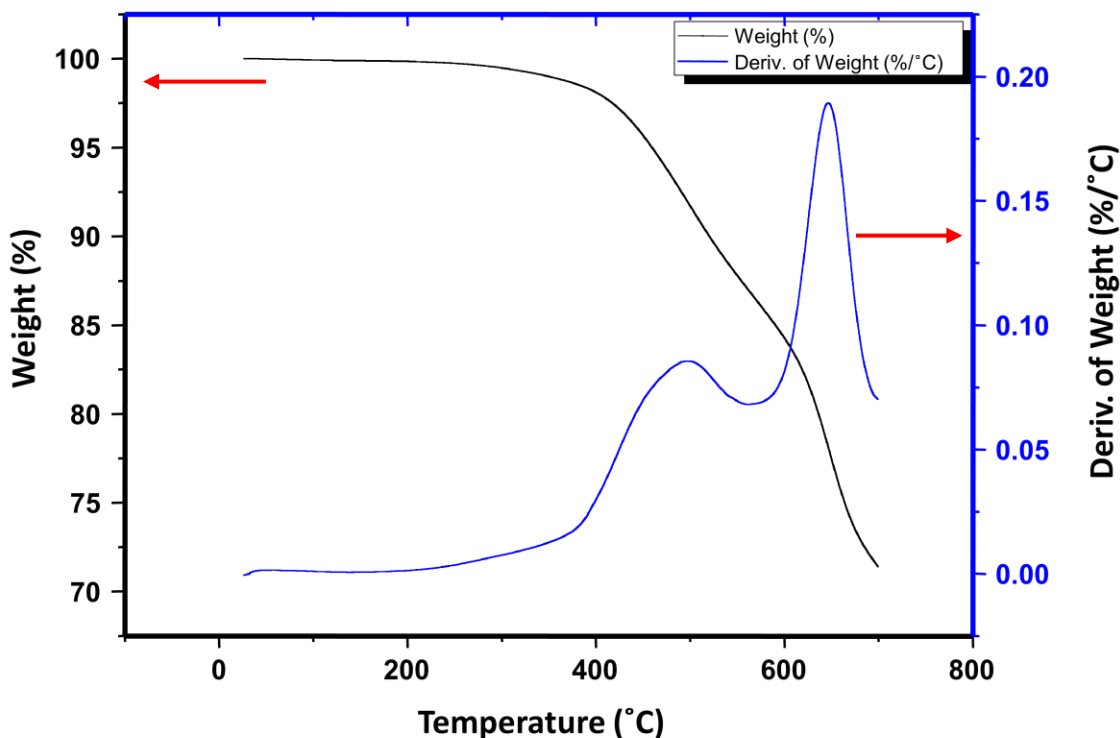
Figure 13: Thermogravimetry analysis of the PDMS (A2000, factor II, Inc) under $N_2$ atmosphere in TGA Q5000 V3.17 from TA Instruments; the rate of increasing temperature was 10 °C/min from room temperature to 700 °C.

The temperature dependence of $TiO_2$ ALD growth was probed on Si and can be seen in Figure 14 using pulse/purge times previously presented in the Method section in the range of 90 °C to 130 °C. It is noted that all runs at 120 °C were done with a new precursor batch/bubbler. These results show no significant temperature dependence on deposition rate within this range indicating a "temperature window" typically seen in ALD type reactions where any potential non-ALD deposition processes such as precursor condensation and thermal decomposition do not occur [19]. These findings are consistent with that of other ALD studies that used the same precursor/oxidizer system [121, 122].
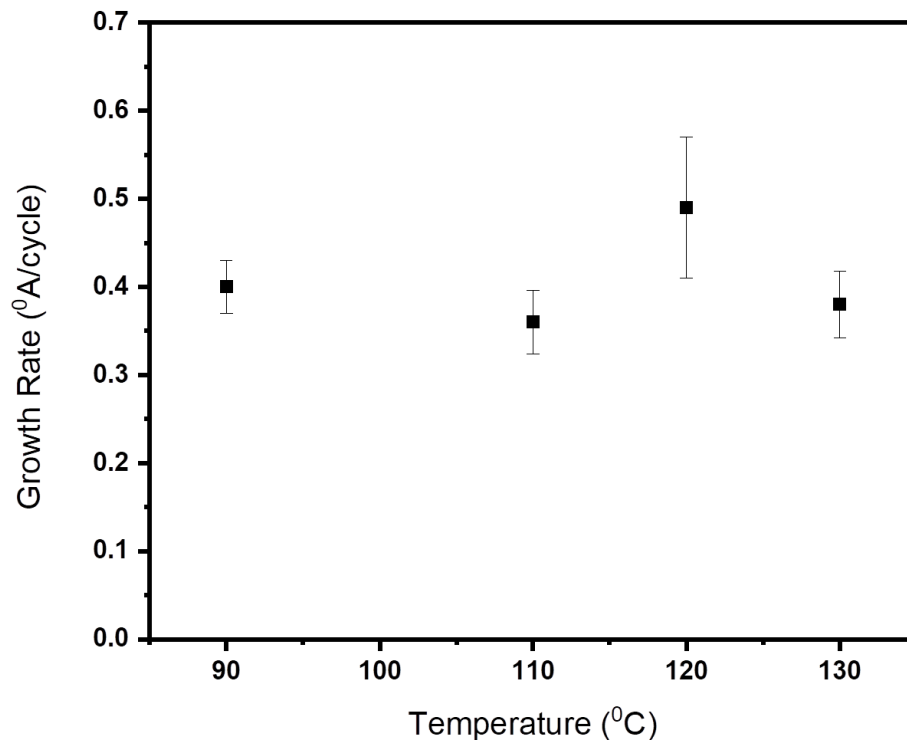
Figure 14: Temperature window of ALD of TDMAT/$O_3$ system on Si wafer alone under operating pressure of 970 mtorr, precursor pulse/purge time 1.7 s/25 s and oxidizer pulse/purge time 1.5 s/20 s, respectively. Error bars represent multiple thickness measurements of samples from different experiments.

Figure 15 depicts the likely surface functionalization for PDMS after oxygen plasma treatment [123] and Figure 16 shows the water contact angle of PDMS before and after the plasma treatment used. Clearly, after 2 minutes of $O_2$ plasma exposure (5 cm$^3$/min, maximum power 400 W), the hydrophilicity of the PDMS surface increased significantly resulting in decreased water contact angle from 99° to 44°. This is likely the result of the formation of silanol group (Si-OH) on the plasma-treated PDMS surface. A similar change in surface properties with plasma treatment was reported in other studies [115, 123]. For instance, XPS data of Roth *et al.* [123] suggested that after $O_2$ plasma treatment, the elemental surface composition of treated

PDMS changed; the relative carbon content decreased while oxygen content increased in the surface region, in agreement with the schematic mechanism depicted in Figure 15.
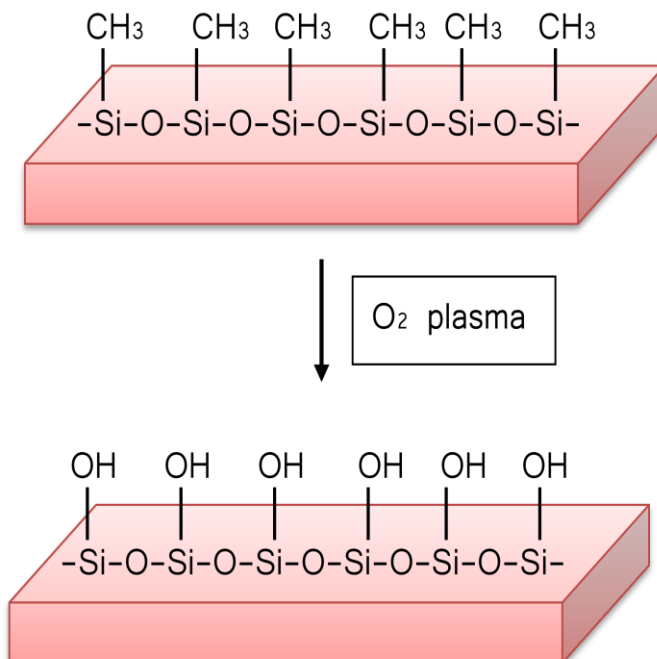


Figure 15: Schematics of the surface treatment mechanism for typical PDMS after 2 minutes of $O_2$ plasma exposure, with the $O_2$ flow of 5 cm$^3$/min at room temperature. This is representative of a single chain of PDMS polymer.
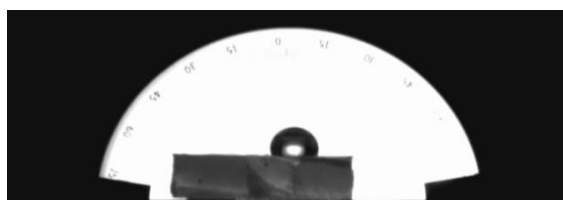


**Pristine PDMS**
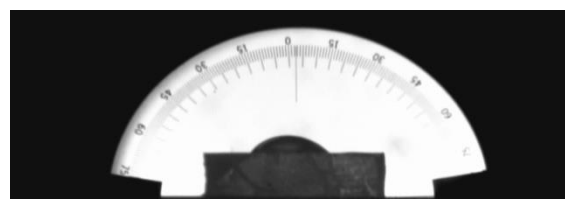
**$O_2$ Plasma treated PDMS**

Figure 16: Water contact angle: a) surface of pristine PDMS, b) 2 minutes oxygen plasma of PDMS under 200 mtorr, at room temperature right after plasma treatment.

Since the PDMS substrate surface was non-specular, the PDMS/TiO$_2$ interface may not be suitable (due to roughness on PDMS) for ellipsometry analysis of the TiO$_2$ thickness. Therefore, a Si control sample was placed on the substrate holder of the reactor along with PDMS samples. The Si wafer sample served as an in-situ reference of the ALD rate. One set of depositions was done with a silicon sample wafer alone in the reactor while the other sets were performed with both PDMS and silicon wafer samples placed in the same reactor as shown as in Figure 1. Figure 17 shows the TiO$_2$ thickness on silicon from the two sets of measurements after different number of ALD cycles is used. In our work, the growth rate on the stand-alone Si wafer is ~ 0.48 Å/cycle which is in good agreement with previously reported values in the literature (0.44-0.65 Å/cycle [82, 121, 122].  Interestingly, the presence of the PDMS substrate with the Si wafer sample appeared to lower the growth of TiO$_2$ thin film on Si wafer by about 25 %. Previous ALD studies of TiO$_2$ on Si have reported that the thin film growth rate on Si could be influenced by other polymers substrates present in the reactor as well. In such cases, some polymers showed a decreased ALD rate, while other polymers resulted in increased ALD rate on Si [70, 124-126], depending on the nature of the polymer, and precursors/oxidizers used. Such polymer influence has been attributed to migration of non-reacted monomers and impurities in the bulk of the polymeric substrate on to the Si wafer. However, in our experiments, all samples were degassed prior to exposure to ALD and so this kind of migration is not likely. Therefore, answering this question requires more detailed investigation on the chemistry and engineering of the material systems involved.

TiO$_2$ films deposited on PDMS are next examined with XPS, which has a probe depth of a few nm, and deep below the surface with XANES which extends a few tens of microns below

the surface of the PDMS.
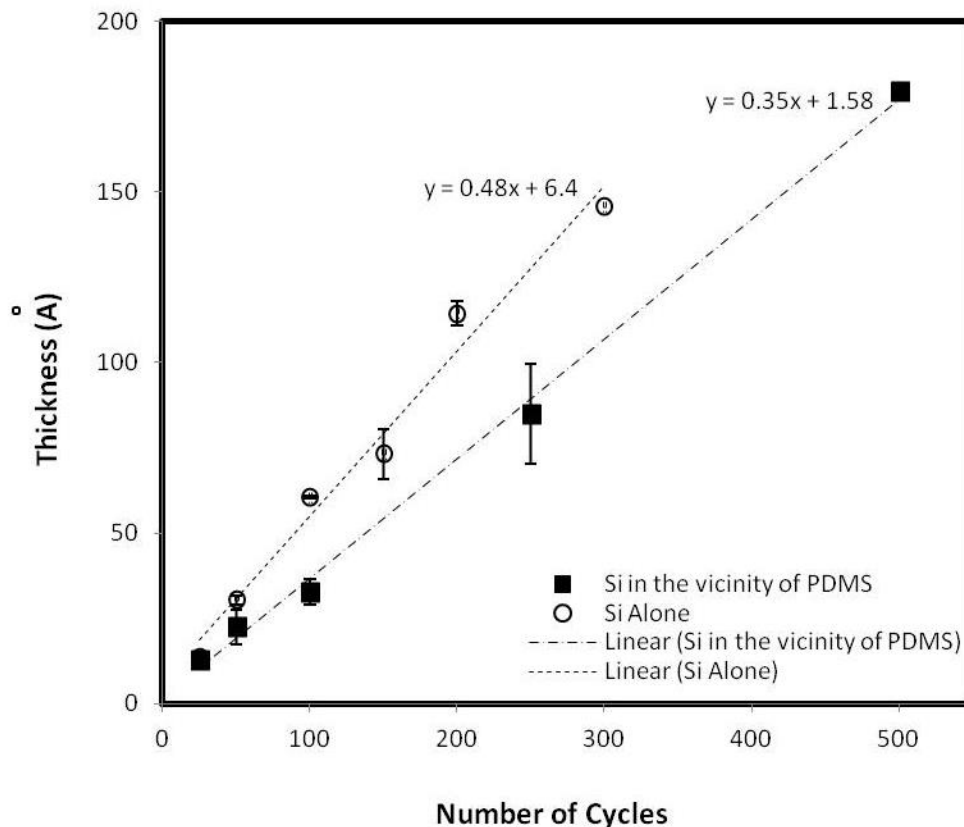


Figure 17: Thickness of $TiO_2$ thin film on Si wafer as a function of number of cycles. ○: typical thickness versus number of cycles for $TiO_2$ on Si wafer without PDMS sample present in reactor; ■: growth of $TiO_2$ on Si wafer with PDMS present in reactor (Figure 1). All depositions were done at 120 °C, 970 mtorr. Precursor pulse/purge time was 1.7 s/25 s and oxidizer pulse/purge time was 1.5 s/20 s. Dashed lines are fitted linear trend line for the growth rates of $TiO_2$ on Si wafer with and without PDMS present in the reactor. Thickness measurements represent averages from at least 3 different samples. Error bars represent multiple thickness measurements of samples from different experiments.

### 2.1.3.1 X-ray Photoelectron Spectroscopy

XPS on the surface of the pristine PDMS sample was done prior to deposition. As can be seen in Figure 18, XPS of the pre-deposition PDMS sample shows Si 2s and 2p (from the backbone of the polymer chain) at 153 and 100 eV, respectively, C 1s (methyl side groups on the polymer chain and ubiquitous C impurities) peak at 284.8 eV, and O 1s (from backbone of

polymer) at 529.2 eV. These XPS peaks for PDMS surfaces are consistent with what other groups have reported [127]. In these spectra, it is noted that no Ti impurity was found in the pristine PDMS which shows that there is no Ti containing contaminants in the PDMS itself that could affect XPS or XANES analyses of ALD films, within the detectability of the instruments used.

In order to evaluate the nucleation and growth of $TiO_2$ on PDMS surfaces with different surface properties, we did XPS after 25 and 50 deposition cycles of $TiO_2$ on both plasma-treated and pristine PDMS (Figure 18). Based on these spectra, there appears to be no evidence of nitrogen (binding energy 402-397 eV) from likely unreacted TDMAT precursor on either pristine or $O_2$ plasma-treated PDMS and therefore reaction between TDMAT precursor and oxidizer ($O_3$) appears to have gone to completion. These XPS spectra also show that after 25 ALD cycles, $TiO_2$ appears mostly on the $O_2$ plasma treated PDMS and not on the surface of pristine PDMS. Thus, the plasma-treated surface was chemically favorable for ALD, presumably due to the silanol groups formed during the plasma treatment, as depicted schematically in Figure 15, whereas the surface of pristine PDMS, lacking silanol groups, does not appear conducive to the ALD reaction. Jur *et al.* [128] reported that for ALD of $Al_2O_3$ on polypropylene there was subsurface formation of $Al_2O_3$ prior to surface deposition. In our study, as the number of ALD cycles of $TiO_2$ increased and reached 50 cycles, the Ti 2p peak, started to show up in the XPS spectra of the surface of pristine PDMS as well. One plausible explanation for this can be the saturation of the PDMS subsurface; further precursor/oxidizer reaction facilitates further film growth of $TiO_2$ from subsurface to surface and thus $TiO_2$ on the PDMS surface starts becoming detectable by XPS on the surface of pristine PDMS as well.
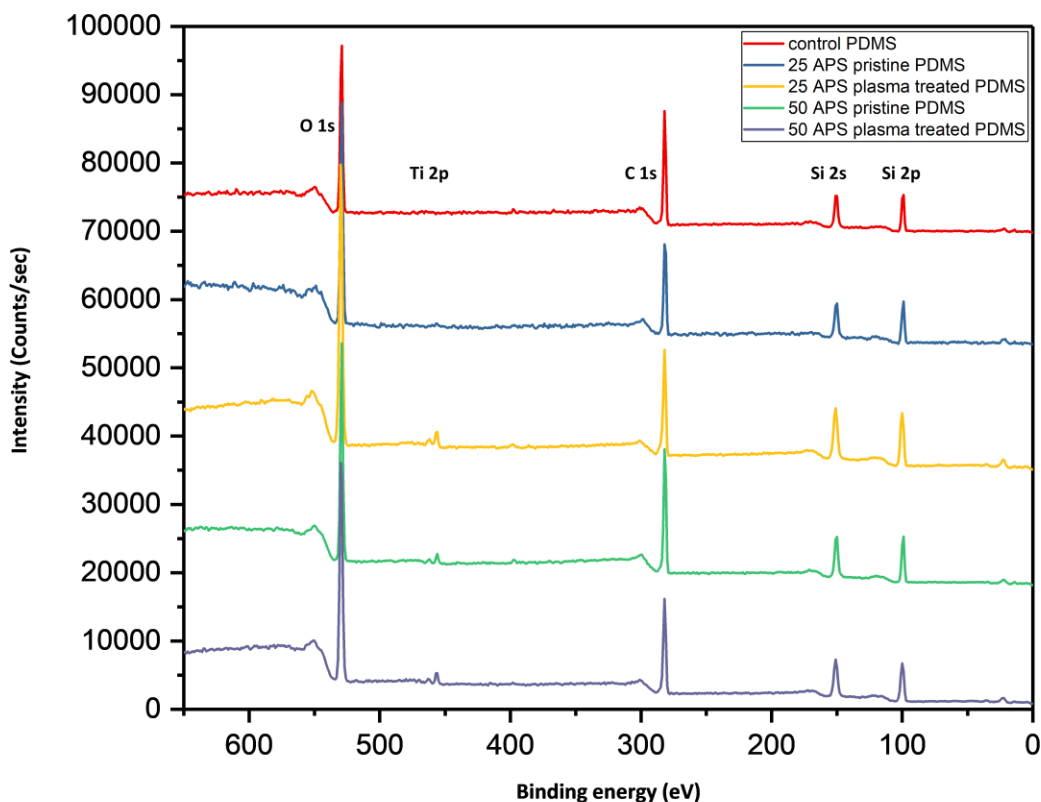
Figure 18: XPS spectra on $O_2$ plasma-treated/ non treated PDMS substrate after a) 25 cycle plasma treated PDMS, b) 25 cycle non-plasma treated PDMS, c) 50 cycle plasma treated PDMS, d) 50 cycle non-plasma treated PDMS at room temperature. ALD processing conditions: operating pressure of 970 mtorr, precursor pulse/purge time 1.7 s/25 s and oxidizer pulse/purge time 1.5 s/20 s, respectively.

XPS is indeed important and informative in the ALD of our material systems; however, XPS probes the surface of the PDMS down to 7-10 nm depth and thus subsurface formation of $TiO_2$ would not be detected by XPS. Therefore, these XPS data are complemented with additional X-ray based techniques, e.g., XANES and EDX analyses, for an improved assessment and understanding of the $TiO_2$ deposition on PDMS substrate surfaces.

**2.1.3.2 <u>X-ray Absorption Near Edge Structure:</u>**

To probe the formation of $TiO_2$ thin films on both surface and subsurface of the PDMS substrates, XANES was performed scanning 4800 to 5350 eV across the Ti K-edge (4966 eV) and monitoring the relative intensity of X-ray fluorescence normalized to the incident X-ray beam flux. The edge step seen at the Ti K-edge is taken to be proportional to the amount of Ti present on the surface and subsurface of PDMS since the X-rays penetrate relatively deep within the PDMS (~40 μm absorption length at Ti K-edge based on X-ray absorption formula calculation from the Hephaestus software of Demeter [129, 130]). We have examined the magnitude of the Ti K edge-step as a function of ALD cycle number on both pristine and plasma-treated PDMS substrates. It can be seen in Figure 19 that as the number of cycles increases, the Ti K edge step increases, which can be attributed to the increase in $TiO_2$ film thickness. The Ti K-edge XANES fingerprint at 4.98 - 5.02 keV range is similar to that reported elsewhere for titanium oxides [131, 132] thus confirming an oxide form of Ti as opposed to Ti from residual unreacted precursor. Surprisingly and contrary to our previous XPS results, at lower number of cycles (e.g., 25 and 50), the edge-steps of the plasma treated samples were actually smaller than the non-plasma treated PDMS indicating more $TiO_2$ present in the non-plasma treated samples for a given number of ALD cycles. Figure 20 shows detailed relation between step edge intensity versus number of ALD cycles.

However, the trend of increasing Ti in the two differently pretreated PDMS samples is not the same. For $O_2$ plasma-treated samples, the K edge step increased almost linearly with the number of cycles, while for the pristine PDMS this increase was not linear. The pristine PDMS had an unusually large Ti K edge step for the lower number of cycles (e.g., 25 and 50 cycles) and then the slope decreased and became similar to that of $O_2$ plasma-treated PDMS for larger

number of cycles. That is, the infiltration gets capped off at some point and new molecules can't make it inside. At that point, titanium dioxide begins to start depositing on the surface [133, 134].

This XANES analytical approach of $TiO_2$ ALD reactions is similar to that done previously by Settapun *et al.* for a totally different system [133]. In that case, they did in-situ X-ray measurements on the Pt $L_3$ edge in an ALD Pt metal deposition reactor and showed that the height of the edge step increased after each cycle due to the greater number of Pt atoms deposited after each cycle [133]. In our work, the increase in Ti K-edge step was seen for both pristine and $O_2$ plasma-treated PDMS (Figure 19).

A plausible explanation of the $TiO_2$/PDMS XANES results is as follows. For the plasma treated PDMS, the exposure of the PDMS to the $O_2$ plasma would functionalize the surface and replace $-CH_3$ groups with $-OH$ groups which can act as surface reaction sites for the upcoming ALD reaction. Therefore, in the case of plasma-treated PDMS, after pulsing/purging of TDMAT (precursor) and pulsing/purging of $O_3$ (oxidizer), nucleation would mostly take place on the exterior functionalized surface and consequently the first layer of $TiO_2$ formed, while diffusion of precursor species into the PDMS subsurface is significantly lowered [135]. With increasing number of cycles, this $TiO_2$ thin film grows thicker on the PDMS external surface. However, in the case of pristine PDMS, the scenario appears to be different because of the higher diffusion of precursor into subsurface of the PDMS and the lack of reactive sites on the surface of PDMS. In this case, after pulsing the first round of precursor and oxidizer, precursor molecules are able to go pass the nonreactive external surface and diffuse/infiltrate into the bulk of polymer. Diffusion into the bulk PDMS coupled with ALD-like reaction within the PDMS matrix would result in $TiO_2$ deposition within the subsurface of PDMS [124, 128]. Thus, for polymers with high density of functional groups on the surface (e.g., plasma-treated PDMS in this study), the deposition

50

tendency is more toward typical ALD-like reaction on the external surface. However, for polymers with no functional groups (e.g., pristine PDMS in this work), the tendency is toward diffusion/infiltration of the precursor/oxidizer into interstitial spaces of the polymer material where precursor-oxidizer reaction takes place [128, 136, 137]. In this scenario, it would be interesting to probe how deep the $TiO_2$ precursor/oxidizer can penetrate into the bulk PDMS. In the case of $Al_2O_3$ ALD on PDMS, Yu *et al.* [117] reported ~3 μm infiltration depth of the TMA precursor into the PDMS polymer.
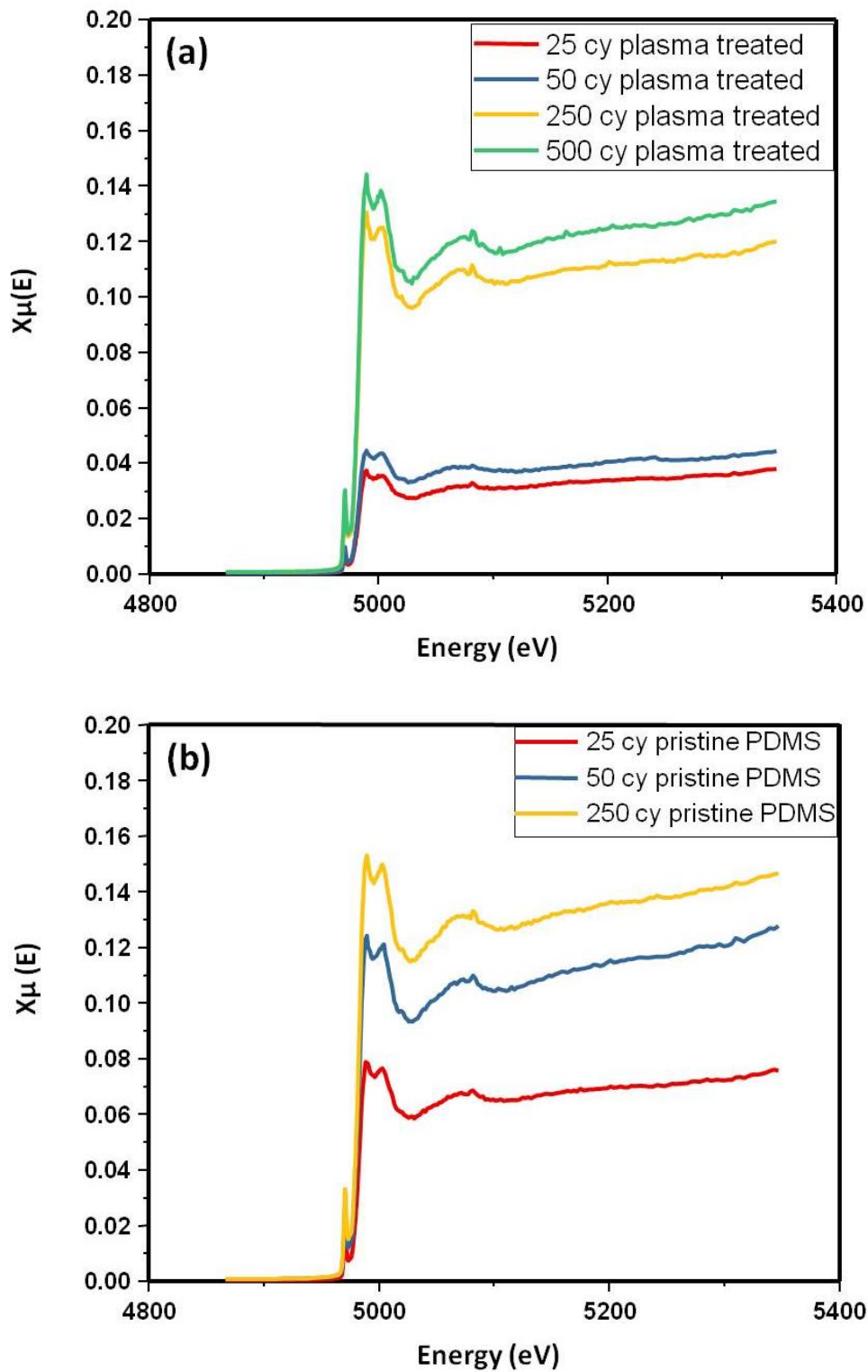
Figure 19: XANES on TiO$_2$ ALD coated a) plasma treated PDMS, b) pristine PDMS after 25, 50, 250, and 500 ALD cycles at room temperature. ALD parameters were as follows, precursor pulse/purge time 1.7 s/25 s, oxidizer pulse/purge time 1.5 s/20 s under 970 mtorr and 120 °C.
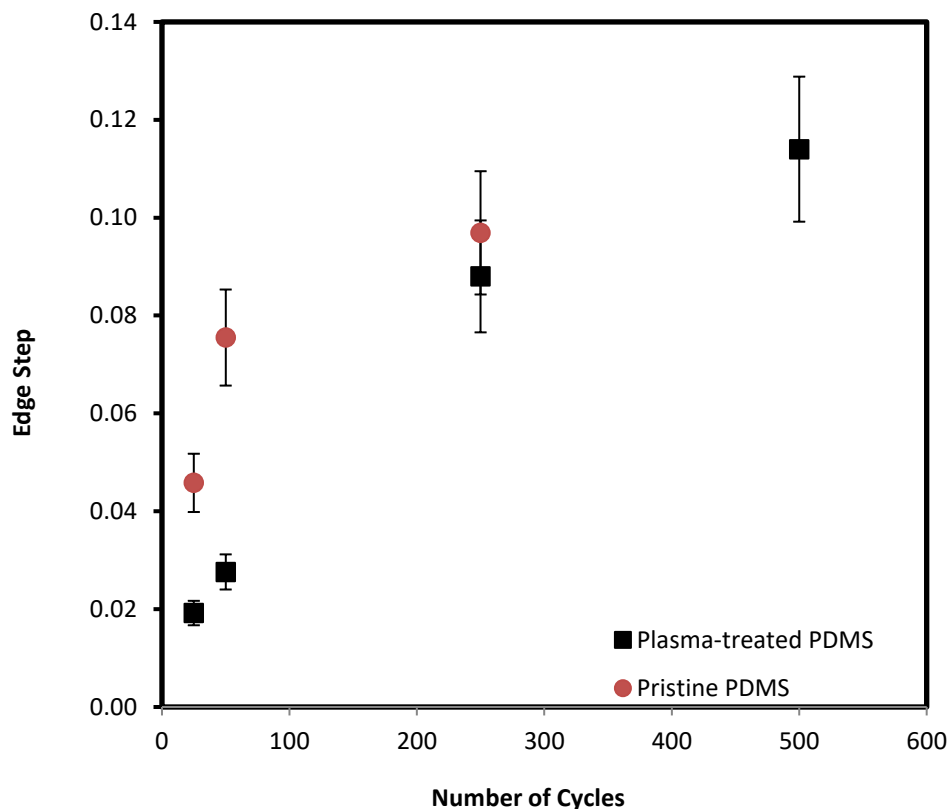
Figure 20: K-edge step XANES of $TiO_2$ thin films deposited on PDMS surface versus number of cycles. ALD parameters were as follows: precursor pulse/purge time 1.7 s/25 s, oxidizer pulse/purge time 1.5 s/20 s, 970 mtorr and 120 °C. Error bars represent estimated uncertainty of the measurement.

### 2.1.3.3 <u>Scanning electron microscopy coupled with energy dispersive X-ray spectroscopy (SEM/EDX)</u>

SEM/EDX was also used to examine the growth and uniformity of $TiO_2$ on both pristine and plasma-treated PDMS substrates at the early stages of $TiO_2$ ALD on PDMS. In these measurements, the probe depth extends to a few microns below the surface of the PDMS which is well beyond that of XPS yet less than that of XANES. Thus EDX analysis probes mainly a short distance below the surface. Each sample was scanned 2 to 3 times on different locations on the deposited PDMS. EDX results show greater amount of Ti on pristine PDMS than that for $O_2$ plasma-treated PDMS. This is consistent with the independent measurements of XANES, Table

1 shows 0.5 – 0.7 % Ti for $TiO_2$ on non-treated PDMS substrates, while the Ti content on

plasma-treated PDMS was less than 0.3 %, the estimated detection limit of the instrument used

for our material systems. Further comparison of SEM/EDX of pristine PDMS with 15 kV and 30

kV showed that Ti was mostly close to its external surface. For the plasma-treated PDMS, the Ti

content was below the estimated detection limit of the instrument.

**Table V: SEM/EDX (15 kV) of 25 cycles of $TiO_2$ on pristine PDMS, 25 cycles of $TiO_2$ on $O_2$ plasma treated PDMS, 50 cycle of $TiO_2$ on pristine PDMS, and 50 cycles of $TiO_2$ on $O_2$ plasma treated PDMS**

| Quantification (atom %) Sample | Si | Ti |
|---|---|---|
| 25 cycle non treated | 40.3±0.3 | 0.51±0.2 |
| 25 cycle Plasma treated | 39.3±0.3 | < 0.3 |
| 50 cycle non treated | 41.2±0.3 | 0.67±0.2 |
| 50 cycle Plasma treated | 42.0±0.3 | < 0.3 |

Comparison of the results of XANES and EDX techniques shows that the measurement

with these two different techniques are in reasonable agreement and for 50 cycle deposition,

there is about 2.5 times more Ti on non-treated PDMS than on plasma-treated PDMS.

Next, we consider the pathways precursor/oxidizer molecules have when they reach the

substrate. Depending on the conditions, they can either react with surface functional groups on

the external surface (for substrates that have external surface functional groups) or

infiltrate/diffuse into the subsurface (for substrates without functional groups on their external

surface). In this study, surface deposition is promptly initiated on plasma-treated PDMS as seen

by XPS measurements, since there are functional groups on the external PDMS surface that also

minimize/prevent subsurface growth of $TiO_2$. According to Markov *et al.* [135], plasma treatment of PDMS can create a layer on the surface that significantly impedes diffusion of oxygen molecules through PDMS. In agreement with these findings, our study suggests that formation of functional groups on the plasma-treated PDMS suppresses subsurface functionalization and impedes infiltration of precursor/oxidizer into the subsurface.

For pristine PDMS, the scenario seems to be different; high amounts of Ti on pristine PDMS can be attributed to the high subsurface area of pristine PDMS compared to the external surface area of PDMS. Subsurface of a typical polymer consists of both microstructural and macrostructural empty spaces. Microstructural empty spaces can be attributed to interstitial and free volumes between polymer chains, while macrostructural voids can be associated with defects and holes in the bulk polymer material. The presence of these free spaces facilitates the diffusion of the precursor/oxidizer into the bulk of the substrate. Further, the non-planar 3D subsurface can host larger amount of deposited oxide as previously reported for other non-planar substrate morphologies like multi-walled carbon nanotubes and collagen fiber [82, 138, 139]. Schematic of the suggested mechanism proposed in this work can be seen in Figure 21 which serves as a plausible explanation of our XANES, XPS and EDX results.

**a) O₂ plasma-treated PDMS**

**b) Pristine PDMS**

Functionalized surface

Number of cycles is increasing

Number of cycles is increasing

Subsurface area

Deposition on functionalized surface

Deposition at crosslinked subsurface, and then continued on surface

Different color used only to differentiate between different layers.
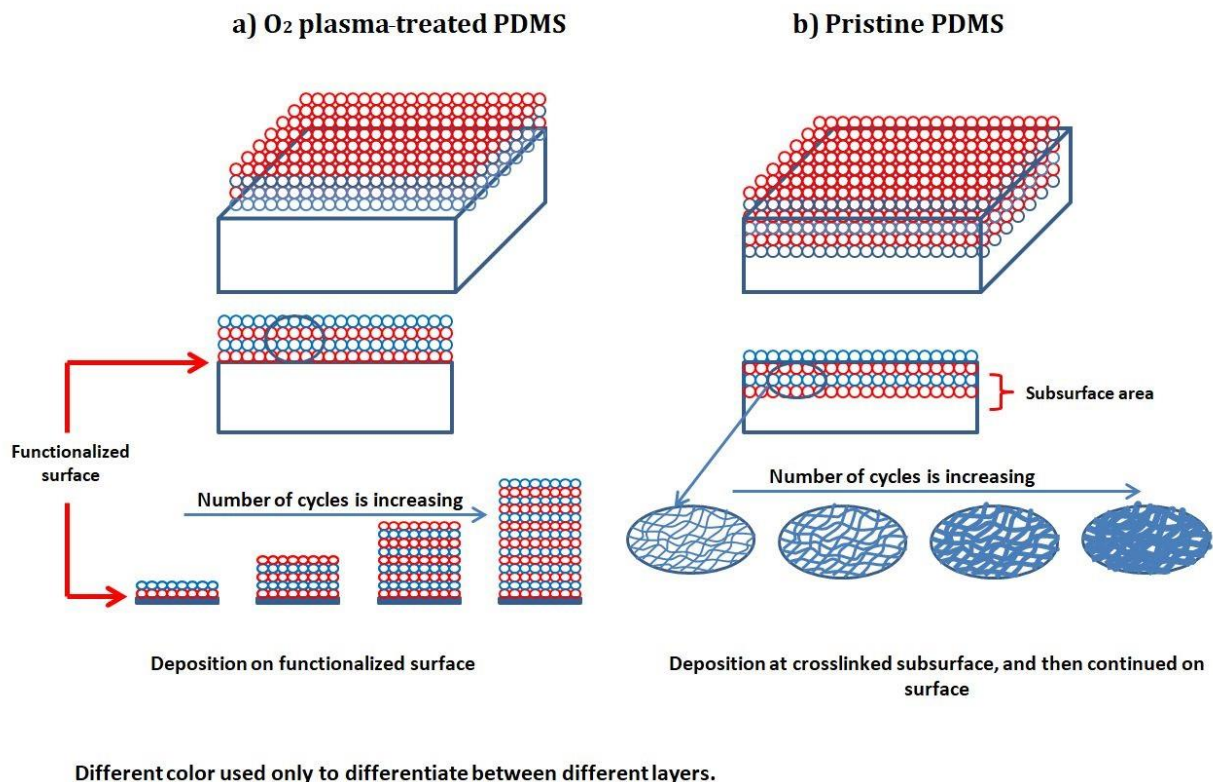
Figure 21: Schematic diagram of the $TiO_2$ formation on a) $O_2$ plasma-treated PDMS, b) pristine PDMS. Different color is used only to differentiate between different layers, and each circle represents 1 unit of $TiO_2$.

In order to examine the dispersion of Ti atoms in pristine PDMS bulk, we did cross-sectional SEM (in line scanning mode) on both plasma treated and pristine PDMS samples which were coated for 25 and 50 cycles. Samples were dipped for 2 minutes in liquid nitrogen and then quickly broken to create a fresh cross section. The resulting cross section was examined with both SEM and EDX. The SEM images up to X40k magnification showed a homogenous material without significant physical defects, voids or cracks. The EDX was performed with ~ 5 μm spot size as a vertical line scan perpendicular to the surface. Silicon and oxygen from the backbone of PDMS chain as well as carbon from methyl side groups of PDMS were constituents of the resulting EDX spectra. No Ti was detected; based on the growth rate of $TiO_2$ (Figure 17), the amount of Ti was estimated to be below the detection limit for the sample preparation and cross-

sectional SEM/EDX used, i.e., ~ 0.3 % [140].

The deposition of $TiO_2$ onto the subsurface PDMS in this process is important because it serves as a foundation for the surface $TiO_2$, likely strengthening the interface of the metal oxide thin film and polymer surface. That is, continuity of $TiO_2$ that diffused and deposited on the subsurface of the substrate and $TiO_2$ deposited on the surface could yield stronger interfacial adhesion of inorganic $TiO_2$ thin films with organic PDMS substrates. The result of having this subsurface deposition, suggests a stronger inorganic/organic interface which is of particular interest in triboelectric nanogenerators [117]; also, combining it with the biocompatibility of some polymers may also be a promising method for tailoring new in-vivo long-term implants such as cardiac pacemakers, maxillofacial and other prostheses.

### 2.1.4   Conclusion

Nucleation and growth of $TiO_2$ thin films deposited on PDMS via ALD were investigated for PDMS substrates with different surface properties. $O_2$ plasma-treated PDMS was used as a hydrophilic surface and pristine PDMS was used as a hydrophobic one. The precursor/oxidizer used were TDMAT and ozone. XANES was used to probe the diffusion of precursor/oxidizer onto the subsurface of the polymeric substrate. XANES data of ALD $TiO_2$ on pristine PDMS showed significantly more Ti than that on plasma-treated PDMS. It also showed that formation of $TiO_2$ on plasma-treated PDMS increased almost linearly with the number of cycles used, which is similar to ALD-like reactions on the surface. For $TiO_2$ ALD on PDMS with hydrophobic surface properties, precursor and oxidizer first diffuse into PDMS prior to having any $TiO_2$ growth on the external substrate surface.

SEM/EDX yielded consistent findings to that of XANES, and indicated more Ti on pristine PDMS than on plasma-treated PDMS. This showed that nonplanar, morphology of the

subsurface of pristine PDMS hosts at least 2.5 times more $TiO_2$ than on the external surface of plasma-treated PDMS. At the early stages of ALD (i.e., after 25 cycle), XPS showed Ti on hydrophilic PDMS but no trace of Ti on hydrophobic PDMS. This 25 cycle delay on $TiO_2$ formation at the surface of pristine PDMS corroborated the infiltration/diffusion mechanism for hydrophobic PDMS ALD substrates. Thus, Ti probed by EDX and XANES in this case is located more than 7-10 nm below the external surface or subsurface area of the PDMS. Therefore, for PDMS with non-functional surface groups, the precursor selectively diffuses into the PDMS where $TiO_2$ deposition takes place, while for polymers with high density of reactive groups on the surface, thin film deposition on the external functionalized surface dominates.

## 2.2 A simple masking method for selective atomic layer deposition of thin films

(Chapter 2.2 was previously published as Hashemi Astaneh, S., Sukotjo, C., Takoudis, C.G., Feinerman, A., Simple masking method for selective atomic layer deposition of thin films, (2020) Journal of Vacuum Science & Technology B, 38, 025001.)

### 2.2.1 Introduction

Atomic layer deposition (ALD) is a vapor phase, layer by layer film deposition technique which is based on self-limiting vapor phase reactions and results in conformal thin films. In ALD, conformality means surface coverage is in the form that can mimic the structure and texture of the substrate. Thickness of such thin films is precisely tunable at Ångström level. In a typical ALD process, two vapor-phase reagents are sequentially exposed to a substrate under high vacuum, separated by inert gas (e.g., $N_2$, Ar) purge steps [141].

Since the vapor phase precursors can reach all exposed areas during each pulse, the growth of ALD thin films is similar to putting a blanket of the intended thin film on the exposed substrate. However, for some applications (like microelectronic and bio-implanted devices)

portions of the substrate need to be uncoated. Selective ALD (SALD) requires coating some portions of the substrate and not other portions.

SALD has attracted a great deal of attention in the last decade. Different approaches developed for depositing patterned thin films via ALD. Most of the approaches are different combinations of lithography and etching. Lithography requires that a resist layer is coated first on the substrate. Then lithography involves patterning this resist layer with different techniques like photons, electrons or imprint (soft) lithography [142]. Choosing between these techniques depends on the chemistry of the resist layer. For some resists, it is recommended to perform physical lithography [143] while for others it is recommended to take advantage of chemical lithographic methods like e-beam and photolithography [144]. Etching requires removing the film chemically or by sputtering, followed by removing the mask layer [145].

Etching and lithography can pattern at the micro and nano scale. However, they are not compatible with ALD on polymeric substrates [78] and are time consuming. We would prefer to utilize a liftoff method that will always work for micro/nano scale patterning. Therefore, some efforts have been undertaken to find and evaluate masking methods other than lithography/etching. Langston *et al.* [146] presented a mechanical masking for ALD thin films which is based on applying pressure to adjust and minimize the clearance between the mask and the substrate. Polished silicon (100), teflon and copper were used as masks and each one was individually connected to a spring assembly; this assembly has control over the pressure on the mask and allowed the pressure to be adjustable. Among these three materials, Si wafer was preferred since its flatness could provide the smallest clearance needed between the mask and substrate [147]. Si mask showed ~ 200 nm diffusion under the mask. The copper mask had 1 mm diffusion under the edge and the Teflon mask led to carbon contamination [146].

In another study Sweet *et al.* evaluated the functionality of a physical mask under compression for patterning on nonwoven fiber mats [148]. They deposited thin films of ZnO via ALD on polypropylene and polyamide. The mask was a patterned aluminum plate which was placed and screwed on top of the fibrous substrate, and then a compression force was applied to the fibers beneath the substrate. They examined the effect of different compression forces on mask ability for fully compressed mask (where the plate spacing was $0.13 \pm 0.02$ mm) and partially compressed mask (where the plate spacing was $0.26 \pm 0.02$ mm). Results showed that the mask partially limited the access of the precursor to the covered area. The color change and EDS analysis within 200 µm of the mask edge indicated that there was some ZnO deposition. In Sweet *et al.* 's work the targeted substrate was nonwoven polymeric fibers; the complexity of the fibers morphology and the differences in the chemical composition (specially functional groups of the surface) of the fibers, made the integrity and resolution of the pattern fully dependent on the characteristic structure and arrangement of the fibers [148].

In the current work, fine iron (Fe) powder and a magnet were used and studied as a masking pair for SALD of silver on Si wafer. To our knowledge, this is the first time this pair is used as a mask in ALD/SALD. Applying this mask, in comparison to other masking methods, was simpler, had no chemical contamination, and it was inexpensive. Fe powder and magnet both have good temperature stability which makes this masking method favorable for depositions performed at temperatures significantly below their Curie temperature (Fe powder has $T_c$ ~770 °C [149] and a NdFeB magnet has $T_c$ ~285 °C [150]). It also can be removed easily without leaving any residue of the masking material behind on the substrate.

### 2.2.2    Experimental

Triethylphosphine(6,6,7,7,8,8,8-heptafluoro-2,2-dimethyl-3,5-octanedionate)        silver(I)

Ag(fod)(Pet$_3$) from Strem Chemicals was used as the silver precursor and its bubbler was maintained at 96 °C during all depositions. Borane dimethylamine complex from Sigma Aldrich was used as a co-reactant/reducer of this ALD reaction and its bubbler was kept at 52 °C. This reducing co-reagent was first introduced by Kalutarage *et al.* [151] for the thermal ALD of copper thin films and then it was used by Makela *et al.* for deposition of silver via thermal ALD [152]. Ultra-high purity N$_2$ (99.999% UHP) was used as carrier gas as well as purging gas for both silver precursor and borane dimethylamine complex co-reactant/reducer. Prior to deposition on Si wafer, the substrates were rinsed with deionized water (> 17.5 MΩ cm), dried with N$_2$, and cut into 2 cm X 1 cm pieces.

NdFeB magnets with approximately 1 Tesla remanence was first placed beneath the Si wafer and then fine Fe powder (American Science and Surplus, Item Number: 91258P1) was carefully put on the part of the Si substrate to mask it from the ALD deposition. It was necessary to carefully pack the Fe powder onto the Si substrate with a thickness of 2-4 mm. If the reactor is magnetic then care must be taken to keep the magnet under the substrate away from the walls of the reactor. It is also helpful to use a non-magnetic sample holder.

After loading the sample, thermal ALD of silver was done in the flow type custom-built ALD system; the details of this system are described elsewhere [120, 153]. This reactor has two precursor delivery lines and a separate line for oxidizer delivery. This design makes this system ideal for depositions with either precursor/oxidizer or precursor/co-reactant. In this work, one of the bubblers was filled with silver precursor and the other one filled with borane dimethylamine complex. Precursor and reducing co-reagent were sequentially introduced into the reactor using a custom-written Labview computer program controlling the open/close of pneumatic Swagelok valves. Both precursor and reducing co-reagent's pulse/purge durations were optimally fixed at 3

s/5 s and 2 s/10 s, respectively. Delivery lines in between bubblers and reactor were set at 120 ⁰C and depositions were done at 120 ⁰C. Base pressure and operating pressure of the system were less than 10 mtorr and 500 mtorr, respectively.

As depicted in Figure 22, for each deposition, a clean Si wafer was first masked with Fe powder/magnet and then loaded into the ALD reactor.
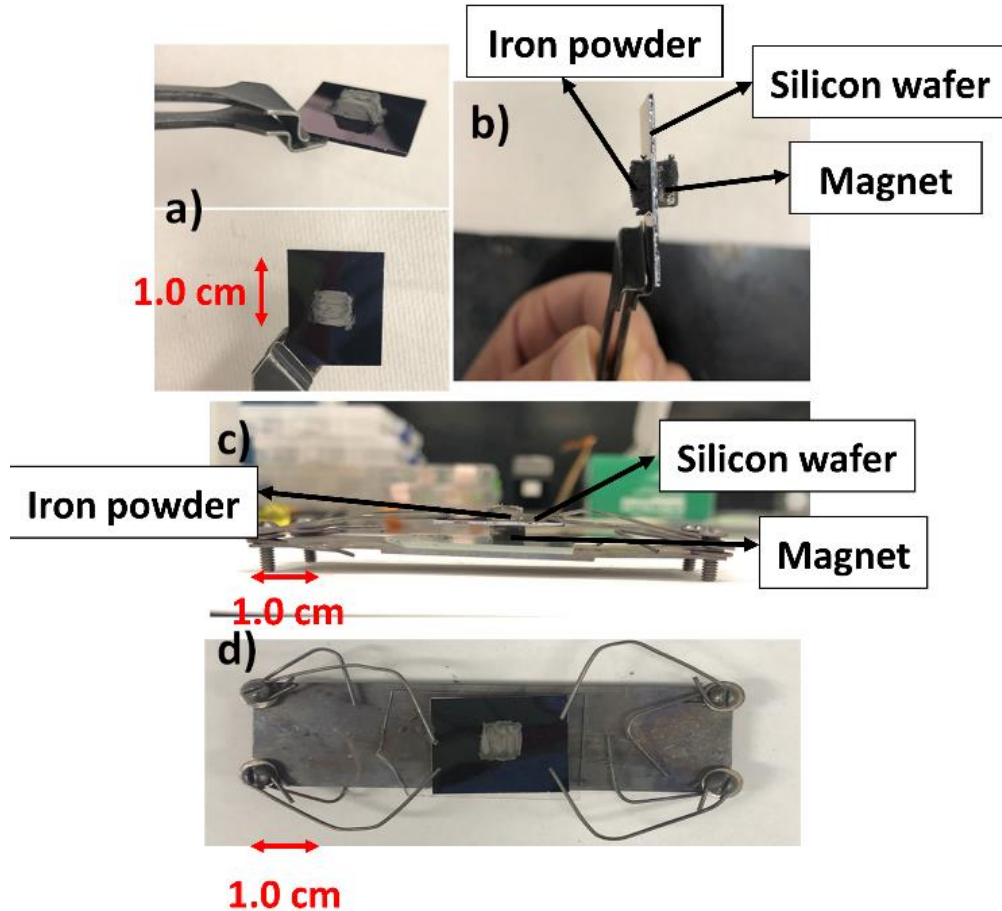


Figure 22: Image of the sample masked with Fe powder from different angles a) top view b) side view c) side view after placing on the custom-built sample holder & d) top view after placing the masked sample on the custom-built sample holder.

In the mechanical mask proposed by Langston *et al*.,[146] one of the limitation was the size of the static and dynamic masks, which makes them not practical for reactors with small size. Our mask is compact and doesn't require a mechanical assembly besides the magnet under the

sample.

Patterned samples (after removing the mask) were studied using x-ray photoelectron spectroscopy (XPS), high resolution field emission scanning electron microscopy (FESEM), and atomic force microscopy (AFM), to determine if there was film deposition under the Fe powder/magnet mask. Water contact angle was measured using Ramé-Hart Contact Angle Goniometer (model No. 100-00). Chemical composition on Si (masked and unmasked) samples were analyzed using Kratos AXIS-165, Kratos Analytical Ltd., UK equipped with monochromatic Al Kα X-ray source. Samples were attached to the sample holder by means of double-sided carbon tape. During XPS, pressure of the chamber was maintained at $10^{-8}$ torr. Atomic force microscopy was done with WITEC-300RA Raman-AFM. Surface morphology was analyzed using high resolution FESEM (JOEL JSM-6320F, JEOL, Inc.).

## 2.2.3   Results and Discussion

The measured water contact angle (WCA) of bare Si wafer is ~36.6° which is in accordance with other reported values in the literature [154]. After 700 cycles of silver ALD, the WCA of the unmasked and masked portions of the sample increased to ~85.0° and ~58.0°, respectively. For the exposed unmasked part of the sample, the WCA is in accordance with that of silver thin films reported elsewhere [155]. Increase in the WCA of the masked part of the sample to ~58.0° was not as high as the WCA of silver thin film and yet it was not close to that of bare Si wafer. It has been established that wetting properties of materials depend on their chemical groups [156] and surface roughness [157]. The increase in WCA of the masked portion can be attributed to Fe powder mask which may enhance the surface roughness of the Si wafer [158].

An advantage of the proposed work is that the Fe powder/magnet mask was easy to

remove after the deposition. For mask removal, the magnet was placed on a thick iron plate. When the sample was lifted up, the magnet remained on the plate. After removing the magnet, the substrate can be cleaned with the flow of the ultra-high purity $N_2$, to remove any possible remaining Fe powder. None of these steps imposed any external compression force to the substrate besides the attraction of the Fe powder to the magnet. The masking methods presented in Langston *et al.* [146] and Sweet *et al.* [148] were based on applying pressure to minimize the clearance between the substrate and the mask. Their approach might be destructive in cases that the substrate has a delicate 3D texture. For such complex and compression sensitive substrates, Fe powder/magnet mask would be a better choice. Fine Fe powder may conformally mask the tiny bumps and pores of the substrate without having any destructive effect on it.

High-resolution SEM images (Figure 23) revealed that after the silver deposition and removal of the mask, there is no silver growth on the masked portion of the Si substrate (Figure 23 b), while the unmasked portion of the sample, which was exposed to precursor/reducing agent (Figure 23 a, c), was covered with Ag particulated thin film.
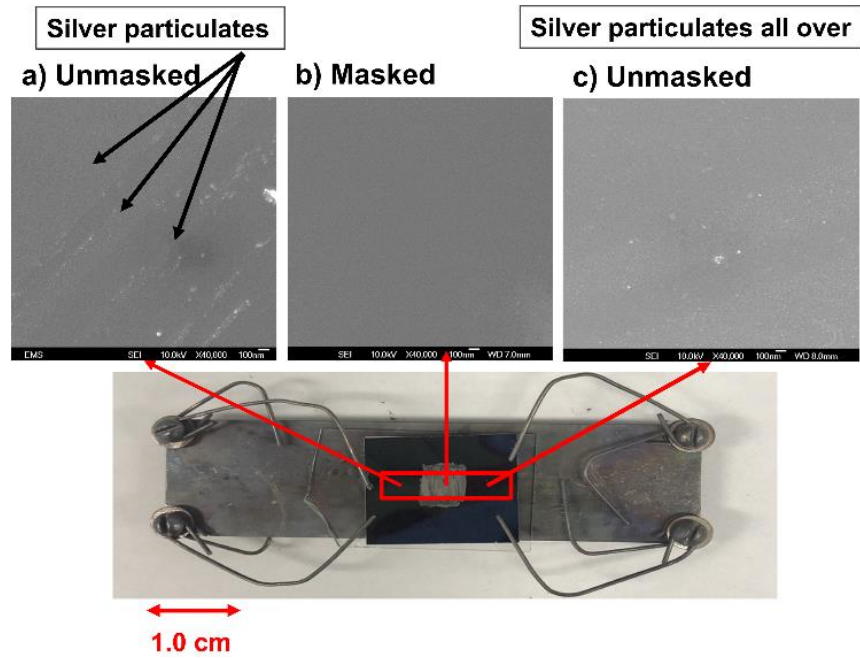
Figure 23: SEM of a) unmasked portion of the sample after Ag deposition, particulated silver thin film was shown by arrow; b) masked portion of the sample after removing the mask, no Ag particles; c) unmasked portion of the sample after Ag deposition. The scale is the same for all SEM images.

AFM was performed on samples of 1300 cycle silver ALD to study the topography and roughness of the sample (Figure 24a-c). The roughness of the unmasked substrate was ~3 nm, that is, higher than that of the masked portion (~1 nm) and the pristine Si wafer (~0.8 nm). Silver deposition was in the form of Volmer-Weber mechanism and resulted into particulated silver thin film on the substrate. AFM images indicated that for the masked portion of the sample, the topography of the surface was smooth, which corroborates that no silver growth happened there. On the unmasked portion of the substrate (Figure 24c), particulated silver thin film covered the entire surface and resulted in different topography from that of the masked part. The size of the Fe powder used in this work were 40-60 microns, which might slightly scratch the Si wafer and make it rougher than the pristine Si sample.
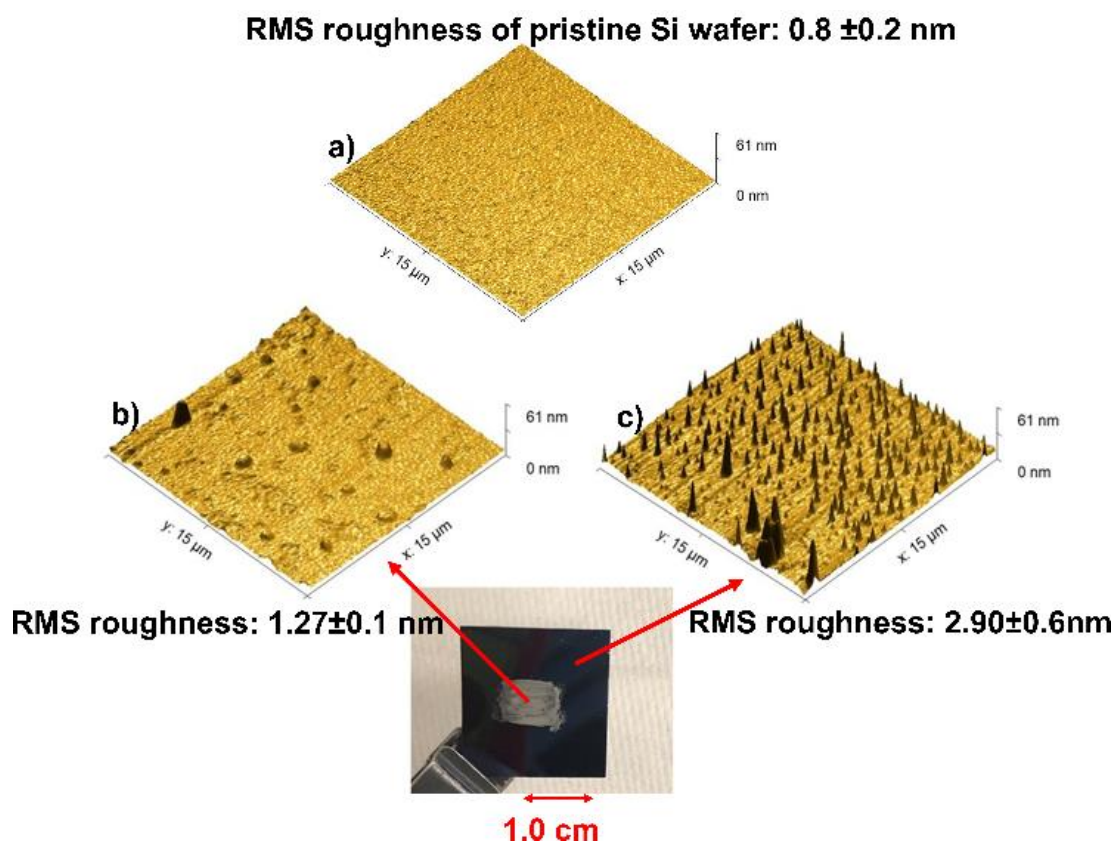
Figure 24: AFM of the patterned sample, a) pristine Si wafer b) masked part of the sample after removing the mask c) unmasked part of the sample after 1300 cycle of Ag deposition.

XPS analysis was performed on the masked and unmasked portions of the substrate to determine the chemical composition of the surface. XPS probes the top 7-10 nm of the surface and surface formation of silver would be detected on the masked portion of the sample. Figure 25 shows XPS of the surface composition for both masked and unmasked portions. As can be seen in the XPS spectra, after 1300 cycles, the unmasked side of the sample showed the characteristic peak of silver. These peaks are in accordance with other studies in the literature [152]. Ag $3p_{1/2}$ and Ag $3p_{3/2}$ appeared at ~602 and ~571 eV, respectively. The double peak of Ag 3d appeared at ~374 and ~368 eV. On the masked side of the Si wafer, the only peaks were O 3s, C 1s, Si 2s and Si 2p; no trace of Ag was observed, which can be attributed to efficient masking of Fe powder/magnet pair.
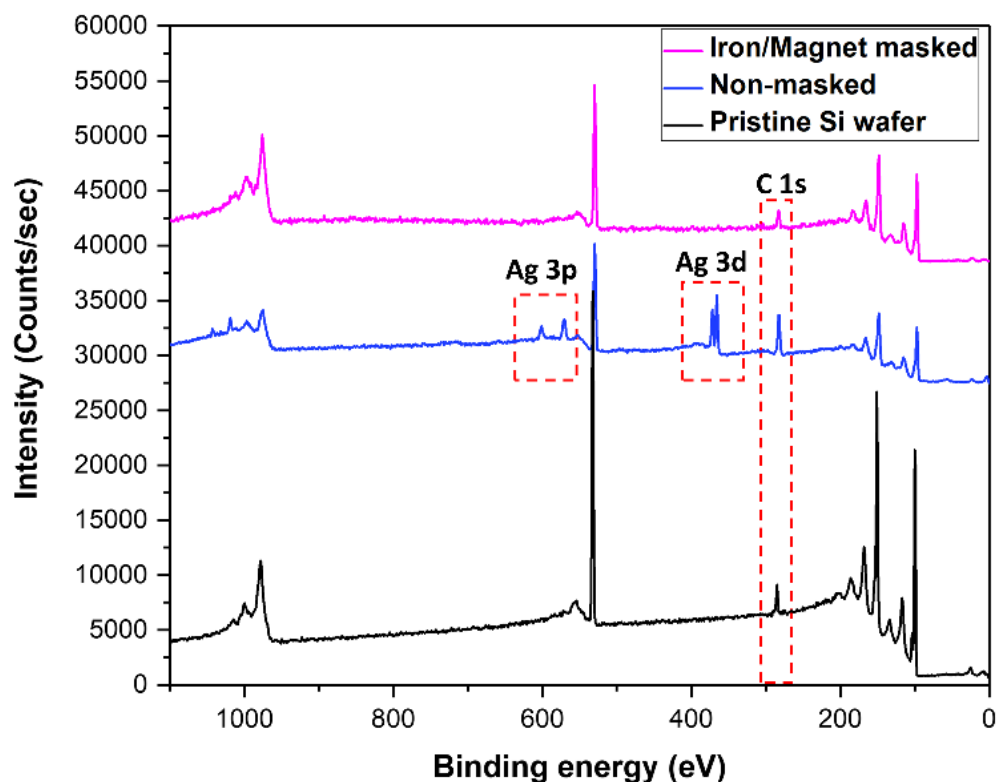
Figure 25: XPS spectra on Silicon wafer substrate a) masked Si wafer b) unmasked Si wafer c) pristine Si wafer. ALD processing conditions: operating pressure of 500 mTorr, precursor pulse/purge time 3 s/5 s and reducing agent pulse/purge time 2 s/10 s, respectively.

XPS of the pristine Si wafer before ALD is also presented in Figure 25 and can be compared to the surface chemical composition of the masked Si wafer. For both pristine and masked Si wafer the main surface chemical species were found to be O 1s, C 1s, Si 2s and Si 2p with peaks at 529 eV, 284 eV, 153 eV and ~100 eV, respectively. This result confirms that Fe powder and magnet prevented Ag growth.

One of the concerns with mechanical masks is that different impurities might be introduced into the reactor and consequently affects the composition of the deposited film. For example, Langston et al.[146] reported that in the case of Teflon mask, XPS spectra showed carbon contamination which was attributed to the presence of Teflon as an organic mask in the ALD reactor. Zhang et al.[159] also studied the masking ability of Parafilm as a physical mask

for $Al_2O_3$, Ir, and $TiO_2$ thin film ALD. Prior to loading the masked samples into the reactor, baking and outgassing of Parafilm were performed at 60 °C/10 min and 200 °C/2h, respectively. In the current study, no time was needed for baking or outgassing the Fe powder mask. Their results revealed that nonuniform growth from the edges is another issue that should be considered with a Parafilm mask. For example, in the case of $Al_2O_3$, the thickness was uniform up to 1 mm from the edges, however in the case of $TiO_2$ it was uniform up to 5 mm from the edges, and for Ir thin film it was ~ 2 mm away from the edges. Outgassing of Parafilm during the ALD could affect the film growth on the unmasked areas differently for the three precursor/oxidizer system that they examined [159]. This effect was reported by Färm *et al.*[160] In Färms work, poly(methyl methacrylate) (PMMA) was used for different precursor/oxidizer systems and reported that passivation of the PMMA mask could be dependent on the nature of the precursor. For instance, halide precursors were reported to be more difficult to passivate than metalorganic precursors [160].

XPS of the unmasked and masked Si wafer did not show any iron or any extra element in the spectra, which suggested that the Fe powder and magnet mask did not leave any impurity or residue behind or react with the precursors or reactants. It also did not impose a significant compression force on the substrate which makes it a good candidate for masking substrates with 3D texture. The proposed mechanism that Fe powder/NdFeB magnet mask the substrate are as follows: the Fe powder behaves like a classical physical mask; alternatively, the fine Fe powder generates an apparent maze that effectively blocks the precursor and co-reactant molecules from reaching the substrate. During the ALD process, the precursor/co-reactant molecules might either be adsorbed on the Fe powder or get trapped in the free voids between the Fe powder grains and never reach the substrate. A summary and comparison of mechanical masks which were used for

thin ALD films is presented in Table VI.

Table VI: Physical masks reported for patterning in ALD

| Substrate<br>Deposited thin film | Mask type | Pros | Cons |
|---|---|---|---|
| $\dfrac{Si\ wafer}{PbS,Al_2O_3,ZrO_2,Pt}$ [146] | Static & dynamic masks with: | Less complicated than lithography/etching processes | -Main limitation of all is this assembly takes up too much space, not suitable for small reactors.<br>-The external force might have destructive effect on 3D substrates |
| | Polished Si (100) | -Provide minimum clearance between mask and substrate<br>-consistent masking material | |
| | Copper | -Effective mask | -~1 mm diffusion of ALD film into the edges |
| | Teflon | | -Imposing carbon contamination in the resulted thin film |
| $\dfrac{Si\ wafer}{Al_2O_3,Ir,TiO_2}$ [159] | Parafilm | -clean & easy method to apply and peel off<br>-applicable up to 300 °C<br>-effective for low resolution patterning | -Outgassing of parafilm at higher temperature had negative effect on film growth<br>-Nonuniform growth around the boundaries (~1 & ~5 mm for $Al_2O_3$ & $TiO_2$, respectively)<br>-Not suitable for flow type reactors with vertical samples at temperature > 275 °C |
| $\dfrac{PP\ and\ Pa6\ fiber}{ZnO}$ [148] | Al metal plates + compression force | Easy to install | -lateral and vertical penetration into the masked part<br>-The external pressure force might have destructive effect on samples with delicate 3D morphology |
| $\dfrac{Silicon\ (100)}{Iriduim,Platinum,Ruthenium}$ [160] $TiO_2,Al_2O_3$ | PMMA | Same method as lithography and patterning with UV light. | -Long pattering duration.<br>-Passivation was dependent on the nature of the metal precursor. |
| $\dfrac{Si\ wafer}{Ag}$ [161] | Iron filings powder/magnet | -Very easy and clean to install & lift off<br>-Doesn't occupy much space<br>-Small assembly<br>-Thermal stability for high temp. ALD<br>-Doesn't contaminate sample | -Not suitable for reactors and sample holders with magnetic properties |

### 2.2.4  Conclusion

In summary, the Iron powder/magnet mask, presented in this work is an inexpensive, easy, and cleaner method for patterning in SALD. This technique can provide an effective method for patterned thin films, especially in research environments. It can also be used in industry for applications which do not need micro/nano scale precision for patterned deposition

on a larger area scale. Employing finer iron powder and a template, may give this method the potential to become a good candidate for higher resolution masking and this is under investigation by our group.

Comparing the roughness and morphology of the masked and unmasked portions of the sample with AFM and SEM showed the absence of silver deposition on the masked part of the sample. XPS showed silver on the unmasked portion of the sample but no trace of silver on the masked portion (after removing the mask). Our XPS results also showed no impurity from the mask material on the Si wafer. These results corroborated the masking efficiency of the iron powder/magnet pair and this method could be extended to other ALD material systems and reactors.

**2.3** **Functionalization of Collagen with Particulated Silver Thin Film via Atomic Layer Deposition**

**2.3.1** **Introduction**

ALD has been established in the semiconductor industry as a promising methods for conformal thin film deposition [162, 163]. In comparison  of ALD with other thin film deposition methods (e.g., electroplating, spin coating, sputtering, physical vapor deposition, and chemical vapor deposition) [21], an advantage of ALD is its excellent controllability of thickness of the targeted thin film down to Ångström length scale [19]. Another outstanding advantage of ALD is the deposition of conformal and uniform thin films especially on three-dimensional structures (3D) [164]. Because of these advantages, applications of ALD have gradually expanded into other fields of research, e.g., medicine and medical devices, wastewater treatment and air purification, solar cell industry [21] and bioengineering [25, 165].

The wide usage of collagen membrane for bone grafting in the dental industry has motivated in part the current research. Collagen is a structural protein and each molecule tends to rearrange its structure into a triple helix (which is called fibril) to maximize its stability [166]. Arrangement of these fibrils results in collagen fiber formation [166]; therefore, the morphology of the collagen membrane is fibrous which results in high surface area. From a clinical point of view, one of the advantages of collagen membranes is its biodegradability and resorbability over time, which means no second surgery is needed for implant removal; however, in some cases it has been reported that collagen dissolved before bone regeneration starts [167]. To overcome this drawback, covalent crosslinking of the collagen membrane was suggested and has been reported to delay its dissolving process [166].

Another level of modification of collagen membrane to overcome its drawbacks is, for example, functionalization of the collagen surface with nanomaterials. As mentioned above, one

of the promising techniques for surface coating, which has precise thickness control at nanometer and Ångström level, is ALD. Among thin film deposition techniques, ALD has attracted lots of interest due to its uniform and conformal film coverage, which is especially preferable in the functionalization of complex 3D surfaces including dental materials like collagen [164, 168]. Collagen is a heat-sensitive material and functionalizing it needs extra care. Bishal et al. [169] used ALD to coat collagen membrane with $TiO_2$ at room temperature. As the number of cycles increased the diameter of the fibers increased; this was a physical representation of thin film growth on the collagen fibers. Their results indicated uniform and conformal coverage of collagen fibers after $TiO_2$ ALD. In another study, bioactivity of these $TiO_2$ collagens were tested and showed improved growth and proliferation of human osteoblastic and mesenchymal stem cells when compared to pristine collagen [83].

There are other studies in the literature on ALD-coated organic materials with complex/3D microstructures/topographies [88, 170, 171]. To our knowledge most of these works were reported on metal oxides, e.g., ZnO [170, 172], $TiO_2$ [172, 173], $Al_2O_3$ [128, 172, 174] and few reports on metal nitride, e.g., TiN [175]. Aside from metal compounds like metal oxides and metal nitrides, there is a strong interest in developing ALD of uniform and conformal pure metal films. There are several established ALD precursor systems for first row transition metals Fe [176], Co [177], Cu [151, 178, 179], and platinoid metals (Ru [180, 181], Rh [182], Pd [183], Pt [184, 185]), W [186, 187]. [186, 187]. There are fewer reports on the ALD of Au and Ag. Possible reasons are their higher cost and the availability of fewer suitable precursors for ALD. One of the proposed pathways for the deposition of elemental metals in a conventional ALD system consists of pulse and then purge of the metal precursor, but instead of an oxidizing agent, a reducing agent is needed to reduce the metal cation of the precursor into its metallic state.

Generally, among noble metals, ALD of silver and gold are reported to be challenging. The low thermal degradation temperature of silver precursors and large ligands connected to silver atoms make the precursor volatility difficult at low temperatures. There are studies on plasma enhanced ALD (PEALD) of silver metal with plasma activated hydrogen, or $NH_3$ as the reducing agents [188-191]. There are a few reports on thermal ALD of silver on silicon and silica gel powder [152, 192]; however, due to the narrow working temperature of silver precursors, silver ALD remains challenging. Ag(fod)(Pet3) is the precursor that was reported to work with both PEALD and thermal ALD. The proposed mechanism for thermal ALD with this precursor is the reduction mechanism. In this reduction reaction, the borane dimethylamine complex reacts with Ag(fod)(Pet3) precursor and eliminates the remaining ligands of Ag(fod)(Pet3) during the borane complex pulse; this yields metallic silver on the surface. The silver deposition mechanism is nucleation and growth. Nucleation of noble metals was reported to start with a delay [193]. After the nucleation step, growth of silver (like other noble metals) continues in the form of Volmer-Weber mechanism because of their high surface energy [189] on the surface of the targeted substrate. As it can be seen, this particulate formation of silver [194] is different from the classical layer by layer ALD growth mechanism reported for metal oxides.

Silver is among the best antibacterial agents [3, 195]. One of the methods that are used for functionalizing surfaces with silver nanoparticles is chemical. For example, Zhang et al. [196] studied the effect of silver nanoparticles on cotton fibers. Their treatment process included an impregnation method: a colloidal solution of silver was prepared, the cotton fabric was stirred in it, the fabric was then washed to remove unfixed nanoparticles, and the final silver treated fabric was left to air dry. The final size of the silver nanoparticles reported was in the range of 10-30 nm (~18 nm average). Their results showed 99.01% and 99.26% reduction in *Staphylococcus*

*aureus* and *Escherichia coli* bacteria, respectively. In the literature, most studies on the potential antibacterial activity of silver used dissolution of silver nanoparticles followed by immersion of the targeted substrate in the solution containing silver nanoparticles [196]. However, making a dispersed medium of silver nanoparticles and immersion of the substrate in that colloidal solution would not be advisable for resorbable materials like collagen. Therefore, functionalization with a method like ALD is of great interest to overcome this challenge.

Silver synthesis methods include arc-discharge [197], physical vapor condensation [198], and ALD on silicon [152, 199]. To study the bioactivity of silver ALD, Delvin-Mullin et al. [66] deposited silver on 3D titanium scaffolds which are being used as orthopedic implants. Bacteria recovery and biofilm formation were studied and compared to that of bare and silver-coated titanium scaffold. In vitro results showed that Ti implants coated with Ag suppressed the growth of osteolytic pathogen (S. Epidermitis) by 2-log fold. Also, Ag did not have any negative effect on newly regenerated bone after 12 weeks in rat tibia, which indicated the efficiency of bone regeneration on silver-coated and uncoated porous Ti implant was similar.

In our study, the objective is to functionalize collagen membrane with particulated silver ALD thin film. Chemical and morphological characterization is done to study and compare the changes before and after silver deposition. Bioactivity of silver-coated collagen is tested in vitro by using "3-(4,5-dimethylthiazol-2-yl)-2,5 diphenyltetrazolium bromide (MTT)" assays. To our knowledge, this is the first report on coating collagen with ALD silver and on studying the biocompatibility of this novel ALD material in oral environments and in biomedical engineering applications in general.

### 2.3.2 <u>Materials</u>

Triethylphosphine(6,6,7,7,8,8,8-heptafluoro-2,2-dimethyl-3,5-octanedione)silver(I)  or Ag(fod)(Pet3) from Strem chemicals was used as the silver precursor and it was maintained in a bubbler at 96 °C during all depositions. As received Ag(fod)(Pet3) was kept at a temperature lower than -18 °C; at that temperature Ag(fod)(Pet3) was white crystalline solid, while at liquid state it turned yellowish. This change was also reported by other researchers [200]. For silver ALD, silver cation in the Ag(fod)(Pet3) precursor needs to be reduced to its metallic state. Conventional reducing agents like $H_2$ and $NH_3$ are not reactive enough to reduce silver in thermal ALD and are reported to only work when plasma is involved to activate them [191, 200]. Therefore, borane dimethylamine complex (($CH_3$)$_2$NH·$BH_3$) from Sigma Aldrich was used as a reducing agent to react with Ag(fod)(Pet3) and leave deposited metallic silver on the substrate [151, 152, 161]. The borane bubbler was kept at 52 ˚C. This reducing co-reagent first introduced by Kalutarage et al. [151] for ALD of copper thin films at low temperature and later it was used by Makela et al. in the deposition of silver thin films via thermal ALD on Si and glass [152]. Here, absorbable collagen membrane from the BIOMEND® distributed by ZIMMER dental was used as received for the substrate.

It has been reported that deposition of metal oxide seed layer could lead to the formation of silver particulated thin film at lower number of ALD cycles. Anders et al. [201] investigated the effect of small amounts of different metal oxide seed layers on nucleation and coalescence of silver thin films. Their results showed that sub-monolayer amount of Ti in $TiO_2$ improved the coalescence of silver islands. To evaluate the role of such interlayer, $TiO_2$ coated collagen was prepared close to room temperature. Room temperature ALD of $TiO_2$ on collagen substrate was first done by Bishal et al. in our custom-built ALD system [169]. In the current study, ALD of

TiO$_2$ thin film was done in a Kurt J. Lesker 150LE ALD System at 40 °C. Tetrakis(dimethylamido) titanium(IV) (TDMAT™) was used as the titanium precursor (Sigma Aldrich). O$_3$ was used as an oxidizer for this ALD reaction and it was prepared using a UV-ozone generator placed immediately upstream of the deposition chamber to minimize ozone decomposition in the delivery line as described in our previous studies [78, 120]. The deposition pressure was 1000 mtorr. The designed recipe for room temperature TiO$_2$ deposition had longer purging times compared to thermal ALD of TiO$_2$, in order to avoid precursor condensation on the linings of the ALD system. Each cycle of the ALD reaction consisted of 1 s/50 s precursor pulse/purge, and 1.8 s/45 s oxidizer pulse/purge. Ultra-high purity N$_2$ (N150 UH-T, Praxair Distribution Inc) was used as a carrier and purging gas for all precursor, oxidizer, and borane dimethylamine complex co-reactant during all experiments. The thickness of the TiO$_2$ interlayer deposited on the reference Si-wafer (using spectral ellipsometer) was 11.1±0.1 nm for 200 cycles.

For all substrates, small cut-outs of silicon (approx. 1.5 cm X 1.0 cm) were used as reference samples for optical thickness measurements. The silicon substrates used had a 525±25 μm thickness and were purchased from WAFERPRO (item number: C04007). Prior to deposition, these silicon cut-outs were rinsed with deionized water from a Barnstead™ Nanopure Infinity lab water system (catalog id: D8961) and then dried with N$_2$ (Praxair NI 4.8-T, purity: 99.998%).

### 2.3.3   Methods

Thermal ALD of silver was performed in patented, custom-built ALD system, the details of which are described in [120, 153]. This flow-type reactor has two stainless steel precursor delivery lines and a separate line for oxidizer delivery. This design makes the system flexible for depositions with either precursor/oxidizer or precursor/co-reactant. For silver ALD, one of the

bubblers was filled with silver precursor and the other one with borane dimethylamine complex. The precursor and the co-reactant were sequentially entered the reactor getting order from a custom-written LabView program controlling the work sequence of pneumatic Swagelok valves. Both precursor and co-reactant pulse/purge times were optimally chosen at 4 s/6 s and 3 s/20 s, respectively. One limitation with the silver precursor is its narrow working temperature. Its degradation temperature was reported as 140 °C, while its evaporation temperature is 91-106 °C [152, 200]. This narrow temperature range imposes limitation on the ALD processing temperature. In this study, delivery lines in between bubblers and reactor were set at 120 ˚C and depositions were done at 120 ˚C. Base pressure and operating pressure of the system were ~9 mtorr and 900 mtorr, respectively.

Spectral Ellipsometry (J. A. Woollam Co., Model: M-44) was used to measure the film thickness of $TiO_2$ thin films on each corresponding Si wafer sample, which was loaded as a control sample in each ALD batch. For silver ALD, the particulated morphology of the thin film caused complex optical behavior, which made it challenging to develop an appropriate spectral ellipsometry model for silver thin films measurements in our work [189]. The chemical composition of the deposited silver was characterized using Kratos AXIS-165, Kratos Analytical Ltd., UK XPS system equipped with monochromatic Al Kα X-ray source on large area mode (1150 μm X 700 μm). Samples were attached to the sample holder using double-sided carbon tape. During XPS, pressure of the chamber was maintained at less than $10^{-8}$ torr. Casa XPS software was used for peak analysis. Surface morphology was analyzed using high resolution field emission scanning electron microscopy (FESEM) (JOEL JSM-6320F, JEOL, Inc.). Prior to FESEM, pristine collagen and silver-coated collagen samples were sputter coated with 6 nm PtPd to make it conductive for the subsequent FESEM.

Human gingival fibroblast (HGF) was cultured via assays employing MTT assay to study the potential cytotoxicity and cell compatibility of silver coated samples to be compared to the pristine collagen membrane. In this test, absorbance is expressed as a measure of gingival cell viability cultured on the silver-coated substrates after day 2 and day 7. Comparing data of control collagen with functionalized collagens is representative of the compatibility of cells with the new functionalized surface.

## 2.3.4   Results and Discussion

### 2.3.4.1 Characterization of collagen samples

Figure 26 shows the collagen membrane before and after silver ALD, it shows that upon silver deposition the sample underwent a color change from white to yellow. It is been reported that nano-silver absorbs light at 435 nm, and due to metallic surface plasmons, unaggregated silver nanoparticles show yellow color [202, 203].
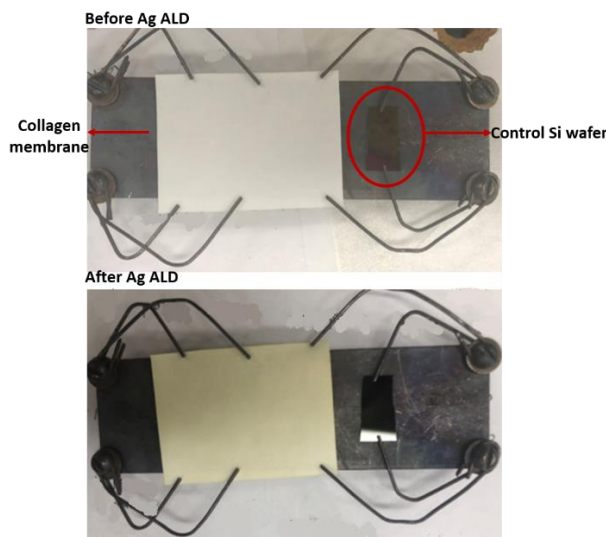


Figure 26: Collagen membrane along with the control Si wafer on the custom-built sample holder, ALD processing conditions: 1300 cycles at operation pressure 900 mtorr, precursor pulse/purge time 3 s/5 s and reducing agent pulse/purge time 2 s/10 s, precursor/co-reactant temperature: 96 ˚C and 52 ˚C, respectively. As can be seen, Ag ALD turned the shade of the collagen membrane yellow.

**2.3.4.2 <u>SEM studies</u>**

Surface morphology of the pristine collagen and silver-coated collagen samples was studied using FESEM (Figure 27). Free image processing software "ImageJ" was used to analyze the SEM images. The main difference between uncoated and coated collagen is the presence of particulated silver on and between collagen fibers. The deposited silver indicated spherical shape, fairly uniform distribution, and conformal deposition. Figure 27a and c, show the microstructure of the samples at X10,000 magnification, while Figure 27b and d give a closer look at X40,000 before and after silver deposition. As SEM suggested after 1300 cycles of silver ALD, silver particulates formed on the collagen fibers and this deposition showed conformality which, means nanosized silver formed on the surface of the collagen and conformally covered all fibers. In real applications, most of these materials are in contact with biofluids that have the ability to flow and wet the top and inside fibers. Therefore, ALD can yield functionalized micro/nanostructure even below the top surface. In our ALD system, upon pulsing of the precursor/reducing agent, molecules of the reactants reached the surface, diffused inwards and reached the fibers which were located below the top surface. The size distribution of the deposited silver is shown in Figure 27e with an average size of 16 nm, assuming a round shape and no particle aggregation. The morphology and size distribution of the Ag ALD on collagen in our study seems to be similar to that in [192] which was reported for plasma-enhanced Ag ALD on silica gel powder, and to the one in [196] obtained via a solution method on cotton fabric.
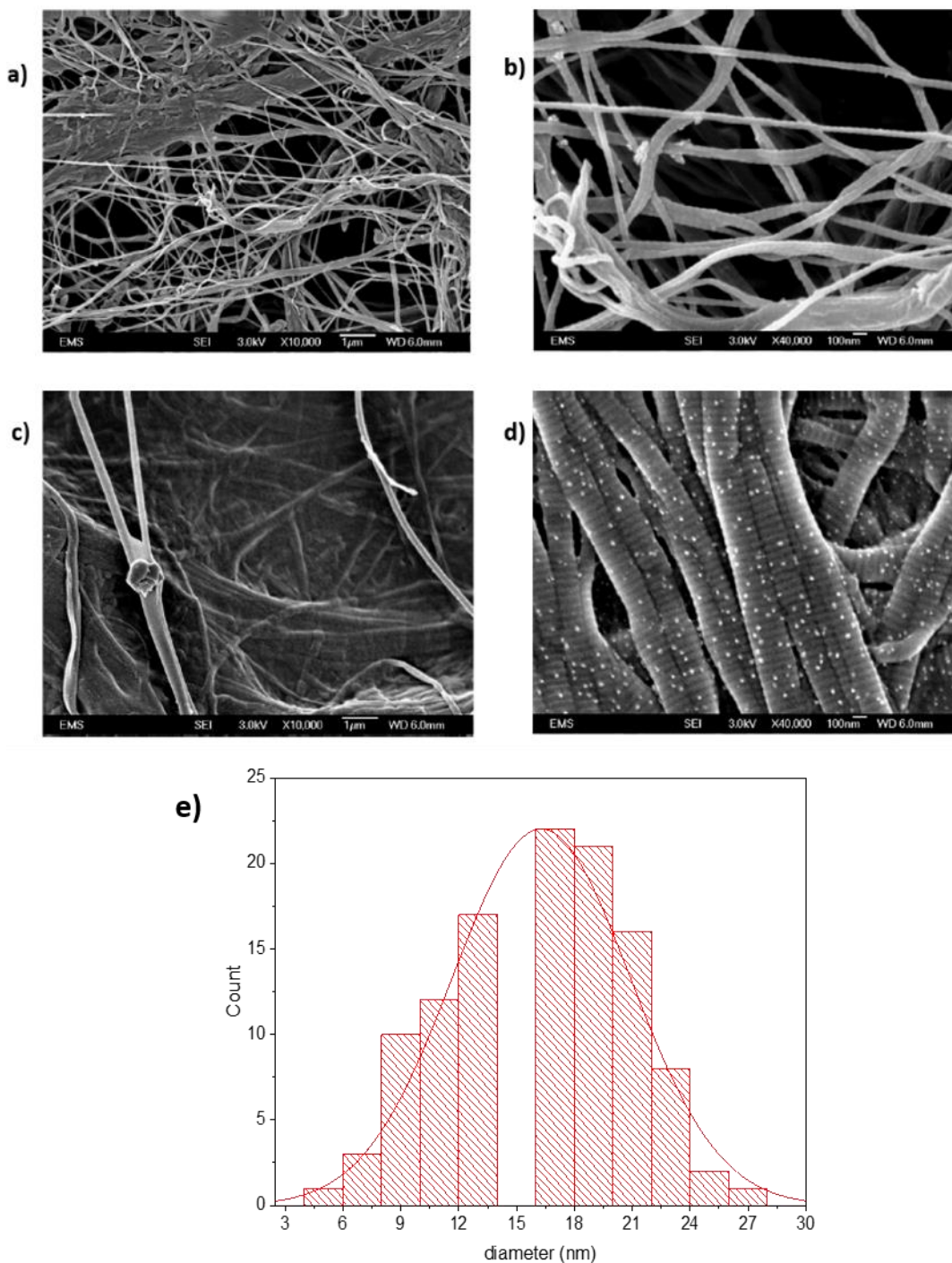
Figure 27: SEM images of the microstructure of a) pristine collagen (Bio-Gide) at X10,000 magnification, b) pristine collagen (Bio-Gide) at X40,000 magnification, c) Ag coated collagen (BioMend) at X10,000 magnification, and d) Ag coated collagen (BioMend) at X40,000 magnification. ALD processing conditions: 1300 cycles at operation pressure 900 mtorr, precursor pulse/purge time 3 s/5 s and reducing agent pulse/purge time 2 s/10 s, precursor/co-reactant temperature: 96 ˚C and 52 ˚C, respectively. e) Statistical particle size distribution of silver.

**2.3.4.3 <u>XPS studies</u>**

XPS is one of the characterization methods for studying the surface chemical composition of samples down to 7-10 nm depth. Figure 28 shows XPS spectra of pristine collagen, silver-coated collagen samples as well as Ag ALD on $TiO_2$-coated collagen.

Samples with ALD silver showed no amount of impurities from the ligands of Ag(fod)(Pet3) (F, P) and the borane dimethylamine complex reducing agents (B, N), demonstrating that the reduction reaction reached completion and all of the $Ag^+$ cation of the precursor could be successfully deposited on the surface without being attached to the unreacted side ligands of Ag(fod)(Pet3) [194].

There are reports showing the positive role of metal oxide interlayer in growth improvement of noble metals due to thermodynamic stability of the metal/oxide interface [204-206]. For example, sub-monolayer amounts of Ti in $TiO_2$ were reported to improve the coalescence of silver islands at thinner silver thickness [201]. Therefore, we also evaluated the role of interlayer in our work through the deposition of 11.1 nm room temperature $TiO_2$ ALD on growth of silver and cell viability.

The elemental composition of pristine and silver coated samples is presented in Figure 28. After silver treatment, all samples showed characteristic Ag $3p_{1/2}$, Ag $3p_{3/2}$ peaks at 601 and 571 eV, respectively, and Ag $3d_{3/2}$ at ~373 and Ag $3d_{5/2}$ at ~367 eV. These peaks are in agreement with silver ALD features reported in the literature using the same or different precursor/co-reactant systems on different substrates, i.e., silicon and glass [152, 199]. Since growth of silver is in the form of particulates, even for samples at higher number of cycles the chemical finger print of the collagen substrate is expected to be observable in XPS spectra, e.g., N 1s at 398 eV

(Figure 28), which corresponds to nitrogen atoms of the collagen backbone. For samples with the TiO₂ interlayer, this fingerprint disappeared which corroborated that ALD of TiO₂ was in the form of an integrated thin film conformally covering the top surface of collagen [169].
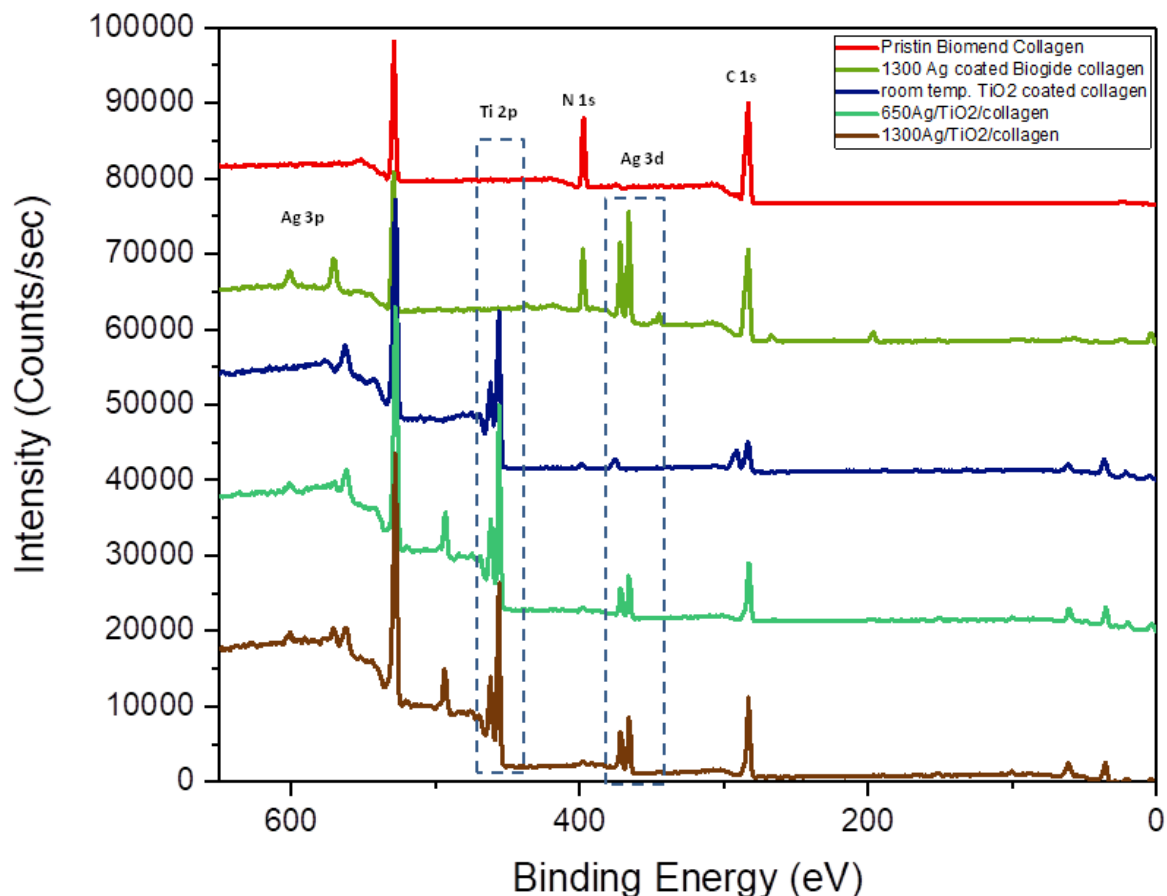


Figure 28: XPS of a) pristine collagen b) 1300 ALD cycles Ag collagen, c) room temperature TiO₂-coated collagen, d) 650 Ag ALD cycles on TiO₂-coated collagen, e) 1300 ALD cycles on TiO₂-coated collagen (3 s/5 s precursor pulse/purge, 2 s/10 s reducing agent pulse/purge), at 115 °C and 900 mtorr.

Main challenges in using silver for functionalization of materials is its higher cost compared to other metals and its toxicity at higher concentrations. Our SEM results showed that thermal ALD of silver after 1300 cycles yields uniform and conformal coverage of collagen fibers achieved at a low concentration of silver, without significantly changing the morphology, especially without blocking the pores of collagen membrane, which is a critical characteristic for

collagen to enable oxygen exchange, micronutrient transfer, blood perfusion, and cell regeneration [166]. As this particulated silver has high surface to volume ratio, this morphology might be preferred over thin film coverage for applications which need high coverage of silver at low concentration, like antibacterial, catalysis, surface plasmon [207] and improvement of near infrared absorption in solar cells [208, 209]. In the following section, cytotoxicity of functionalized collagen with silver is further investigated.

Base on the results of XPS and SEM the morphology of the silver ALD appears to be in the form of Volmer-Weber mechanism. Schematics of our proposed mechanism is presented in Figure 29.
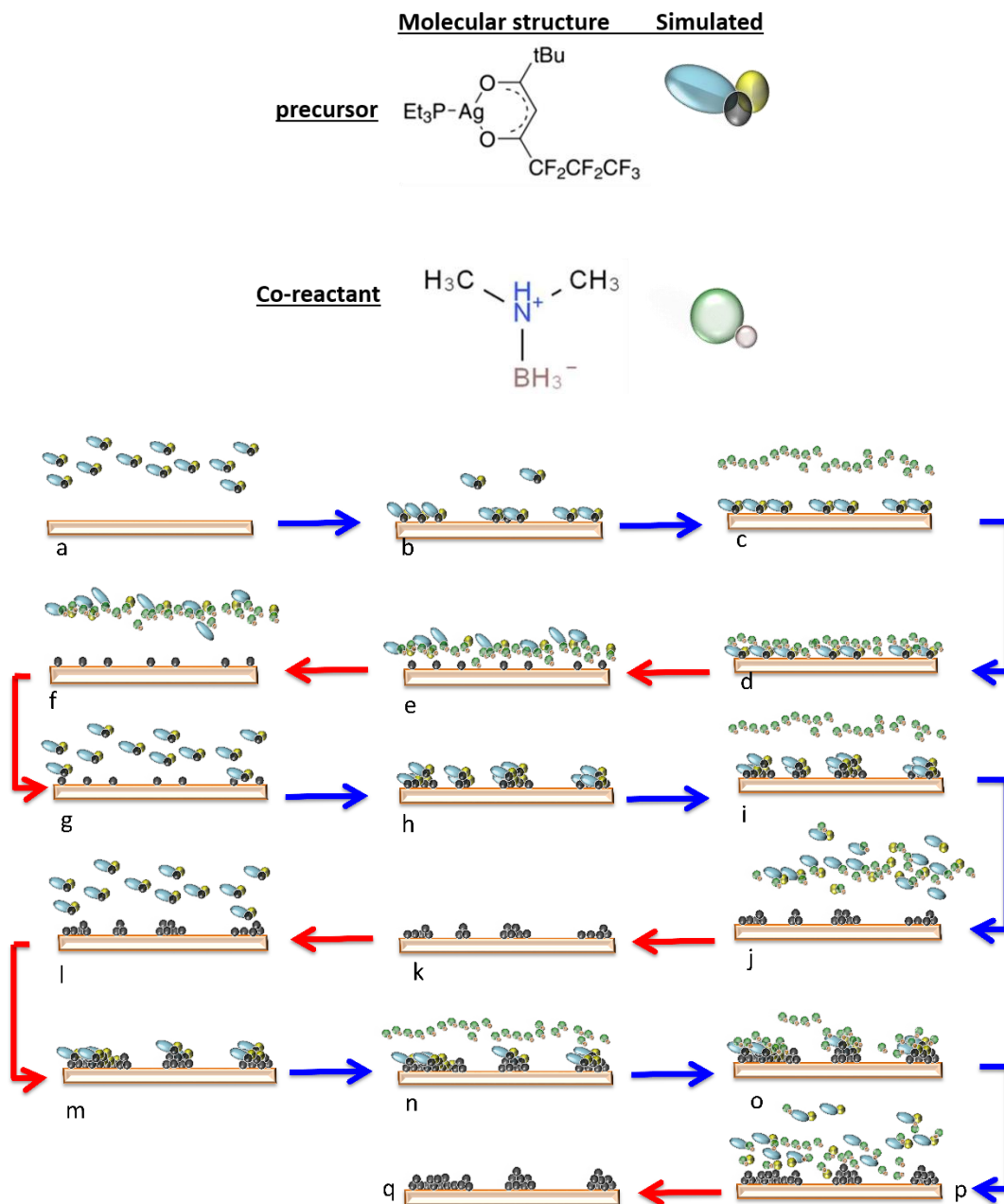
Figure 29: Schematic of Volmer-Weber nucleation and growth mechanism for silver thermal ALD, a) Silver precursor pulse. b) Chemisorbed silver precursor on the surface. c) Borane dimethylamine complex (as reducing agent of the reaction) pulsed. d) The reduction reaction between silver precursor and reducing agent. e) $Ag^+$ reduced to its metallic state. f) By-products and left over of reducing agent purge. g) 2nd cycle of Ag precursor pulse. h) Because of the nature of silver atoms tend to agglomerate, so next round of precursor adsorbs on or very close to previous silver atoms. i) 2nd cycle of reducing agent pulse. j) Reducing agent and by products purged after the second round of silver reduction reaction. k) Silver atoms deposited on previous silver atoms or very close to previously deposited silver. L) $3^{rd}$ cycle of precursor pulse. m) Chemisorption of silver precursor happens on/next to previously deposited silver atoms to connect islands to each other or make them bigger. n) $3^{rd}$ cycle of reducing agent pulse. o) Reduction reaction like step d and j. p) Byproducts and left over of reducing agent purge. q)

84

Island growth and neighboring island get close to each other for coalescence.

### 2.3.4.4 Biocompatibility Test

Although silver is the most preferred commercial antibacterial additive [3], it has been reported that silver can have toxic effect on human cells. Taleghani et al. [210] studied the toxicity of different concentrations of silver nanoparticle solutions on human gingival cells in-vitro. In their study, commercially purchased Plasmachem silver nanoparticles of ~10nm were used. Their results showed that toxicity of silver nanoparticles is time and dose dependent; for example, for high concentrations (> 10 μg/ml) the viability of cell decreased while lower concentrations did not show significant toxicity. In our work, assays using "3-(4,5-dimethylthiazol-2-yl)-2,5-diphenyltetrazolium bromide (MTT)" and according to the application of these collagen membranes, gingival cells were selected to study the potential cytotoxicity of silver-coated samples. The cell culture test was done on a control sample, and 1300 cycles Ag on collagen, 1300 cycles Ag and 650 cycles Ag on collagen coated with $TiO_2$ interlayer (11.1±0.1 nm). In this test, absorbance is expressed as a measure of gingival cell viability. For all tested samples cell proliferation were improved after 5 days. Based on the absorbance values in Figure 30, one can conclude that the cell response of silver coated collagens are higher than the pristine collagen for both day 2 and day 7. That is, our results showed that cell proliferation was not negatively affected by the presence of silver particulated thin films. Hence, this ALD silver is below cytotoxicity level. Therefore, due to the established antibacterial nature of silver, membranes coated with silver ALD can be antibacterial and biocompatible.
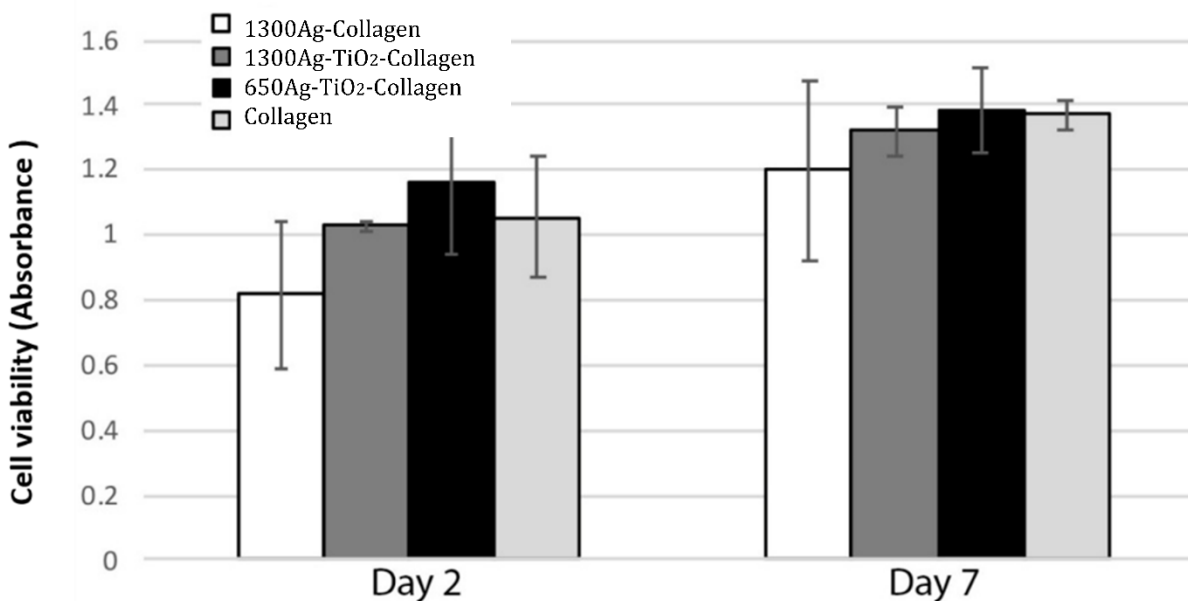
Figure 30: MTT Viability assay results indicating absorbance as a measure of cell viability of gingival cells cultured on the silver coated samples for day 2 and day 7. collagen represents the pristine collagen, 650Ag-TiO$_2$-collagen and 1300Ag-TiO$_2$-Collagen represent 650 and 1300 cycles of Ag-ALD on interlayer of TiO$_2$ (11.1$\pm$0.1 nm), and 1300Ag-Collagen represents 1300 cycles of Ag-ALD on pristine collagen. ALD processing conditions: pressure 900 mtorr, precursor pulse/purge time 3 s/5 s and reducing agent pulse/purge time 2 s/10 s, precursor/co-reactant temperature: 96 ˚C and 52 ˚C, respectively.

### 2.3.5   Summary and Conclusions

Commercially available collagen was functionalized with particulated silver thin film via thermal ALD. Surface characterization of the samples demonstrated that silver was successfully deposited on collagen samples. Our study on the role of metal oxide interlayer showed a predisposition of collagen with ALD TiO$_2$ to promote silver deposition and shorten its nucleation delay. SEM revealed that silver deposition is in the form of relatively uniform particulated thin film with an average size of ~16 nm. Silver-coated collagen and silver-coated TiO$_2$/collagen samples were found to be biologically compatible with gingival cells and they exhibited no negative effect on the biocompatibility of the collagen, and growth and proliferation of cells. Collagen is bioresorbable membrane which makes it difficult to get functionalized via methods

which involve solvents. Therefore, our proposed solvent-free silver ALD process is novel and favorable to surface functionalize such a bioresorbable substrate without any adverse effect on the collagen membrane.

## 2.4    ALD of Silver on N95 mask

### 2.4.1    Introduction

Personal protective equipment (PPE) is being used by healthcare personnel (HCP) and ordinary people which keeps HPC, patients safe from the potential transmission of disease and/or toxic materials [211]. Due to recent SARS-CoV-2 pandemic in 2019 and 2020, the Center for Disease Control and Protection (CDC) has recommended healthcare personnel to use N95 respirator. Originally, N95 respirators were designed for one time usage and were worn by HCP to reduce exposure to airborne infectious agents, including the SARS-CoV-2 virus. Unfortunately, the ongoing pandemic has caused worldwide shortages of effective respiratory masks. The shortages of supply and high demand may have increased the price significantly, causing consumers to use them beyond their service life. Extended use of respirators, however, may not advisable, as air-borne bacteria may be intercepted by respirators' filter media [212]. Recent studies also indicated that SARS-CoV-2 virus may oculate and remain viable on the outer side of the respirator for 3 days [213]. Further, the host's saliva and sweat may have nurtured and created an ideal environment for the bacteria and viruses to remain viable and pose unexpected threats to the wearers' health [214, 215]. Several decontaminated procedures, such as disinfection via ultra violet and 70°C dry heat [216-218], have been proposed to extend the longevity of that PPE; however, these decontaminated procedures may negatively affect its function. Recently, there is a huge interest in re-engineering or improving the existing N95 mask, which can maximize the protection and can have antibacterial and antiviral properties [219-221].

Engineered silver (Ag) nanoparticles are reported to effectively inactivate bacteria without showing cytotoxicity [222]. In one recent report, researchers functionalized particulate respirator with Ag-NP by sodium oleate technique that could inhibit the growth of Staphylococcus Aureus and Pseudomonas Aeruginosa in real time [219].

Lately, we have successfully functionalized collagen membranes with $TiO_2$ at room temperature [169] and with Ag via ALD. Polypropylene (PP) and polyesters are being used as the main materials for the filter of N95 respirators [223]. The microstructure of such PP filter media is fibrous and similar to the microstructure of collagen membrane. In our earlier studies, coating collagen membrane with $TiO_2$ were successfully performed and documented [83, 169]. Our results showed that via ALD one can deposit uniform and conformal thin film of $TiO_2$ on the surface of fibrous collagen [169]. In the case of collagen membrane, $TiO_2$ ALD successfully functionalized the surface and made it biocompatible while promoting growth of osteoblastic and mesenchymal stem cells when compared to uncoated collagen [83].

Due to the complex 3D microstructure of the filters of the N95 mask (PP), ALD can be an effective technique to uniformly functionalize its surface, and engineer N95 masks (or help create other masks) with longer usage life and antibacterial and COVID19 inactivation properties. There are silver-containing materials/pads that are used for covering superficial wounds, minor burns, abrasions and lacerations (e.g., Silverlon™ [224]). Yet, such masks are not designed as PPE for clinical environment where the infection risk level is high since they do not provide a liquid barrier protection, therefore, they are not substitutes for surgical face masks. The aims of current study is to conduct the functionalization of N95 respirators by using ALD Ag with a recently patented ALD system [120, 225] achieving nanometer length scale films; to characterize the functionalized samples chemically and morphologically; and to obtain process – structure –

performance inter-relationships of the resulting systems.

## 2.4.2    Materials and Methods

N95 mask was cut into pieces and used as received. All ALD processes were done using a custom-built ALD reactor. A photograph and schematic of the linings representation of the ALD system is shown in Figure 31. Due to the nature of the precursor and the co-reactant that was used, the oxidizer line was shut down and the alternate pulse/purge of the silver precursor and borane complex from the bubblers was leading the ALD reaction.
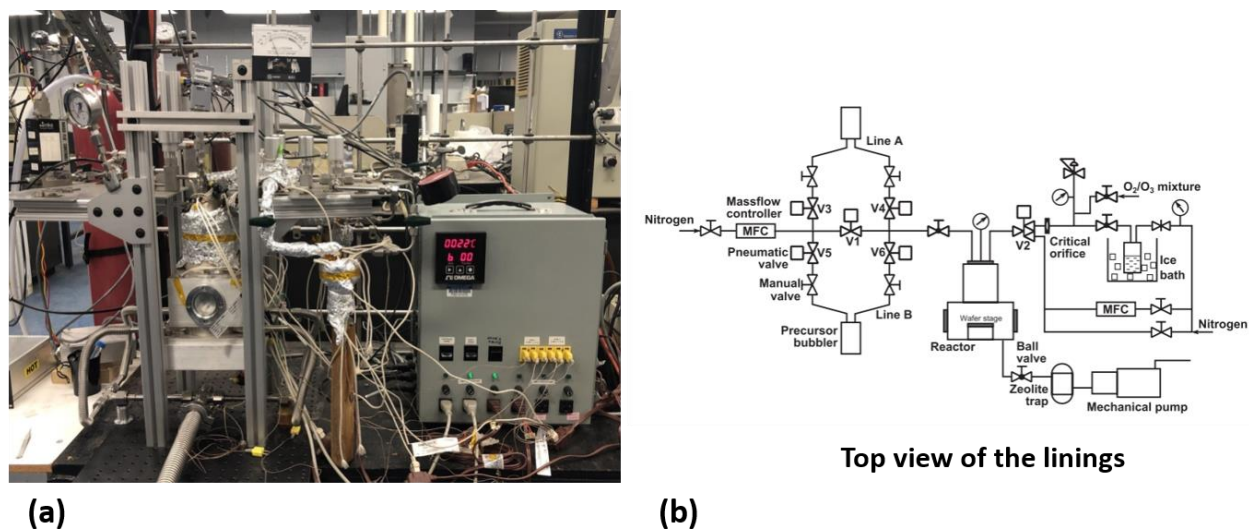


Figure 31: a) photograph of the custom-built ALD system, b) Schematic of the lining arrangements from top view [120].

Ag(fod)(Pet3) from Strem chemicals was used as the silver precursor and it was kept at 96 °C during all depositions. Borane dimethylamine complex $((CH_3)_2NH \cdot BH_3)$ from Sigma Aldrich was used as a reducing agent/co-reactant to react with Ag(fod)(Pet3) and leave deposited metallic silver on the substrate [151, 152, 161]. The borane bubbler was kept at 52 °C. Four groups of samples were prepared for this study on N95 filters: 1100 cycles Ag ALD deposited at 90 ˚C, 1500 cycles Ag ALD deposited at 90 ˚C, 1100 cycles Ag ALD deposited at 120 ˚C, and

1500 cycles Ag ALD deposited at 120 ˚C.

Residual gas analysis (RGA) was done to study the thermal stability of the N95 mask filter. RGA200 from Stanford Research System connected to Pfeiffer, TCP 015 was used for this purpose. For surface characterization, XPS (Kratos AXIS-165, from Kratos Analytical Ltd., United Kingdom) equipped with a monochromic Al K$\alpha$ (1486.6 eV) x-ray source operating at 15 kV and 10 mA. High resolution spectra of Ag 3d was collected using step size of 0.1 eV, and dwell time of 200 ms. Atomic force microscopy was done with WITEC-300RA Raman-AFM. Water contact angle (WCA) were conducted to study the surface wettability. A micro-syringe was used to place 5 µL of DI water droplet onto sample surfaces according to sessile drop method. To calculate the WCA values, captured photos were analyzed via "contact angle" Plugins of ImageJ software.

To test the effect of the developed surfaces on fabric respirators in controlling bacterial growth, the air-borne pathogen *Staphylococcus aureus* was used as a model strain for microbiological assay. For this, the experiment was carried out in triplicate in two separate occasion to investigate the effect of developed surfaces on both stages of bacterial adhesion to the substrate and biofilm formation (n = 6). Hence, prior to the experiments, *S. aureus* ATCC 14458 strain was grown on Mannitol Salt Agar (MSA, BD Difco) plates at 37 °C for 24 h. Then, loopfuls of MSA-grown colonies were inoculated into a tube containing 5 mL of sterilized Tryptic Soy Broth (TSB, BD Difco), and grown overnight aerobically at 37 °C [226]. After this period, overnight culture (1 mL) was added to 5 mL of fresh TSB and incubated until it had reached the exponential growth phase, with an optical density of 0.3 at 550 nm. Bacterial cells were then diluted 1:10 in TSB to approximate $10^7$ cells/mL. Subsequently, the fabric discs (6 mm in diameter) previously sterilized by autoclaving process (121 °C for 15 min) [219] were

placed in a 96-well microplate and aerobically incubated with the bacteria inoculum in TSB (1:10 v/v) for 2 h and 24 h at 37 °C. Finally, after each period of bacterial adhesion (2 h) and biofilm formation (24 h), the discs were gently washed in 0.9% NaCl, and a serial dilution of a vortexed suspension (0.9% NaCl, 1 min) [227] was plated in duplicate on Brain Heart Infusion agar (BD Difco). The agar plates were incubated aerobically at 37 °C for 24 h for colony-forming unit (CFU) counts. Data were expressed as the logarithm of CFU per milliliter (log10 CFU/mL), and the antibacterial efficiency of the biofilm-formed samples was calculated using eq 1 [228]:

$$R = \frac{(B-A) \times 100}{B} \%$$ (1)

where R is the ratio of bacteria reduction (%), A is the mean number of viable bacteria colonies after contacting with uncoated control fabric, and B is the mean number of viable bacteria colonies after contacting with coated fabric samples.

### 2.4.3 Results and Discussions

Silver ALD was conducted on silicon wafer substrate and N95 mask filter. Chemical analysis of the deposited silver was probed with x-ray photoelectron spectroscopy (XPS). Surface morphology was characterized using atomic force microscopy (AFM).
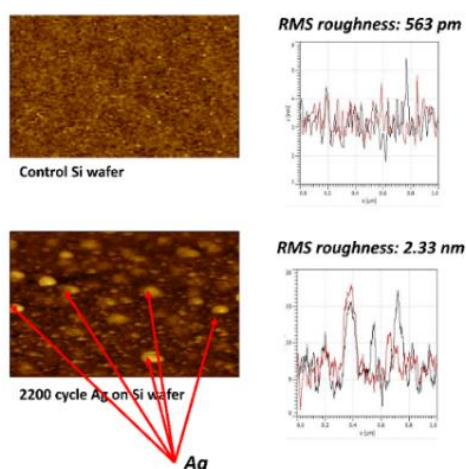
Figure 32: AFM images of pristine Si wafer sample (top-left), Ag coated Si wafer (bottom-left) roughness profile of pristine Si wafer (top-right), and roughness profile of Ag coated Si wafer (bottom-right).

As it can be clearly seen in Figure 32, silver particulated thin film was successfully deposited on Si wafer and changed the surface topography and roughness of the substrate. Data showed that after silver deposition, the roughness of the surface increased from 563 pm for pristine Si wafer to 2.33 nm after silver ALD; this is attributed to the island growth of silver on the surface.

Our results suggested that thermal ALD of silver was successfully done on Si wafer sample. These Ag ALD processing conditions can be expanded to N95 filter media. But before that, potential thermal degradation of PP at 120 ˚C was investigated prior to silver deposition. For atomic mass of 16 (potential methane), 14 (potential -$CH_2$-), and 12 (potential C), after about 1 hour degassing at 120 ˚C, the background and sample data showed similar trend; for atomic mass of 15 (potential -$CH_3$), the pressure is lower than $2 * 10^{-11}$ torr, which suggested that any potential release of atomic mass 15 is negligible. Comparing the residual gas data of the background and the as received N95 filter sample at 120 ˚C, RGA results suggested that 1.0 hour of degassing is sufficient prior to silver deposition at 120 ˚C (Figure 33).
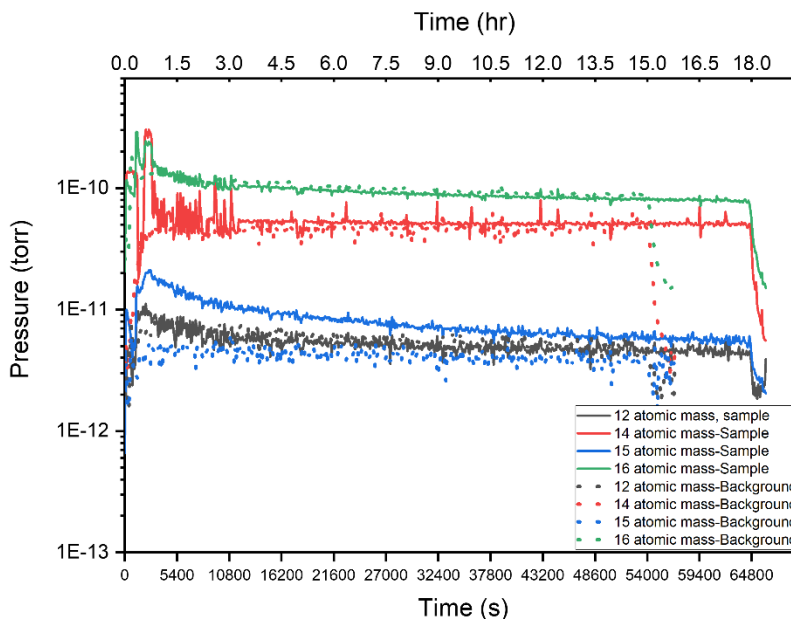
Figure 33: RGA of N95 mask filter media at 120 ˚C, for atomic mass number of 12, 14, 15, and 16. Scatter points are the background data, lines relates to the N95 filter media.

PP is hydrocarbon and its molecular structure consists of carbon (C) and hydrogen (H) atoms (Figure 34a). XPS of the pristine N95 mask was done prior to the Ag deposition. As it can be seen in Figure 34d, XPS of pristine N95 filter media shows C-C bond (from the backbone of the polypropylene chain) at 285.0 eV which is consistent with literature results [229]. This N95 filter has not been washed prior to deposition and used as received, therefore, the O 1s peak at 529.2 eV could in part be related to ambient contamination (Figure 34d). After 1500 cycles ALD on N95 mask, in addition to the 2 peaks of pristine N95, the silver peak (Ag 3d) was observed on the top layer of the N95 mask. As presented in Figure 34d, the results on the mid-layer of N95 mask show that, due to the fibrous nature of the N95 filter media, silver was able to infiltrate into the bottom layer and also coat the mid-layer. We previously reported such infiltration in our study on another polymer [230]. Yellow color of the samples after silver ALD (Figure 34c) is another physical evidence for the formation of un-aggregated silver nanoparticles [202, 203].
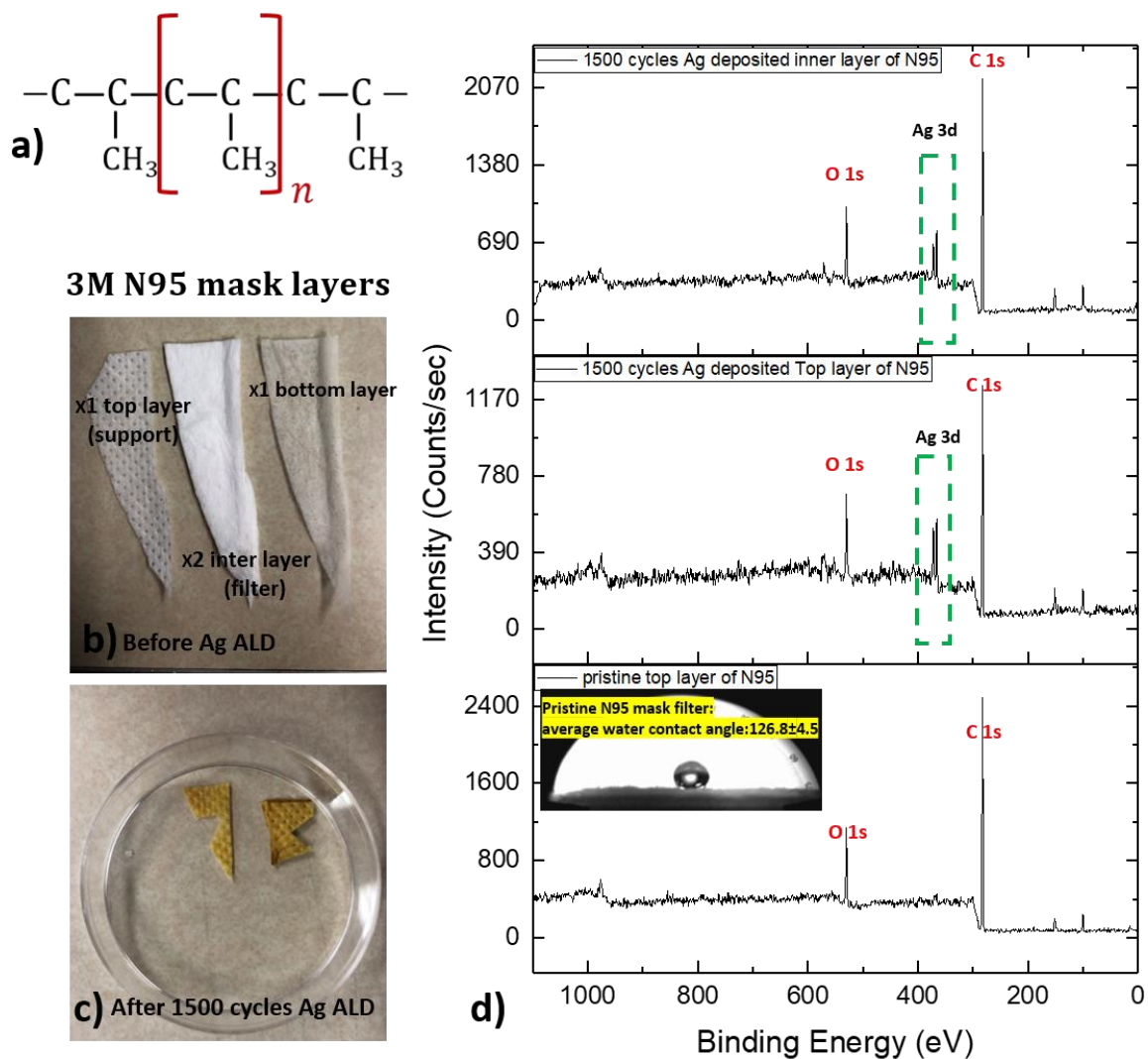
Figure 34: a) Molecular structure of polypropylene (PP), b) layers of N95 mask before ALD (3M), c) pieces of N95 mask after silver ALD, d) XPS spectra on N95 filter media as received N95 filter media b) 1500 cycle Ag ALD on N95 top layer, c)1500 cycle Ag ALD on N95 mid-layer. ALD processing conditions: operating pressure of 800 mTorr, precursor pulse/purge time 3 s/5 s and reducing agent pulse/purge time 2 s/10 s, respectively.

Generally, the respirators in the market do not have antibacterial properties and using them beyond their service life shows lower efficiency and provides a suitable environment for growth and proliferation of bacteria, especially on the mid-layer [219]. Therefore, it is highly preferable to focus on the N95 mid-layer filter for silver treatment to promote its antibacterial

properties. XPS results of the silver deposition on N95 mid-layer are presented in Figure 35; high resolution Ag 3d is also included. Due to lack of polar components in the chemical formula of PP, N95 filter is hydrophobic in nature with 126.8±4.5 degrees, which is in good agreement with WCA reported in the literature for the melt blown N95 filter [231].
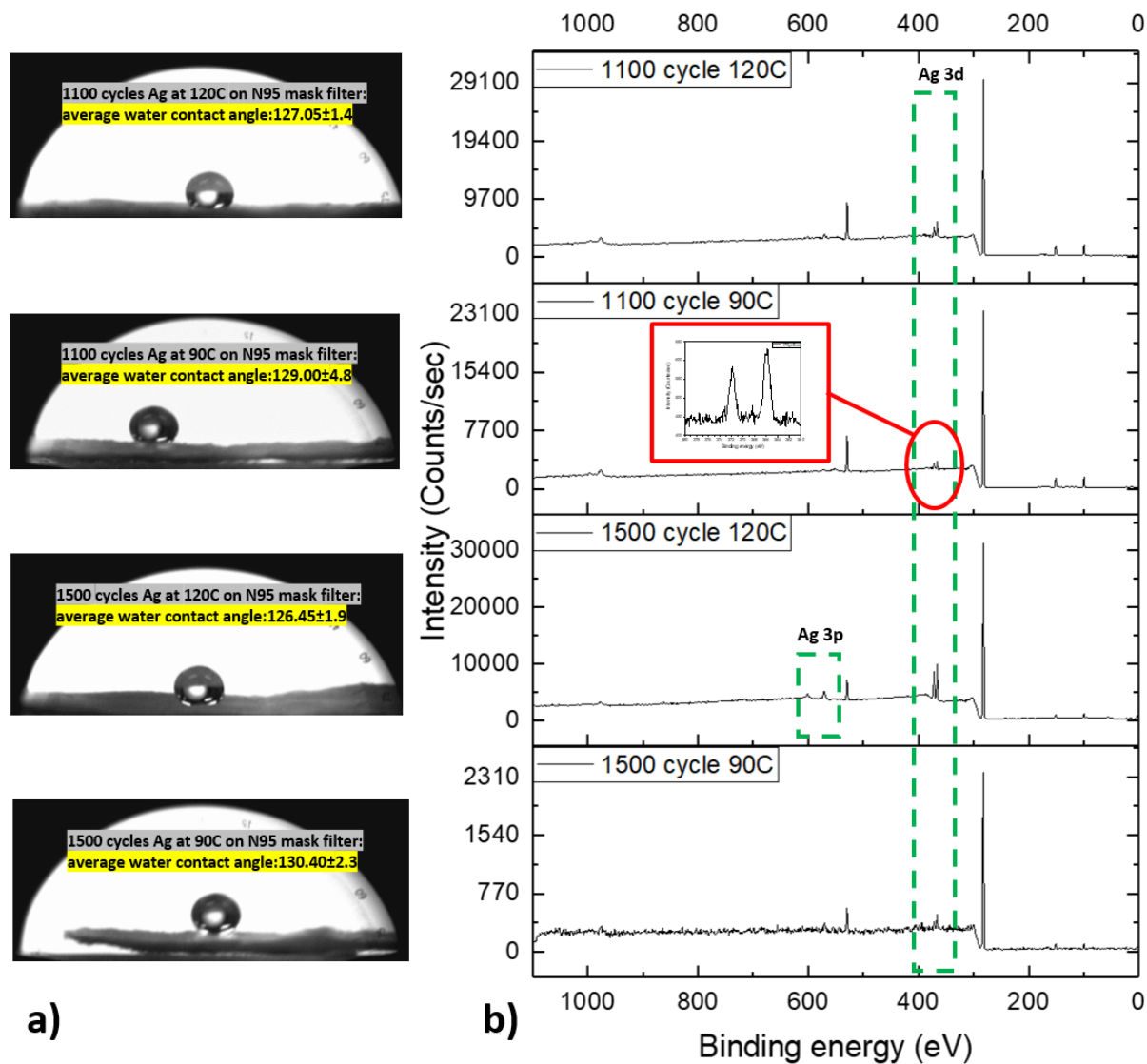


Figure 35: a) Water contact angle measurements of four groups of Ag coated N95 mask filter, b) XPS spectra of silver ALD on mid-layer of N95 mask and high resolution Ag 3d peak on mid-layer N95 for sample which was functionalized at 90 ˚C and 1100 cycle counts of Ag ALD.

XPS analysis confirmed the formation of silver on the filter media of N95 on all the four groups of samples: 1100 cycles Ag deposited at 90 ˚C, 1100 cycles Ag deposited at 120 ˚C, 1500 cycles Ag deposited at 90 ˚C, and 1500 cycles Ag deposited at 120 ˚C. As presented in the survey spectra, in addition to O and C, silver peak (Ag 3d) was observed on all our samples. 3p peak is typically less intense than 3d, therefore, comparing samples which were fabricated at 120 ˚C with samples which prepared at 90 ˚C, due to higher intensity of Ag 3d, less intense Ag 3p was also observable, but for samples which were fabricated at 90 ˚C, due to the less intense Ag 3d compared to 120 ˚C samples, Ag 3p might have been buried under the noise (Figure 35b).

Our SEM results on collagen membrane (which has similar microstructure to N95 filter) (Figure 27) showed that silver ALD resulted uniformly distributed silver nanoparticles on the surface and below surface. Expanding this morphology to the nonwoven PP (N95 filter) suggests that this micro/nanostructure would be preferable for respiratory filters since it does not block the flow of the air during inhalation and exhalation process.

**2.4.3.1 <u>Wash test</u>**

Our proposed practical method to study the adherence of Ag ALD particulates to N95 filter media is washing test. Sample with 1500 cycles Ag deposited at 120 ˚C was selected for wash test. Two washing methods (normal wash with running DI water and washing under sonication in DI water) each one for 1 minute and 10 minutes were chosen. To investigate the stability of Ag particulates on N95 filter media, XPS characterization was done and compared for functionalized samples before and after wash test. Our washing results (Figure 36) revealed that neither washing with running DI water nor sonication in DI negatively affected the adhesion between particulated Ag ALD deposited on N95 filter media.
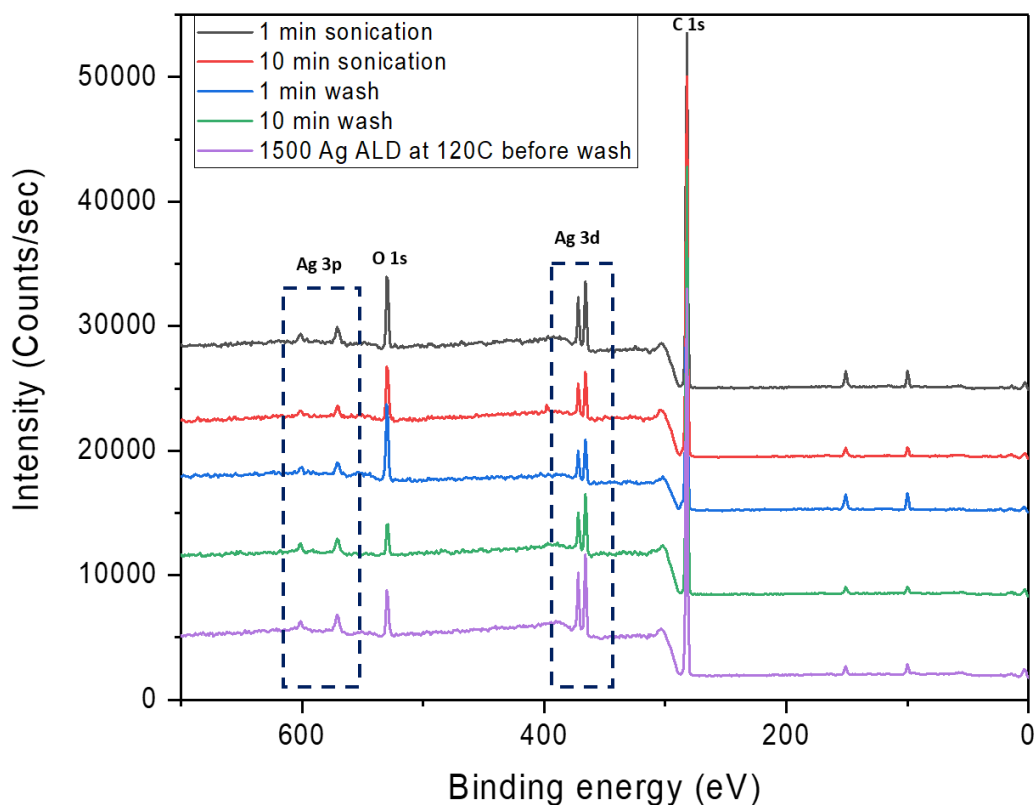
Figure 36: XPS of the functionalized sample with 1500 cycles Ag ALD at 120 °C before wash test and after 1 minute and 10 minutes washing with running water and washing under sonication.

## 2.4.3.2 Bacterial adhesion behavior and antibacterial properties of Ag-coated fabrics dependent on treatment parameters

Because surface properties are known to influence bacterial attachment behavior, we investigated whether the modification of the respirator fabric surfaces with different silver ALD treatment parameters would influence the bacterial adhesion (2 h) of the air-borne pathogen *S. aureus*. Interestingly, when the surface treatment was performed at 120 °C a statistically significant increase on bacterial adhesion was observed for both Ag ALD number of cycles: 1100 ($p < 0.01$) and 1500 ($p < 0.0001$) compared to the control group. These fabric surfaces also showed higher *S. aureus* loads compared to those functionalized at 90 °C ($p < 0.05$). Conversely,

no significant difference in viable cell count was noted between control and the groups treated at 90°C for 1100 cycles (p = 0.9987) and 1500 cycles (p = 0.9866); this suggests that at initial stages of biofilm development these surfaces had no effect on the adherence of bacterial cells to the fabric samples (Figure 37A).

Once the biofilm buildup begins with the bacterial adhesion to the surface and it is followed by the co-aggregation and proliferation of bacterial cells into cell clusters, an approach providing an antibacterial control during this time would be of great relevance to respirator wearers' health. Thus, to further evaluate the antibacterial properties of the developed surfaces under biofilm establishment, it was investigated by CFU counts after a culture period of 24 h. As shown in Figure 37B, for the sample which functionalized at 120°C for 1500 cycles, surface continued allowing more S. aureus to adhere and proliferate than the control group (p < 0.001). In contrast, all other experimental surfaces reduced the average viable CFU counts. According to the microbiological results, besides the 1100 cycles deposited at 90°C does not influence 2 h bacterial adhesion, it was also able to significantly reduce the viable bacterial count after 24 h of biofilm development than the control surface (p < 0.01). Quantitatively, the S. aureus CFU content was reduced by about 76%. Altogether, it indicates that the sample which functionalized for 1100 Ag ALD cycles at 90°C surface was potent for maintain initial bacteria adherence and suppress subsequent biofilm formation.
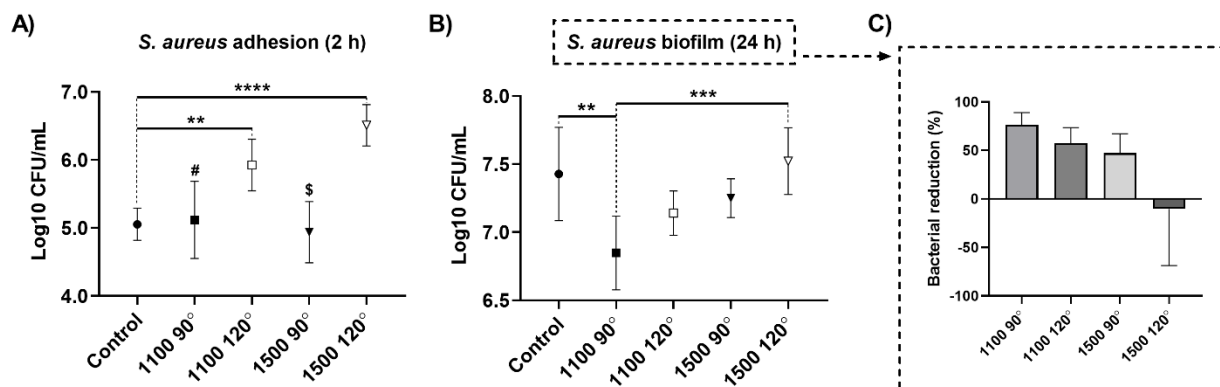
Figure 37: Microbiological assay for control and experimental samples using S. aureus. (A) Average CFU counts (log10 CFU/mL) after 2 hours of testing bacterial adhesion and (B) 24 hours of testing biofilm formation on surfaces. (C) Bacterial reduction (%) demonstrate the antibacterial efficiency of treated surfaces in relation to control against S. aureus in 24 h biofilm. **$p < 0.01$, ***$p<0.001$, and ****$p < 0.0001$, using Tukey HSD test. In panel A, # indicate significant differences between 1100 90°C vs. 1100 120°C ($p < 0.05$) and 1500 120°C ($p < 0.0001$), and $ indicate significant differences between 1500 90°C vs. 1100 120°C ($p < 0.01$) and 1500 120°C ($p < 0.0001$). The error bars indicate standard deviations.

Considering XPS and antibacterial data, results showed improvement in suppressing the biofilm formation on samples with smaller size silver which was deposited at 90 °C for 1100 ALD cycles. Ag is well known for its antimicrobial effect; however, it depends on the type of the microorganism, different antibacterial characteristics were reported for it. It has been reported that Ag effectively suppressed E. coli and yeast growth, while for S. aureus there are some studies which showed that the inhibitory effect reported to be mild to not effective [232, 233]. Thicker membrane wall of S. Aureus was reported to be the reason of such resistance. Different mechanisms are proposed for antibacterial activity of silver, some reported that positive charge on $Ag^+$ is responsible for Ag antimicrobial activity [234, 235]. It is also mentioned that the ability of Ag in "pits" formation on the cell membrane is the crucial factor [236]. Smaller particles have a larger surface area per unit mass and can diffuse easier through the membrane wall destroying the internal cellular components of bacteria. According to our proposed

mechanism in Figure 29, lower number of cycles (in this case 1100 cycle) resulted in smaller size silver particulates on the surface and consequently more effective against biofilm formation after 24 hours.

### 2.4.4   Conclusion

The current study presented a successful silver functionalization method on non-woven PP. Ag metal particulated thin film was deposited on filter on N95 mask using Ag(fod)(Pet3) precursor and borane complex reducing agent. The deposition process was ALD. This method is solvent free and efficient in achieving respirators without blocking the pores and negatively affecting air permeability of the mask. The potential application of such Ag ALD coated filter media can be as antibacterial wound dressings, face masks or other PPEs with the target of longer-term service life.

# 3      CONSCLUSION AND FUTURE WORK

Section 3.1 was previously published as Hashemi Astaneh, S., Faverani, L., Sukotjo, C., Takoudis, C.G., Atomic layer deposition on dental materials: processing conditions and surface functionalization to improve physical, chemical, and clinical properties- A Review (2021) <u>Acta Biomaterialia</u>, 121, 103-118.

## 3.1 <u>Conclusion</u>

The translation of newly developed biomaterial can be categorized as the following four stages [237]:

Stage 1: fabrication of the material, microstructure characterizations, physical and mechanical properties.

Stage 2: In vitro tests for different cell types, cytotoxicity, genotoxicity.

Stage 3: In vivo implantation to study tissue viability, histology, and inflammatory effects.

Stage 4: Human trials for clinical feasibility and efficiency.

The ALD-fabricated materials, which were designed for dental applications or can be considered as a potential candidate for clinical practice, are summarized in Table I- IV. The type of the study and the bottom line of each research is presented in there as well.

According to Table I-IV, the majority of the proposed ALD coated materials showed promising properties at stage 1. Some of the studies reached stage 2 (in vitro tests) and in the specific cell and bacteria environment, showed improvement. However, the number of in vivo studies (stage 3) is rare, therefore this part has great potential for defining new projects and future studies. Depending on the material system, using Table I-IV of this work, one can find a good starting point for recommending processing conditions, and favorable microstructure for reaching tunable in vitro results. Also, within our efforts for new materials, new cell and bacteria environments can always be considered for future studies. There is a wide range of dental

material which were so far coated via ALD. Possible clinical applications of ALD-coated materials are like pristine materials but with improved properties. For instance, in the case of metal substrates (e.g., dental implants) coating them with different ALD films showed different improvements: better osteointegration properties, improved osteoblast compatibility, improved antibacterial properties, and improved corrosion properties. In the case of polymeric dental materials, similar improvement in properties is expected; for example, $TiO_2$-coated collagen membranes can enhance the bone growth properties and antibacterial activities. ALD coated polymeric dentures can result in better mechanical properties, and improved wear resistance and antibacterial properties. ALD coated maxillofacial prostheses could yield improved aging properties and more stable color.

Theoretically, ALD technique imposes outstanding properties: reduction in the chance of infection, reduction in the chance of second surgeries, and improvements in the pace of healing for dental materials that are being used in the body. For materials that are being used for external applications, longevity improvement in clinical practice is the outcome of ALD thin film on those materials. With all these potential clinical applications mentioned above, more effort is needed to move forward to stages 3 and 4 and study the long-term property changes in vivo and in the human body. Also, safety concerns in terms of potential cytotoxic and inflammatory responses in clinical use needs to be more investigated. Another noteworthy idea for future work can be on dental materials which are subject to mechanical stresses like fatigue and wear. The risk of delamination and the consequent biocompatibility concerns need to be studied in detail.

## 3.2 Future Work

### 3.2.1  Silver ALD on Ti alloy and PDMS

As presented in introduction of this thesis, Ti alloys and PDMS are two of the materials

which have numerous applications in biomedical field of science. Deposition of silver is of interest. Our preliminary results of silver deposition on PDMS and Ti is presented in Appendix B which can be an informative starting point for further future studies on these substrates.

### 3.2.2 Animal Studies of ALD-Ag Collagen

Silver coated collagen was achieved in this thesis. This type of collagen is being used as bone growth agent in dental surgeries, and this is its major application. Invivo bioactivity involving animal tests needs to be done to assess the antibacterial activity, bone regeneration capability, toxicity, and side effects of the silver functionalized collagen.

### 3.2.3 Copper ALD on N95 mask

In the context of functionalized face mask, to improve the performance of N95 mask against COVID19, it is reported that metal copper showed outstanding properties in inactivating HuCoV-229E virus [238]. In this thesis, functionalization of N95 mask with Ag metal was achieved in order to deposit antibacterial functional agents on N95 filter without blocking the pores of the filter media. Copper ALD on N95 mask can also be applied to study and potential development of N95 mask (or any other type) with antivirus properties.

For copper atomic layer deposition on PPEs, including N95 mask, which are mostly made of polymers, one should be careful with the choice of processing conditions such as temperature. We have recently done a review on Cu ALD and successful precursor/co-reactant systems and processing temperatures; Cu ALD systems are presented in Table VII; considering the melting and degradation temperature of typical PPE materials, low temperature processes should be considered.

## Table VII: Summary of Cu ALD precursors and processing temperature window

| Year | Journal | Deposited Film | Precursor | T-window (°C) | Growth rate (Å/cycle) |
|---|---|---|---|---|---|
| **Efficient Process for Direct Atomic Layer Deposition of Metallic Cu Thin Films Based on an Organic Reductant [239]** |||||| 
| 2017 | Chemistry of materials | Cu | Cu(acac)2-$H_2O$/ HQ | 170-230 | 2 |
| **Low Temperature Growth of High Purity, Low Resistivity Copper Films by Atomic Layer Deposition [179]** |||||| 
| 2011 | Chemistry of materials | Cu | Cu- (OCHMeCH2NMe$_2$)$_2$ (1), formic acid, and hydrazine | 110-160 | 0.5 |
| **Atomic Layer Deposition of Ultrathin Copper Metal Films from a Liquid Copper(I) Amidinate Precursor [240]** |||||| 
| 2006 | J. of the Electrochemical society | Cu | copper_I_ N,N_-di-sec-butylacetamidinate, and molecular hydrogen gas as the reducing agent. | 150-190 | On SiO2, Si3N4: 1.5-2 On Ru,Cu,Co: 0.1-0.5 |
| **Atomic layer chemical vapor deposition of copper [241]** |||||| 
| 2004 | Materials sci. in semiconductor | Cu On Si/SiO$_2$ Glass TiN coated Si | bis[2,2,6,6-tetramethyl-3,5-heptadionato] Cu(II), Cu(thd)2/ UHP hydrogen | 350 | 2 |
| **Investigation of AlMe3, BEt3, and ZnEt2 as Co-Reagents for Low-Temperature Copper Metal ALD/Pulsed-CVD [178]** |||||| 
| 2010 | Chem. Mater. | Cu on Ruthenium SiO$_2$ | [CuL2] / ZnEt2 L=acetylacetonate (acac; 1), hexafluoroacetylacetonate (hfac; 2), N-isopropyl-β-ketiminate (acnac; 3), N,N-dimethyl-β-diketiminate (nacnac; 4), 2-pyrrolylaldehyde (PyrAld; 5), N-isopropyl-2-pyrrolylaldiminate (PyrImiPr; 6a), N-ethyl-2-pyrrolylaldiminate (PyrImEt; 6b), and N-isopropyl-2-salicylaldiminate (IPSA; 7) | 130-150 | 0.1 |
| **Low-Temperature Atomic Layer Deposition of Copper Metal Thin Films: Self-Limiting Surface Reaction of Copper Dimethylamino-2-propoxide with Diethylzinc [242]** |||||| 
| 2009 | communications | Cu On patterned alkyl siloxane (SAMs) | [Cu(dmap)2] / Et2Zn | 100-120 | 0.2 |
| **Low-Temperature Atomic Layer Deposition of Copper Films Using Borane Dimethylamine as the Reducing Co-reagent [151]** |||||| 
| 2014 | Chemistry of materials | Cu On Ru | Cu(OCHMeCH2NMe$_2$)$_2$/ BH3(NHMe$_2$) | 130-160 | 0.13 |

| | | | | | |
|---|---|---|---|---|---|
| **Low-Temperature Atomic Layer Deposition of Copper Films Using Borane Dimethylamine as the Reducing Co-reagent [151]** | | | | | |
| **2 0 1 4** | **Chemistry of materials** | **Cu On Pd & Pt** | $Cu(OCHMeCH2NMe_2)_2$/formic acid/$BH_3(NHMe_2)$ | **135-165** | **0.2** |
| **Copper reduction and atomic layer deposition by oxidative decomposition of formate by hydrazine [243]** | | | | | |
| **2 0 1 4** | communication | **Cu** | Cu(+1)(dmap) /Formate /hydrazine | | |
| **Atomic layer deposition of copper nitride film and its application to copper seed layer for electro deposition [244]** | | | | | |
| **2 0 1 4** | **The solid thin films** | **Cu On Si & Ru** | bis(1-dimethylamino-2-methyl-2-butoxy)copper(II) and NH3 and reduced tometallic copper film by annealing at 200 °C or higher | **100-140 Anneal at 200** | **0.8** |

# CITED LITERATURE

1.      Rasouli, R., A. Barhoum, and H. Uludag, *A review of nanostructured surfaces and materials for dental implants: surface coating, patterning and functionalization for improved performance.* Biomaterials Science, 2018. **6**(6): p. 1312-1338.

2.      Gaviria, L., et al., *Current trends in dental implants.* J Korean Assoc Oral Maxillofac Surg, 2014. **40**(2): p. 50-60.

3.      Makvandi, P., et al., *Polymeric and inorganic nanoscopical antimicrobial fillers in dentistry.* Acta Biomaterialia, 2020. **101**: p. 69-101.

4.      Kadiyala, U., et al., *Unexpected insights into antibacterial activity of zinc oxide nanoparticles against methicillin resistant Staphylococcus aureus (MRSA).* Nanoscale, 2018. **10**(10): p. 4927-4939.

5.      Din, M.I., et al., *Green Adeptness in the Synthesis and Stabilization of Copper Nanoparticles: Catalytic, Antibacterial, Cytotoxicity, and Antioxidant Activities.* Nanoscale Research Letters, 2017. **12**(1): p. 638.

6.      Rodrigues, C.T., et al., *Antibacterial properties of silver nanoparticles as a root canal irrigant against Enterococcus faecalis biofilm and infected dentinal tubules.* International Endodontic Journal, 2018. **51**(8): p. 901-911.

7.      Yao, C., E.B. Slamovich, and T.J. Webster, *Enhanced osteoblast functions on anodized titanium with nanotube-like structures.* Journal of Biomedical Materials Research Part A, 2008. **85A**(1): p. 157-166.

8.      Bosco, R., et al., *Surface Engineering for Bone Implants: A Trend from Passive to Active Surfaces.* Coatings, 2012. **2**: p. 95-119.

9.      Matykina, E., et al., *Transmission electron microscopy of coatings formed by plasma electrolytic oxidation of titanium.* Acta Biomaterialia, 2009. **5**(4): p. 1356-1366.

10.     Li, P.H. and P.K. Chu, *1 - Thin film deposition technologies and processing of biomaterials*, in *Thin Film Coatings for Biomaterials and Biomedical Applications*, H.J. Griesser, Editor. 2016, Woodhead Publishing. p. 3-28.

11.     Roy, P., S. Berger, and P. Schmuki, *TiO2 Nanotubes: Synthesis and Applications.* Angewandte Chemie International Edition, 2011. **50**(13): p. 2904-2939.

12.     Yang, B., et al., *Preparation of bioactive titanium metal via anodic oxidation treatment.* Biomaterials, 2004. **25**(6): p. 1003-1010.

13.     Lee, B.-H., et al., *In vivo behavior and mechanical stability of surface-modified titanium implants by plasma spray coating and chemical treatments.* Journal of Biomedical

Materials Research Part A, 2004. **69A**(2): p. 279-285.

14.     Baryshnikova, M., et al., *Formation of hydroxylapatite on CVD deposited titania layers.* physica status solidi c, 2015. **12**(7): p. 918-922.

15.     Arbenin, A.Y., et al., *Characteristics of the synthesis of TiO2 films on a titanium surface by the sol-gel technique.* Russian Journal of General Chemistry, 2014. **84**(12): p. 2453-2454.

16.     Chen, X. and S.S. Mao, *Titanium Dioxide Nanomaterials: Synthesis, Properties, Modifications, and Applications.* Chemical Reviews, 2007. **107**(7): p. 2891-2959.

17.     George, S.M., *Atomic Layer Deposition: An Overview.* Chemical Reviews, 2010. **110**(1): p. 111-131.

18.     Doll, G.L., et al., *Chemical Vapor Deposition and Atomic Layer Deposition of Coatings for Mechanical Applications.* Journal of Thermal Spray Technology, 2010. **19**(1): p. 510-516.

19.     Johnson, R.W., A. Hultqvist, and S.F. Bent, *A brief review of atomic layer deposition: from fundamentals to applications.* Materials Today, 2014. **17**(5): p. 236-246.

20.     Fraga, M. and R. Pessoa, *Progresses in Synthesis and Application of SiC Films: From CVD to ALD and from MEMS to NEMS.* Micromachines, 2020. **11**.

21.     Oviroh, P.O., et al., *New development of atomic layer deposition: processes, methods and applications.* Science and Technology of Advanced Materials, 2019. **20**(1): p. 465-496.

22.     Muñoz-Rojas, D., et al., *Spatial Atomic Layer Deposition, Chemical Vapor Deposition for Nanotechnology*. 2019.

23.     Leskelä, M. and M. Ritala, *Atomic layer deposition (ALD): from precursors to thin film structures.* Thin Solid Films, 2002. **409**(1): p. 138-146.

24.     Puurunen, R.L., *A Short History of Atomic Layer Deposition: Tuomo Suntola's Atomic Layer Epitaxy.* Chemical Vapor Deposition, 2014. **20**(10-11-12): p. 332-344.

25.     Bishal, A.K., et al., *Atomic Layer Deposition in Bio-Nanotechnology: A Brief Overview.* 2015. **43**(4): p. 255-276.

26.     Groner, M.D., et al., *Low-Temperature Al2O3 Atomic Layer Deposition.* Chemistry of Materials, 2004. **16**(4): p. 639-645.

27.     Klaus, J.W., O. Sneh, and S.M. George, *Growth of SiO2 at Room Temperature with the Use of Catalyzed Sequential Half-Reactions.* Science, 1997. **278**(5345): p. 1934.

28.     Shahmohammadi, M., B. Yang, and C.G. Takoudis, *Applications of Titania Atomic Layer Deposition in the Biomedical Field and Recent Updates.* American Journal of Biomedical Science & Research, 2020. **8**(6): p. 465-4658.

29.     Leppäniemi, J., et al., *Non-stick properties of thin-film coatings on dental-restorative instruments.* European journal of oral sciences, 2017. **125**(6): p. 495-503.

30.     Lin, H.-C., et al., *Atomic Layer Deposited Al2O3 Films on NiTi Shape Memory Alloys for Biomedical Applications.* Procedia Manufacturing, 2019. **37**: p. 431-437.

31.     Zhang, J., et al., *Conformal oxide nanocoatings on electrodeposited 3D porous Ni films by atomic layer deposition.* Journal of Materials Chemistry C, 2016. **4**(37): p. 8655-8662.

32.     Bae, C., H. Shin, and K. Nielsch, *Surface modification and fabrication of 3D nanostructures by atomic layer deposition.* MRS Bulletin, 2011. **36**(11): p. 887-897.

33.     Lautenschlager, E.P. and P. Monaghan, *Titanium and titanium alloys as dental materials.* International dental journal, 1993. **43**(3): p. 245-253.

34.     Silva-Bermudez, P. and S.E. Rodil, *An overview of protein adsorption on metal oxide coatings for biomedical implants.* Surface and Coatings Technology, 2013. **233**: p. 147-158.

35.     Bilo, F., et al., *Atomic layer deposition to prevent metal transfer from implants: An X-ray fluorescence study.* Applied Surface Science, 2015. **359**: p. 215-220.

36.     Nazarov, D.V., et al., *Formation of Micro- and Nanostructures on the Nanotitanium Surface by Chemical Etching and Deposition of Titania Films by Atomic Layer Deposition (ALD).* Materials (Basel, Switzerland), 2015. **8**(12): p. 8366-8377.

37.     Dobrzanski, L., et al., *Atomic layer deposition of TiO2 onto porous biomaterials.* 2015. **75**: p. 5-11.

38.     Dobrzanski, L., et al., *Metallic skeletons as reinforcement of new composite materials applied in orthopaedics and dentistry.* Archives of Materials Science and Engineering, 2018. **2**: p. 53-85.

39.     Dobrzański, L.A., et al. *Structure and Properties of the Skeleton Microporous Materials with Coatings Inside the Pores for Medical and Dental Applications*. in *Frontiers in Materials Processing, Applications, Research and Technology*. 2018. Singapore: Springer Singapore.

40.     Liu, L., R. Bhatia, and T.J. Webster, *Atomic layer deposition of nano-TiO2 thin films with enhanced biocompatibility and antimicrobial activity for orthopedic implants.* Int J Nanomedicine, 2017. **12**.

41. Grigal, I.P., et al., *Correlation between bioactivity and structural properties of titanium dioxide coatings grown by atomic layer deposition.* Applied Surface Science, 2012. **258**(8): p. 3415-3419.

42. Solovyev, A.A., et al., *Correlation between structural and bioactive properties of titanium dioxide formed by atomic layer deposition.* Nanotechnologies in Russia, 2013. **8**(5): p. 388-391.

43. Alekhin, A.P., et al., *Atomic layer deposition of thin films of titanium dioxide from titanium tetramethoxide and water.* Russian Journal of Applied Chemistry, 2013. **86**(3): p. 326-331.

44. Daugaard, H., et al., *The effect on bone growth enhancement of implant coatings with hydroxyapatite and collagen deposited electrochemically and by plasma spray.* Journal of biomedical materials research. Part A, 2010. **92**(3): p. 913-921.

45. Radtke, A., et al., *Titania Nanotubes/Hydroxyapatite Nanocomposites Produced with the Use of the Atomic Layer Deposition Technique: Estimation of Bioactivity and Nanomechanical Properties.* Nanomaterials (Basel, Switzerland), 2019. **9**(1): p. 123.

46. Putkonen, M., et al., *Atomic layer deposition and characterization of biocompatible hydroxyapatite thin films.* Thin Solid Films, 2009. **517**(20): p. 5819-5824.

47. Gittens, R.A., et al., *The roles of titanium surface micro/nanotopography and wettability on the differential response of human osteoblast lineage cells.* Acta Biomaterialia, 2013. **9**(4): p. 6268-6277.

48. Olivares-Navarrete, R., et al., *Direct and indirect effects of microstructured titanium substrates on the induction of mesenchymal stem cell differentiation towards the osteoblast lineage.* Biomaterials, 2010. **31**(10): p. 2728-2735.

49. Padial-Molina, M., et al., *Role of wettability and nanoroughness on interactions between osteoblast and modified silicon surfaces.* Acta Biomaterialia, 2011. **7**(2): p. 771-778.

50. Basiaga, M., et al., *Evaluation of physicochemical properties of surface modified Ti6Al4V and Ti6Al7Nb alloys used for orthopedic implants.* Materials Science and Engineering: C, 2016. **68**: p. 851-860.

51. Patel, S., et al., *Novel functionalization of Ti-V alloy and Ti-II using atomic layer deposition for improved surface wettability.* Colloids and Surfaces B: Biointerfaces, 2014. **115**: p. 280-285.

52. Kang, H., et al., *Photocatalytic effect of thermal atomic layer deposition of TiO2 on stainless steel.* Applied Catalysis B: Environmental, 2011. **104**(1): p. 6-11.

53. Pantaroto, H.N., et al., *Antibacterial photocatalytic activity of different crystalline TiO2*

*phases in oral multispecies biofilm.* Dental Materials, 2018. **34**(7): p. e182-e195.

54. Marin, E., et al., *Multilayer Al2O3/TiO2 Atomic Layer Deposition coatings for the corrosion protection of stainless steel.* Thin Solid Films, 2012. **522**: p. 283-288.

55. Radi, P.A., et al., *Tribocorrosion behavior of TiO2/Al2O3 nanolaminate, Al2O3, and TiO2 thin films produced by atomic layer deposition.* Surface and Coatings Technology, 2018. **349**: p. 1077-1082.

56. Kassapidou, M., et al., *Cobalt-chromium alloys in fixed prosthodontics in Sweden.* Acta biomaterialia odontologica Scandinavica, 2017. **3**(1): p. 53-62.

57. Bhaskar, V. and V. Subba Reddy, *Biodegradation of nickel and chromium from space maintainers: An in vitro study.* J Indian Soc Pedod Prev Dent, 2010. **28**(1): p. 6-12.

58. Ziębowicz, A., et al., *The effect of atomic layer deposition of ZrO2 on the physicochemical properies of cobalt based alloys intended for prosthetic dentistry.* Archives of Metallurgy and Materials, 2018. **63**: p. 1077-1082.

59. Plecko, M., et al., *Osseointegration and biocompatibility of different metal implants--a comparative experimental investigation in sheep.* BMC musculoskeletal disorders, 2012. **13**: p. 32-32.

60. Gotman, I., *Characteristics of Metals Used in Implants.* Journal of Endourology, 1997. **11**(6): p. 383-389.

61. Shan, C.-X., X. Hou, and K.-L. Choy, *Corrosion resistance of TiO2 films grown on stainless steel by atomic layer deposition.* Surface and Coatings Technology, 2008. **202**: p. 2399–2402.

62. Yang, Q., et al., *Atomic layer deposited ZrO2 nanofilm on Mg-Sr alloy for enhanced corrosion resistance and biocompatibility.* Acta Biomaterialia, 2017. **58**: p. 515-526.

63. Testoni, G.E., et al., *Influence of the Al2O3partial-monolayer number on the crystallization mechanism of TiO2in ALD TiO2/Al2O3nanolaminates and its impact on the material properties.* Journal of Physics D: Applied Physics, 2016. **49**(37): p. 375301.

64. Li, J., et al., *Balancing Bacteria–Osteoblast Competition through Selective Physical Puncture and Biofunctionalization of ZnO/Polydopamine/Arginine-Glycine-Aspartic Acid-Cysteine Nanorods.* ACS Nano, 2017. **11**(11): p. 11250-11263.

65. Zhu, Y., et al., *Biofunctionalization of carbon nanotubes/chitosan hybrids on Ti implants by atom layer deposited ZnO nanostructures.* Applied Surface Science, 2017. **400**: p. 14-23.

66. Devlin-Mullin, A., et al., *Atomic Layer Deposition of a Silver Nanolayer on Advanced*

*Titanium Orthopedic Implants Inhibits Bacterial Colonization and Supports Vascularized de Novo Bone Ingrowth.* Advanced Healthcare Materials, 2017. **6**(11): p. 1700033.

67.   Geng, H., et al., *Biotransformation of Silver Released from Nanoparticle Coated Titanium Implants Revealed in Regenerating Bone.* ACS Applied Materials & Interfaces, 2017. **9**(25): p. 21169-21180.

68.   Darwish, G., et al., *Improving Polymethyl Methacrylate Resin Using a Novel Titanium Dioxide Coating.* Journal of Prosthodontics, 2019. **28**(9): p. 1011-1017.

69.   Zane, A., et al., *Biocompatibility and antibacterial activity of nitrogen-doped titanium dioxide nanoparticles for use in dental resin formulations.* International journal of nanomedicine, 2016. **11**: p. 6459-6470.

70.   Kemell, M., et al., *Surface modification of thermoplastics by atomic layer deposition of Al2O3 and TiO2 thin films.* European Polymer Journal, 2008. **44**(11): p. 3564-3570.

71.   Paul, P., K. Pfeiffer, and A. Szeghalmi, *Antireflection Coating on PMMA Substrates by Atomic Layer Deposition.* Coatings, 2020. **10**.

72.   Napari, M., et al., *Nucleation and growth of ZnO on PMMA by low-temperature atomic layer deposition.* Journal of Vacuum Science & Technology A, 2014. **33**(1): p. 01A128.

73.   Vähä-Nissi, M., et al., *Antibacterial and barrier properties of oriented polymer films with ZnO thin films applied with atomic layer deposition at low temperatures.* Thin Solid Films, 2014. **562**: p. 331-337.

74.   Park, K.-H., et al., *Antibacterial activity of the thin ZnO film formed by atomic layer deposition under UV-A light.* Chemical Engineering Journal, 2017. **328**: p. 988-996.

75.   Li, J., et al., *Light-Activated Rapid Disinfection by Accelerated Charge Transfer in Red Phosphorus/ZnO Heterointerface.* Small Methods, 2019. **3**(3): p. 1900048.

76.   Zhang, K., et al., *Sr/ZnO doped titania nanotube array: An effective surface system with excellent osteoinductivity and self-antibacterial activity.* Materials & Design, 2017. **130**: p. 403-412.

77.   Choi, S.-W., et al., *Inflammatory Bone Resorption and Antiosteosarcoma Potentials of Zinc Ion Sustained Release ZnO Chips: Friend or Foe?* ACS Biomaterials Science & Engineering, 2016. **2**(4): p. 494-500.

78.   Astaneh, S.H., et al., *Surface and subsurface film growth of titanium dioxide on polydimethylsiloxane by atomic layer deposition.* Applied Surface Science, 2019. **493**: p. 779-786.

79.   Pessoa, R.S., et al., *TiO2 coatings via atomic layer deposition on polyurethane and*

*polydimethylsiloxane substrates: Properties and effects on C. albicans growth and inactivation process.* Applied Surface Science, 2017. **422**: p. 73-84.

80.     Goldfinger, Y., et al., *Biofilm prevention on cochlear implants.* Cochlear Implants International, 2014. **15**(3): p. 173-178.

81.     Bishal, A.K., et al., *Color stability of maxillofacial prosthetic silicone functionalized with oxide nanocoating.* The Journal of Prosthetic Dentistry, 2019. **121**(3): p. 538-543.

82.     Bishal, A.K., C. Sukotjo, and C.G. Takoudis, *Room temperature TiO2 atomic layer deposition on collagen membrane from a titanium alkylamide precursor.* Journal of Vacuum Science & Technology A, 2016. **35**(1): p. 01B134.

83.     Bishal, A.K., et al., *Enhanced Bioactivity of Collagen Fiber Functionalized with Room Temperature Atomic Layer Deposited Titania.* ACS Applied Materials & Interfaces, 2018. **10**(40): p. 34443-34454.

84.     Rezwan, K., et al., *Biodegradable and bioactive porous polymer/inorganic composite scaffolds for bone tissue engineering.* Biomaterials, 2006. **27**(18): p. 3413-3431.

85.     Chusuei, C.C., et al., *Solid−Liquid Adsorption of Calcium Phosphate on TiO2.* Langmuir, 1999. **15**(21): p. 7355-7360.

86.     Järn, M., et al., *Topography and Surface Energy Dependent Calcium Phosphate Formation on Sol−Gel Derived TiO2 Coatings.* Langmuir, 2006. **22**(19): p. 8209-8213.

87.     Kmiec, M., et al., *Chitosan-Properties and Applications in Dentistry.* Advances in Tissue Engineering and Regenerative Medicine, 2017. **2**: p. 1-7.

88.     Choy, S., et al., *Tough and Immunosuppressive Titanium-Infiltrated Exoskeleton Matrices for Long-Term Endoskeleton Repair.* ACS Applied Materials & Interfaces, 2019. **11**(10): p. 9786-9793.

89.     Bathala, L., et al., *The Role of Polyether Ether Ketone (Peek) in Dentistry - A Review.* Journal of medicine and life, 2019. **12**(1): p. 5-9.

90.     Pessoa, R.S. and M.A. Fraga, *Biomedical applications of ultrathin atomic layer deposited metal oxide films on polymeric materials*, in *Frontiers of Nanoscience*. 2019. p. 291-307.

91.     Shahmohammadi, M., et al., *Enhancing the surface properties and functionalization of polymethyl methacrylate with atomic layer-deposited titanium(IV) oxide.* Journal of Materials Science, 2020.

92.     Apratim, A., et al., *Zirconia in dental implantology: A review.* Journal of International Society of Preventive & Community Dentistry, 2015. **5**(3): p. 147-156.

93.    Yao, L., et al., *Atomic layer deposition of zinc oxide on microrough zirconia to enhance osteogenesis and antibiosis.* Ceramics International, 2019. **45**(18, Part A): p. 24757-24767.

94.    Al-Sanabani, F., A. Madfa, and N. Al-Qudaimi, *Alumina ceramic for dental applications: A review article.* American Journal of Materials Research, 2014. **1**: p. 26-34.

95.    Narayan, R.J., et al., *Atomic layer deposition of TiO2 thin films on nanoporous alumina templates: Medical applications.* JOM, 2009. **61**(6): p. 12-16.

96.    Weimer, A.W., et al., *DENTAL COMPOSITE FILLER PARTICLES.* 2008: USA.

97.    Müller, B., et al., *Atomic layer deposited TiO2 protects porous ceramic foams from grain boundary corrosion.* Corrosion Science, 2016. **106**: p. 35-42.

98.    Maitz, M.F., *Applications of synthetic polymers in clinical medicine.* Biosurface and Biotribology, 2015. **1**(3): p. 161-176.

99.    Boudot, C., et al., *Vacuum arc plasma deposition of thin titanium dioxide films on silicone elastomer as a functional coating for medical applications.* Materials Science and Engineering: C, 2017. **74**: p. 508-514.

100.   Abbasi, F., H. Mirzadeh, and M. Simjoo, *Hydrophilic interpenetrating polymer networks of poly(dimethyl siloxane) (PDMS) as biomaterial for cochlear implants.* Journal of Biomaterials Science, Polymer Edition, 2006. **17**(3): p. 341-355.

101.   Sia Samuel, K. and M. Whitesides George, *Microfluidic devices fabricated in Poly(dimethylsiloxane) for biological studies.* ELECTROPHORESIS, 2003. **24**(21): p. 3563-3576.

102.   Trantidou, T., et al., *Hydrophilic surface modification of PDMS for droplet microfluidics using a simple, quick, and robust method via PVA deposition.* Microsystems &Amp; Nanoengineering, 2017. **3**: p. 16091.

103.   Sopyan, I., et al., *An efficient TiO2 thin-film photocatalyst: photocatalytic properties in gas-phase acetaldehyde degradation.* Journal of Photochemistry and Photobiology A: Chemistry, 1996. **98**(1): p. 79-86.

104.   Wei-guo, X., C. An-min, and Z. Qiang, *Preparation of TiO2 thin film and its antibacterial activity.* Journal of Wuhan University of Technology-Mater. Sci. Ed., 2004. **19**(1): p. 16-18.

105.   Joost, U., et al., *Photocatalytic antibacterial activity of nano-TiO2 (anatase)-based thin films: Effects on Escherichia coli cells and fatty acids.* Journal of Photochemistry and Photobiology B: Biology, 2015. **142**: p. 178-185.

106.    Yeung, K.S. and Y.W. Lam, *A simple chemical vapour deposition method for depositing thin TiO2 films.* Thin Solid Films, 1983. **109**(2): p. 169-178.

107.    Arturo, I.M., R.A. Dwight, and A.L. Alcides, *Effect of deposition methods on the properties of photocatalytic TiO 2 thin films prepared by spray pyrolysis and magnetron sputtering.* Journal of Physics: Condensed Matter, 2004. **16**(22): p. S2335.

108.    Tiwary, R., et al. *Characterization of TiO2 Thin Film Deposited by RF Sputtering Method.* in *2014 International Conference on Devices, Circuits and Communications (ICDCCom).* 2014.

109.    Ahn, J., et al. *Comparison study from sputtering, sol-gel, and ALD processes developing embedded thin film capacitors.* in *2006 8th Electronics Packaging Technology Conference.* 2006.

110.    Miikkulainen, V., et al., *Crystallinity of inorganic films grown by atomic layer deposition: Overview and general trends.* Journal of Applied Physics, 2013. **113**(2): p. 021301.

111.    Ganta, D., et al., *Hydrophobic recovery in ultrathin PDMS-coated long and short silicon nanowires.* Chemical Physics Letters, 2016. **647**: p. 175-180.

112.    Kim, J., et al., *The Mechanisms of Hydrophobic Recovery of Polydimethylsiloxane Elastomers Exposed to Partial Electrical Discharges.* Journal of Colloid and Interface Science, 2001. **244**(1): p. 200-207.

113.    Hillborg, H. and U.W. Gedde, *Hydrophobicity recovery of polydimethylsiloxane after exposure to corona discharges.* Polymer, 1998. **39**(10): p. 1991-1998.

114.    Spagnola, J.C., B. Gong, and G.N. Parsons, *Surface texture and wetting stability of polydimethylsiloxane coated with aluminum oxide at low temperature by atomic layer deposition.* Journal of Vacuum Science & Technology A, 2010. **28**(6): p. 1330-1337.

115.    Bodas, D. and C. Khan-Malek, *Hydrophilization and hydrophobic recovery of PDMS by oxygen plasma and chemical treatment—An SEM investigation.* Sensors and Actuators B: Chemical, 2007. **123**(1): p. 368-373.

116.    Gong, B., J.C. Spagnola, and G.N. Parsons, *Hydrophilic mechanical buffer layers and stable hydrophilic finishes on polydimethylsiloxane using combined sequential vapor infiltration and atomic/molecular layer deposition.* Journal of Vacuum Science & Technology A, 2011. **30**(1): p. 01A156.

117.    Yu, Y., et al., *Sequential Infiltration Synthesis of Doped Polymer Films with Tunable Electrical Properties for Efficient Triboelectric Nanogenerator Development.* Advanced Materials, 2015. **27**(33): p. 4938-4944.

118.    Poodt, P., et al., *Spatial atomic layer deposition: A route towards further industrialization of atomic layer deposition.* Journal of Vacuum Science & Technology A, 2011. **30**(1): p. 010802.

119.    Ferguson, J.D., A.W. Weimer, and S.M. George, *Atomic Layer Deposition of Al2O3 Films on Polyethylene Particles.* Chemistry of Materials, 2004. **16**(26): p. 5602-5609.

120.    Selvaraj, S.K., G. Jursich, and C.G. Takoudis, *Design and implementation of a novel portable atomic layer deposition/chemical vapor deposition hybrid reactor.* Review of Scientific Instruments, 2013. **84**(9): p. 095109.

121.    Kim, Y.-W. and D.-H. Kim, *Atomic layer deposition of TiO2 from tetrakis-dimethylamido-titanium and ozone.* Korean Journal of Chemical Engineering, 2012. **29**(7): p. 969-973.

122.    Jin, C., et al., *Structure and photoluminescence of the TiO2 films grown by atomic layer deposition using tetrakis-dimethylamino titanium and ozone.* Nanoscale Research Letters, 2015. **10**: p. 95-95.

123.    Roth, J., et al., *Surface Functionalization of Silicone Rubber for Permanent Adhesion Improvement.* Langmuir, 2008. **24**(21): p. 12603-12611.

124.    Wilson, C.A., R.K. Grubbs, and S.M. George, *Nucleation and Growth during Al2O3 Atomic Layer Deposition on Polymers.* Chemistry of Materials, 2005. **17**(23): p. 5625-5634.

125.    Aghaee, M., et al., *Low temperature temporal and spatial atomic layer deposition of TiO2 films.* Journal of Vacuum Science & Technology A, 2015. **33**(4): p. 041512.

126.    Pensa, E., *Enhanced properties of polymethyl methacrylate coated with atomic layer deposited ceramic nanofilm*, in *bioengineering* 2018, university of Illinois at Chicago: Chicago. p. 101.

127.    Louette, P., F. Bodino, and J.-J. Pireaux, *Poly(dimethyl siloxane) (PDMS) XPS Reference Core Level and Energy Loss Spectra.* Surface Science Spectra, 2005. **12**(1): p. 38-43.

128.    Jur, J.S., et al., *Temperature-Dependent Subsurface Growth during Atomic Layer Deposition on Polypropylene and Cellulose Fibers.* Langmuir, 2010. **26**(11): p. 8239-8244.

129.    Ravel, B. and M. Newville, *ATHENA, ARTEMIS, HEPHAESTUS: data analysis for X-ray absorption spectroscopy using IFEFFIT.* Journal of Synchrotron Radiation, 2005. **12**(4): p. 537-541.

130.    *http://xafs.org/Software/Demeter*. 2019  [cited 2019.

131.    *X-ray Absorption Near-Edge Structure (XANES) Spectroscopy.* Reviews in Mineralogy and Geochemistry, 2014. **78**(1): p. 75-138.

132.    Angelomé, P.C., et al., *Mesoporous Anatase TiO2 Films: Use of Ti K XANES for the Quantification of the Nanocrystalline Character and Substrate Effects in the Photocatalysis Behavior.* The Journal of Physical Chemistry C, 2007. **111**(29): p. 10886-10893.

133.    Setthapun, W., et al., *Genesis and Evolution of Surface Species during Pt Atomic Layer Deposition on Oxide Supports Characterized by in Situ XAFS Analysis and Water−Gas Shift Reaction.* The Journal of Physical Chemistry C, 2010. **114**(21): p. 9758-9771.

134.    Christensen Steven, T., et al., *Controlled Growth of Platinum Nanoparticles on Strontium Titanate Nanocubes by Atomic Layer Deposition.* Small, 2009. **5**(6): p. 750-757.

135.    Markov, D.A., et al., *Variation in diffusion of gases through PDMS due to plasma surface treatment and storage conditions.* Biomedical microdevices, 2014. **16**(1): p. 91-96.

136.    Guo, H.C., et al., *Recent progress of atomic layer deposition on polymeric materials.* Materials Science and Engineering: C, 2017. **70**: p. 1182-1191.

137.    Parsons, G.N., *Atomic Layer Deposition on Soft Materials*, in *Atomic Layer Deposition of Nanostructured Materials*. 2012.

138.    Deng, S., et al., *Atomic layer deposition-based synthesis of photoactive TiO2 nanoparticle chains by using carbon nanotubes as sacrificial templates.* RSC Advances, 2014. **4**(23): p. 11648-11653.

139.    Spagnola, J.C., et al., *Surface and sub-surface reactions during low temperature aluminium oxide atomic layer deposition on fiber-forming polymers.* Journal of Materials Chemistry, 2010. **20**(20): p. 4213-4222.

140.    Liao, Y., *Practical Electron Microscopy and Database*. 2007.

141.    Leskelä, M., M. Mattinen, and M. Ritala, *Review Article: Atomic layer deposition of optoelectronic materials.* Journal of Vacuum Science & Technology B, 2019. **37**(3): p. 030801.

142.    Mackus, A.J.M., A.A. Bol, and W.M.M. Kessels, *The use of atomic layer deposition in advanced nanopatterning.* Nanoscale, 2014. **6**(19): p. 10941-10960.

143.    Chou, S.Y., P.R. Krauss, and P.J. Renstrom, *Nanoimprint lithography.* Journal of Vacuum Science & Technology B: Microelectronics and Nanometer Structures Processing, Measurement, and Phenomena, 1996. **14**(6): p. 4129-4133.

144.   Acikgoz, C., et al., *Polymers in conventional and alternative lithography for the fabrication of nanostructures.* European Polymer Journal, 2011. **47**(11): p. 2033-2052.

145.   Fang, C., et al., *Thermal atomic layer etching: Mechanism, materials and prospects.* Progress in Natural Science: Materials International, 2018. **28**(6): p. 667-675.

146.   Langston, M.C., T. Usui, and F.B. Prinz, *Mechanical masking of films deposited by atomic layer deposition.* Journal of Vacuum Science & Technology A, 2012. **30**(1): p. 01A153.

147.   Elam, J.W., et al., *Conformal Coating on Ultrahigh-Aspect-Ratio Nanopores of Anodic Alumina by Atomic Layer Deposition.* Chemistry of Materials, 2003. **15**(18): p. 3507-3517.

148.   Sweet, W.J., C.J. Oldham, and G.N. Parsons, *Atomic Layer Deposition of Metal Oxide Patterns on Nonwoven Fiber Mats using Localized Physical Compression.* ACS Applied Materials & Interfaces, 2014. **6**(12): p. 9280-9289.

149.   Hasier, J., M.A. Riolo, and P. Nash, *Curie temperature determination via thermogravimetric and continuous wavelet transformation analysis.* EPJ Techniques and Instrumentation, 2017. **4**(1): p. 5.

150.   Coey, J.M.D., *Perspective and Prospects for Rare Earth Permanent Magnets.* Engineering, 2019.

151.   Kalutarage, L.C., S.B. Clendenning, and C.H. Winter, *Low-Temperature Atomic Layer Deposition of Copper Films Using Borane Dimethylamine as the Reducing Co-reagent.* Chemistry of Materials, 2014. **26**(12): p. 3731-3738.

152.   Mäkelä, M., et al., *Studies on Thermal Atomic Layer Deposition of Silver Thin Films.* Chemistry of Materials, 2017. **29**(5): p. 2040-2045.

153.   Takoudis, C.G., M. Singh, and S.K. Selvaraj, *Multi-metal films, alternating film multilayers, formation methods and deposition system.* 2019, The Board of Trustees of the University of Illinois (Urbana, IL): United States.

154.   Thomas, R.R., et al., *Wettability of Polished Silicon Oxide Surfaces.* Journal of The Electrochemical Society, 1996. **143**(2): p. 643-648.

155.   Foadi, F., et al., *Roughness-dependent wetting behavior of vapor-deposited metallic thin films.* Physical Review E, 2019. **100**(2): p. 022804.

156.   Kakade, B.A. and V.K. Pillai, *Tuning the Wetting Properties of Multiwalled Carbon Nanotubes by Surface Functionalization.* The Journal of Physical Chemistry C, 2008. **112**(9): p. 3183-3186.

157.    Kubiak, K.J., et al., *Wettability versus roughness of engineering surfaces.* Wear, 2011. **271**(3): p. 523-528.

158.    Han, S., et al., *The Wettability and Numerical Model of Different Silicon Microstructural Surfaces.* Applied Sciences, 2019. **9**(3): p. 566.

159.    Zhang, C., et al., *Patterned films by atomic layer deposition using Parafilm as a mask.* Journal of Vacuum Science & Technology A, 2018. **36**(1): p. 01B102.

160.    Färm, E., et al., *Selective-Area Atomic Layer Deposition Using Poly(methyl methacrylate) Films as Mask Layers.* The Journal of Physical Chemistry C, 2008. **112**(40): p. 15791-15795.

161.    Hashemi Astaneh, S., et al., *Simple masking method for selective atomic layer deposition of thin films.* Journal of Vacuum Science & Technology B, 2020. **38**(2): p. 025001.

162.    Kim, H., *Atomic layer deposition of metal and nitride thin films: Current research efforts and applications for semiconductor device processing.* Journal of Vacuum Science & Technology B: Microelectronics and Nanometer Structures Processing, Measurement, and Phenomena, 2003. **21**(6): p. 2231-2261.

163.    Sneh, O., et al., *Thin film atomic layer deposition equipment for semiconductor processing.* Thin Solid Films, 2002. **402**(1): p. 248-261.

164.    Cremers, V., R.L. Puurunen, and J. Dendooven, *Conformality in atomic layer deposition: Current status overview of analysis and modelling.* Applied Physics Reviews, 2019. **6**(2): p. 021302.

165.    Skoog, S.A., J.W. Elam, and R.J. Narayan, *Atomic layer deposition: medical and biological applications.* International Materials Reviews, 2013. **58**(2): p. 113-129.

166.    Sbricoli, L., et al., *Selection of Collagen Membranes for Bone Regeneration: A Literature Review.* Materials, 2020. **13**: p. 786.

167.    Zenóbio, E.G., et al., *Morphological Analysis of Resorbable Collagen Membranes by Scanning Electron Microscopy.* Journal of the International Academy of Periodontology, 2018. **20/1**: p. 19-24.

168.    Hashemi Astaneh, S., et al., *Atomic Layer Deposition on Dental Materials: Processing Conditions and Surface Functionalization to Improve Properties - a Critical Review.* 2020.

169.    Bishal, A.K., C. Sukotjo, and C.G. Takoudis, *Room temperature TiO2 atomic layer deposition on collagen membrane from a titanium alkylamide precursor.* Journal of Vacuum Science & Technology A, 2017. **35**(1): p. 01B134.

170.    Lee, S.-M., et al., *Low-temperature ZnO atomic layer deposition on biotemplates: flexible photocatalytic ZnO structures from eggshell membranes.* Physical Chemistry Chemical Physics, 2009. **11**(19): p. 3608-3614.

171.    Zhao, Y., et al., *Biotemplated Hierarchical Nanostructure of Layered Double Hydroxides with Improved Photocatalysis Performance.* ACS Nano, 2009. **3**(12): p. 4009-4016.

172.    Lee, S.-M., et al., *Greatly Increased Toughness of Infiltrated Spider Silk.* Science, 2009. **324**(5926): p. 488.

173.    Kemell, M., et al., *Atomic Layer Deposition in Nanometer-Level Replication of Cellulosic Substances and Preparation of Photocatalytic TiO2/Cellulose Composites.* Journal of the American Chemical Society, 2005. **127**(41): p. 14178-14179.

174.    Hyde, G.K., et al., *Atomic Layer Deposition of Conformal Inorganic Nanoscale Coatings on Three-Dimensional Natural Fiber Systems: Effect of Surface Topology on Film Growth Characteristics.* Langmuir, 2007. **23**(19): p. 9844-9849.

175.    Hyde, G.K., et al., *Atomic layer deposition and biocompatibility of titanium nitride nano-coatings on cellulose fiber substrates.* Biomedical Materials, 2009. **4**(2): p. 025001.

176.    Maruyama, T., et al., *Large voltage-induced magnetic anisotropy change in a few atomic layers of iron.* Nature nanotechnology, 2009. **4**(3): p. 158-161.

177.    Klesko, J.P., M.M. Kerrigan, and C.H. Winter, *Low Temperature Thermal Atomic Layer Deposition of Cobalt Metal Films.* Chemistry of Materials, 2016. **28**(3): p. 700-703.

178.    Vidjayacoumar, B., et al., *Investigation of AlMe3, BEt3, and ZnEt2 as Co-Reagents for Low-Temperature Copper Metal ALD/Pulsed-CVD.* Chemistry of Materials, 2010. **22**(17): p. 4844-4853.

179.    Knisley, T.J., et al., *Low Temperature Growth of High Purity, Low Resistivity Copper Films by Atomic Layer Deposition.* Chemistry of Materials, 2011. **23**(20): p. 4417-4419.

180.    Aaltonen, T., et al., *Ruthenium Thin Films Grown by Atomic Layer Deposition.* Chemical Vapor Deposition, 2003. **9**(1): p. 45-49.

181.    Popovici, M., et al., *Atomic Layer Deposition of Ruthenium Thin Films from (Ethylbenzyl) (1-Ethyl-1,4-cyclohexadienyl) Ru: Process Characteristics, Surface Chemistry, and Film Properties.* Chemistry of Materials, 2017. **29**(11): p. 4654-4666.

182.    Park, K.J. and G.N. Parsons, *Selective area atomic layer deposition of rhodium and effective work function characterization in capacitor structures.* Applied Physics Letters, 2006. **89**(4): p. 043111.

183.    Weber, M.J., et al., *Atomic Layer Deposition of High-Purity Palladium Films from*

*Pd(hfac)2 and H2 and O2 Plasmas.* The Journal of Physical Chemistry C, 2014. **118**(16): p. 8702-8711.

184. Lee, J., et al., *Highly conductive and flexible fiber for textile electronics obtained by extremely low-temperature atomic layer deposition of Pt.* Npg Asia Materials, 2016. **8**: p. e331.

185. Dendooven, J., et al., *Low-Temperature Atomic Layer Deposition of Platinum Using (Methylcyclopentadienyl)trimethylplatinum and Ozone.* The Journal of Physical Chemistry C, 2013. **117**(40): p. 20557-20561.

186. Elam, J.W., et al., *Nucleation and growth during tungsten atomic layer deposition on SiO2 surfaces.* Thin Solid Films, 2001. **386**(1): p. 41-52.

187. Wilson, C.A., et al., *Tungsten atomic layer deposition on polymers.* Thin Solid Films, 2008. **516**(18): p. 6175-6185.

188. Niskanen, A., et al., *Radical-Enhanced Atomic Layer Deposition of Silver Thin Films Using Phosphine-Adducted Silver Carboxylates.* Chemical Vapor Deposition, 2007. **13**(8): p. 408-413.

189. van den Bruele, F.J., et al., *Atmospheric pressure plasma enhanced spatial ALD of silver.* Journal of Vacuum Science & Technology A, 2014. **33**(1): p. 01A131.

190. Amusan, A.A., et al., *Ag films grown by remote plasma enhanced atomic layer deposition on different substrates.* Journal of Vacuum Science & Technology A, 2015. **34**(1): p. 01A126.

191. Minjauw, M.M., et al., *Plasma-Enhanced Atomic Layer Deposition of Silver Using Ag(fod)(PEt3) and NH3-Plasma.* Chemistry of Materials, 2017. **29**(17): p. 7114-7121.

192. Masango, S.S., et al., *Nucleation and Growth of Silver Nanoparticles by AB and ABC-Type Atomic Layer Deposition.* The Journal of Physical Chemistry C, 2014. **118**(31): p. 17655-17661.

193. Hämäläinen, J., M. Ritala, and M. Leskelä, *Atomic Layer Deposition of Noble Metals and Their Oxides.* Chemistry of Materials, 2014. **26**(1): p. 786-801.

194. Wack, S., et al., *Large-Scale Deposition and Growth Mechanism of Silver Nanoparticles by Plasma-Enhanced Atomic Layer Deposition.* The Journal of Physical Chemistry C, 2019. **123**(44): p. 27196-27206.

195. Siddiqi, K.S., A. Husen, and R.A.K. Rao, *A review on biosynthesis of silver nanoparticles and their biocidal properties.* Journal of Nanobiotechnology, 2018. **16**(1): p. 14.

196.    Zhang, F., et al., *Application of silver nanoparticles to cotton fabric as an antibacterial textile finish.* Fibers and Polymers, 2009. **10**(4): p. 496-501.

197.    Tien, D.-C., et al., *Discovery of ionic silver in silver nanoparticle suspension fabricated by arc discharge method.* Journal of Alloys and Compounds, 2008. **463**(1): p. 408-411.

198.    Abou El-Nour, K.M.M., et al., *Synthesis and applications of silver nanoparticles.* Arabian Journal of Chemistry, 2010. **3**(3): p. 135-140.

199.    Golrokhi, Z., et al., *The influence of tertiary butyl hydrazine as a co-reactant on the atomic layer deposition of silver.* Applied Surface Science, 2017. **399**: p. 123-131.

200.    Kariniemi, M., et al., *Plasma-Enhanced Atomic Layer Deposition of Silver Thin Films.* Chemistry of Materials, 2011. **23**(11): p. 2901-2907.

201.    Anders, A., et al., *Smoothing of ultrathin silver films by transition metal seeding.* Solid State Communications, 2006. **140**(5): p. 225-229.

202.    González, A.L., et al., *Size, Shape, Stability, and Color of Plasmonic Silver Nanoparticles.* The Journal of Physical Chemistry C, 2014. **118**(17): p. 9128-9136.

203.    Kobayashi, Y., V. Salgueiriño-Maceira, and L.M. Liz-Marzán, *Deposition of Silver Nanoparticles on Silica Spheres by Pretreatment Steps in Electroless Plating.* Chemistry of Materials, 2001. **13**(5): p. 1630-1633.

204.    Campbell, C.T., *Ultrathin metal films and particles on oxide surfaces: structural, electronic and chemisorptive properties.* Surface Science Reports, 1997. **27**(1): p. 1-111.

205.    Todeschini, M., et al., *Influence of Ti and Cr Adhesion Layers on Ultrathin Au Films.* ACS Applied Materials & Interfaces, 2017. **9**(42): p. 37374-37385.

206.    Bishal, A.K., et al., *Highly Conductive Collagen by Low Temperature Atomic Layer Deposition of Platinum.* ACS Applied Materials & Interfaces, 2020.

207.    Hegazy, M.A. and E. Borham, *Preparation and characterization of silver nanoparticles homogenous thin films.* NRIAG Journal of Astronomy and Geophysics, 2018. **7**(1): p. 27-30.

208.    Pillai, S., et al., *Surface plasmon enhanced silicon solar cells.* Journal of Applied Physics, 2007. **101**(9): p. 093105.

209.    Wei, H. and H. Eilers, *From silver nanoparticles to thin films: Evolution of microstructure and electrical conduction on glass substrates.* Journal of Physics and Chemistry of Solids, 2009. **70**(2): p. 459-465.

210.    Taleghani, F., et al., *Cytotoxicity of Silver Nanoparticles on Human Gingival Epithelial*

*Cells: An In Vitro Study.* Journal of Dental School, 2014. **32**: p. 30-36.

211. CDC, C.f.D.C.a.P. *Optimizing Supply of PPE and Other Equipment during Shortages.* 2020 July 16, 2020; Available from: https://www.cdc.gov/coronavirus/2019-ncov/hcp/ppe-strategy/general-optimization-strategies.html.

212. CDC, C.f.D.C.a.P. *Recommended Guidance for Extended Use and Limited Reuse of N95 Filtering Facepiece Respirators in Healthcare Settings.* 2020 [cited 2020 Nov. 2020]; Available from: https://www.cdc.gov/niosh/topics/hcwcontrols/recommendedguidanceextuse.html.

213. Chin, A.W.H., et al., *Stability of SARS-CoV-2 in different environmental conditions.* The Lancet Microbe, 2020. **1**(1): p. e10.

214. S., P., *Wearing Face Masks Is The "new Normal": Know These Tips and Tricks to Avoid Common Side Effects. .* The Times Now, 2020.

215. Spitzer, M., *Masked education? The benefits and burdens of wearing face masks in schools during the current Corona pandemic.* Trends in neuroscience and education, 2020. **20**: p. 100138-100138.

216. Anderegg, L., et al., *A scalable method of applying heat and humidity for decontamination of N95 respirators during the COVID-19 crisis.* PLOS ONE, 2020. **15**(7): p. e0234851.

217. Oh, C., et al., *Dry Heat as a Decontamination Method for N95 Respirator Reuse.* Environmental Science & Technology Letters, 2020: p. acs.estlett.0c00534.

218. Juang, P.S.C. and P. Tsai, *N95 Respirator Cleaning and Reuse Methods Proposed by the Inventor of the N95 Mask Material.* The Journal of emergency medicine, 2020. **58**(5): p. 817-820.

219. Zheng, C.R., et al., *Particulate Respirators Functionalized with Silver Nanoparticles Showed Excellent Real-Time Antimicrobial Effects against Pathogens.* Environmental Science & Technology, 2016. **50**(13): p. 7144-7151.

220. Sportelli, M.C., et al., *Can Nanotechnology and Materials Science Help the Fight against SARS-CoV-2? .* Nanomaterials, 2020. **10**.

221. Zhong, H., et al., *Plasmonic and Superhydrophobic Self-Decontaminating N95 Respirators.* ACS Nano, 2020. **14**(7): p. 8846-8854.

222. Makvandi, P., et al., *Metal-Based Nanomaterials in Biomedical Applications: Antimicrobial Activity and Cytotoxicity Aspects.* Advanced Functional Materials, 2020. **30**(22): p. 1910021.

223.  3M.  *https://multimedia.3m.com/mws/media/1538980O/3m-disposable-respirator-1870-technical-data-sheet.pdf*. 2020  [cited 2020 Sep. 2nd].

224.  *Silverlon*. 2020  [cited 2020 Nov.]; Available from: https://www.silverlon.com/.

225.  Takoudis, C.G., M. Singh, and S.K. Selvaraj, *Multi-metal films, alternating film multilayers, formation methods and deposition system*, U. patent, Editor. 2019: United States

226.  Nagay, B.E., et al., *Visible-Light-Induced Photocatalytic and Antibacterial Activity of TiO2 Codoped with Nitrogen and Bismuth: New Perspectives to Control Implant-Biofilm-Related Diseases.* ACS Applied Materials & Interfaces, 2019. **11**(20): p. 18186-18202.

227.  Lorenzetti, M., et al., *The Influence of Surface Modification on Bacterial Adhesion to Titanium-Based Substrates.* ACS Applied Materials & Interfaces, 2015. **7**(3): p. 1644-1651.

228.  Wang, J., et al., *Antibacterial Surface Design of Titanium-Based Biomaterials for Enhanced Bacteria-Killing and Cell-Assisting Functions Against Periprosthetic Joint Infection.* ACS Applied Materials & Interfaces, 2016. **8**(17): p. 11162-11178.

229.  Lannon, J.M. and Q. Meng, *Analysis of a Poly(propylene)(PP) Homopolymer by XPS.* Surface Science Spectra, 1999. **6**(2): p. 79-82.

230.  Hashemi Astaneh, S., et al., *Surface and subsurface film growth of titanium dioxide on polydimethylsiloxane by atomic layer deposition.* Applied Surface Science, 2019. **493**: p. 779-786.

231.  Ullah, S., et al., *Reusability Comparison of Melt-Blown vs Nanofiber Face Mask Filters for Use in the Coronavirus Pandemic.* ACS Applied Nano Materials, 2020: p. acsanm.0c01562.

232.  Kim, J.S., et al., *Antimicrobial effects of silver nanoparticles.* Nanomedicine: Nanotechnology, Biology and Medicine, 2007. **3**(1): p. 95-101.

233.  Wady, A.F., et al., *Effect of a Silver Nanoparticles Solution on Staphylococcus aureus and Candida spp.* Journal of Nanomaterials, 2014. **2014**: p. 545279.

234.  Hamouda T, et al., *A novel surfactant nanoemulsion with a unique non-irritant topical antimicrobial activity against bacteria, enveloped viruses and fungi.* Microbiol Res., 2001. **156**: p. 1-7.

235.  Dibrov, P., et al., *Chemiosmotic mechanism of antimicrobial activity of Ag(+) in Vibrio cholerae.* Antimicrobial agents and chemotherapy, 2002. **46**(8): p. 2668-2670.

236.  Sondi, I. and B. Salopek-Sondi, *Silver nanoparticles as antimicrobial agent: a case study*

*on E. coli as a model for Gram-negative bacteria.* Journal of Colloid and Interface Science, 2004. **275**(1): p. 177-182.

237. Velu, R., et al., *A Comprehensive Review on Bio-Nanomaterials for Medical Implants and Feasibility Studies on Fabrication of Such Implants by Additive Manufacturing Technique.* Materials (Basel, Switzerland), 2019. **13**(1): p. 92.

238. Warnes, S.L., Z.R. Little, and C.W. Keevil, *Human Coronavirus 229E Remains Infectious on Common Touch Surface Materials.* mBio, 2015. **6**(6): p. e01697-15.

239. Tripathi, T.S. and M. Karppinen, *Efficient Process for Direct Atomic Layer Deposition of Metallic Cu Thin Films Based on an Organic Reductant.* Chemistry of Materials, 2017. **29**(3): p. 1230-1235.

240. Li, Z., A. Rahtu, and R.G. Gordon, *Atomic Layer Deposition of Ultrathin Copper Metal Films from a Liquid Copper(I) Amidinate Precursor.* Journal of The Electrochemical Society, 2006. **153**(11): p. C787.

241. Mane, A.U. and S.A. Shivashankar, *Atomic layer chemical vapour deposition of copper.* Materials Science in Semiconductor Processing, 2004. **7**(4): p. 343-347.

242. Lee, B.H., et al., *Low-Temperature Atomic Layer Deposition of Copper Metal Thin Films: Self-Limiting Surface Reaction of Copper Dimethylamino-2-propoxide with Diethylzinc.* Angewandte Chemie International Edition, 2009. **48**(25): p. 4536-4539.

243. Dey, G. and S.D. Elliott, *Copper reduction and atomic layer deposition by oxidative decomposition of formate by hydrazine.* RSC Advances, 2014. **4**(65): p. 34448-34453.

244. Park, J.-M., et al., *Atomic layer deposition of copper nitride film and its application to copper seed layer for electrodeposition.* Thin Solid Films, 2014. **556**: p. 434-439.

245. Hashemi Astaneh, S., et al., *Atomic layer deposition on dental materials: processing conditions and surface functionalization to improve physical, chemical, and clinical properties - A Review.* Acta Biomaterialia, 2020.

# APPENDICES

# Appendix A

## PERMISSION TO USE PREVIOUSLY PUBLISHED MATERIALS

Chapter 1 and part of chapter 3 was previously published as "Atomic layer deposition on dental materials: processing conditions and surface functionalization to improve physical, chemical, and clinical properties - A Review" in Acta Biomaterialia [245]. According to the journal:

Figure 3 is adapted from Procedia Manufacturing 37 [30], and for noncommercial purposes, full or partial parts of paper is allowed to be used in this thesis.

Figure 5 is adapted from Applied Surface Science 258 (2012) 3415– 3419 [41], the permission is as follow:

| | |
|---|---|
| Licensed Content Title | Correlation between bioactivity and structural properties of titanium dioxide coatings grown by atomic layer deposition |
| Licensed Content Author | I.P. Grigal,A.M. Markeev,S.A. Gudkova,A.G. Chernikova,A.S. Mityaev,A.P. Alekhin |
| Licensed Content Date | Feb 1, 2012 |
| Licensed Content Volume | 258 |
| Licensed Content Issue | 8 |
| Licensed Content Pages | 5 |
| Start Page | 3415 |
| End Page | 3419 |
| Type of Use | reuse in a thesis/dissertation |
| Portion | figures/tables/illustrations |
| Number of figures/tables/illustrations | 1 |
| Format | both print and electronic |
| Are you the author of this Elsevier article? | No |
| Will you be translating? | No |
| Title | thesis |
| Institution name | University of Illinois at Chicago |
| Expected presentation date | Dec 2020 |
| Portions | only figure 5 |
| Requestor Location | University of Illinois at Chicago 900 West Taylor Street 1215 CHICAGO, IL 60607 United States Attn: University of Illinois at Chicago |
| Publisher Tax ID | 98-0397604 |
| Total | 0.00 USD |

Figure 6 is adapted from Nanotechnologies in Russia 8, 388–391(2013) [42], the reprint permission is as follow:

| | |
|---|---|
| SPRINGER NATURE LICENSE TERMS AND CONDITIONS Nov 10, 2020 | |
| This Agreement between University of Illinois at Chicago -- Sarah Hashemi Astaneh ("You") and Springer Nature ("Springer Nature") consists of your license details and the terms and conditions provided by Springer Nature and Copyright Clearance Center. | |
| License Number | 4945580907394 |
| License date | Nov 10, 2020 |
| Licensed Content Publisher | Springer Nature |

| | |
|---|---|
| Licensed Content Publication | Nanotechnologies in Russia |
| Licensed Content Title | Correlation between structural and bioactive properties of titanium dioxide formed by atomic layer deposition |
| Licensed Content Author | A. A. Solovyev et al |
| Licensed Content Date | Jun 28, 2013 |
| Type of Use | Thesis/Dissertation |
| Requestor type | academic/university or research institute |
| Format | print and electronic |
| Portion | figures/tables/illustrations |
| Number of figures/tables/illustrations | 1 |
| Will you be translating? | no |
| Circulation/distribution | 500 - 999 |
| Author of this Springer Nature content | no |
| Title | thesis |
| Institution name | University of Illinois at Chicago |
| Expected presentation date | Dec 2020 |
| Portions | figure 5 |
| Requestor Location | University of Illinois at Chicago 900 West Taylor Street 1215 CHICAGO, IL 60607 United States Attn: University of Illinois at Chicago |
| Total | 0.00 USD |

Figure 7 is adapted from Nanomaterials (Basel) 2019 9: 123, which is an open source journal and according to the following statement no permission is needed to reprint it.

Figure 8 is adapted from Applied Surface Science Volume 359, 30 (2015) 215-220 [35], the information of reprint permission is as follow:

| | |
|---|---|
| License Number | 4945590394863 |
| License date | Nov 10, 2020 |
| Licensed Content Publisher | Elsevier |
| Licensed Content Publication | Applied Surface Science |
| Licensed Content Title | Atomic layer deposition to prevent metal transfer from implants: An X-ray fluorescence study |
| Licensed Content Author | Fabjola Bilo,Laura Borgese,Josef Prost,Mirjam Rauwolf,Anna Turyanskaya,Peter Wobrauschek,Peter Kregsamer,Christina Streli,Ugo Pazzaglia,Laura E. Depero |
| Licensed Content Date | Dec 30, 2015 |
| Licensed Content Volume | 359 |
| Licensed Content Issue | n/a |
| Licensed Content Pages | 6 |
| Start Page | 215 |
| End Page | 220 |
| Type of Use | reuse in a thesis/dissertation |
| Portion | figures/tables/illustrations |
| Number of figures | 1 |
| Format | both print and electronic |
| Are you the author of this Elsevier article? | No |
| Will you be translating? | No |
| Title | thesis |
| Institution name | University of Illinois at Chicago |
| Expected presentation date | Dec 2020 |
| Portions | figure 6 |
| Requestor Location | University of Illinois at Chicago 900 West Taylor Street 1215 CHICAGO, IL 60607 United States Attn: University of Illinois at Chicago |
| Publisher Tax ID | 98-0397604 |
| Total | 0.00 USD |

Figure 9 is adapted from ACS Appl. Mater. Interfaces 10 (2018) 34443−34454 [83], the permission is as follow:

Figure 10 is adapted from Ceramics International 45 (2019) 24757–24767, the permission information is as follow:

| | |
|---|---|
| Title | thesis |
| Institution name | University of Illinois at Chicago |
| Expected presentation date | Dec 2020 |
| Portions | figure 7C |
| Requestor Location | University of Illinois at Chicago<br>900 West Taylor Street<br>1215<br>CHICAGO, IL 60607<br>United States<br>Attn: University of Illinois at Chicago |
| Publisher Tax ID | 98-0397604 |
| Total | 0.00 USD |

Figure 11 is adapted from Corrosion Science 106 (2016) 35-42 [97], the permission information is as follow:

ELSEVIER LICENSE
TERMS AND CONDITIONS

Nov 10, 2020

This Agreement between University of Illinois at Chicago -- Sarah Hashemi Astaneh ("You") and Elsevier ("Elsevier") consists of your license details and the terms and conditions provided by Elsevier and Copyright Clearance Center.

| | |
|---|---|
| License Number | 4945610620123 |
| License date | Nov 10, 2020 |
| Licensed Content Publisher | Elsevier |
| Licensed Content Publication | Corrosion Science |
| Licensed Content Title | Atomic layer deposited TiO2 protects porous ceramic foams from grain boundary corrosion |
| Licensed Content Author | Benjamin Müller,Håvard Haugen,Ola Nilsen,Hanna Tiainen |
| Licensed Content Date | May 1, 2016 |
| Licensed Content Volume | 106 |
| Licensed Content Issue | n/a |
| Licensed Content Pages | 8 |
| Start Page | 35 |
| End Page | 42 |
| Type of Use | reuse in a thesis/dissertation |
| Portion | figures/tables/illustrations |
| Number of figures/tables/illustrations | 1 |
| Format | both print and electronic |
| Are you the author of this Elsevier article? | No |
| Will you be translating? | No |

| | |
|---|---|
| Title | thesis |
| Institution name | University of Illinois at Chicago |
| Expected presentation date | Dec 2020 |
| Portions | figure 5 |
| Requestor Location | University of Illinois at Chicago<br>900 West Taylor Street<br>1215<br>CHICAGO, IL 60607<br>United States<br>Attn: University of Illinois at Chicago |
| Publisher Tax ID | 98-0397604 |
| Total | 0.00 USD |

Chapter 2.2 was previously published in Journal of Vacuum Science & Technology B, the permission to use this paper in this thesis is as follow [161]:

This Agreement between University of Illinois at Chicago -- Sarah Hashemi Astaneh ("You") and AIP Publishing ("AIP Publishing") consists of your license details and the terms and conditions provided by AIP Publishing and Copyright Clearance Center.

| | |
|---|---|
| License Number | 4943830842923 |
| License date | Nov 07, 2020 |
| Licensed Content Publisher | American Vacuum Society |
| Licensed Content Publication | Journal of Vacuum Science & Technology B |
| Licensed Content Title | Simple masking method for selective atomic layer deposition of thin films |
| Licensed Content Author | Sarah Hashemi Astaneh, Cortino Sukotjo, Christos G. Takoudis, et al |
| Licensed Content Date | Mar 1, 2020 |
| Licensed Content Volume | 38 |
| Licensed Content Issue | 2 |
| Type of Use | Thesis/Dissertation |
| Requestor type | Author (original article) |
| Format | Print and electronic |
| Portion | Excerpt (> 800 words) |
| Will you be translating? | No |
| Title | thesis |
| Institution name | University of Illinois at Chicago |
| Expected presentation date | Dec 2020 |
| Order reference number | 161 |
| Portions | full paper |
| Requestor Location | University of Illinois at Chicago<br>900 West Taylor Street |

| | |
|---|---|
| | 1215<br>CHICAGO, IL 60607<br>United States<br>Attn: University of Illinois at Chicago |
| Total | 0.00 USD |

**PRELIMINARY STUDIES AND RESULTS FOR FUTURE PROJECTS**

This section is dedicated to other projects and studies which have been done by me during my Ph.D. studies.

## B.1 Silver ALD on other dental materials

As it was mentioned in the introduction of this thesis, titanium is one of the materials which is widely being used in dental industry. After achieving the processing conditions for silver ALD, preliminary studies were conducted with the objective of functionalizing Ti and PDMS with Ag. Figure 38 shows XPS result of the 1300 cycles of Ag ALD on Ti alloy at 115 ˚C and 95 ˚C deposition temperature.
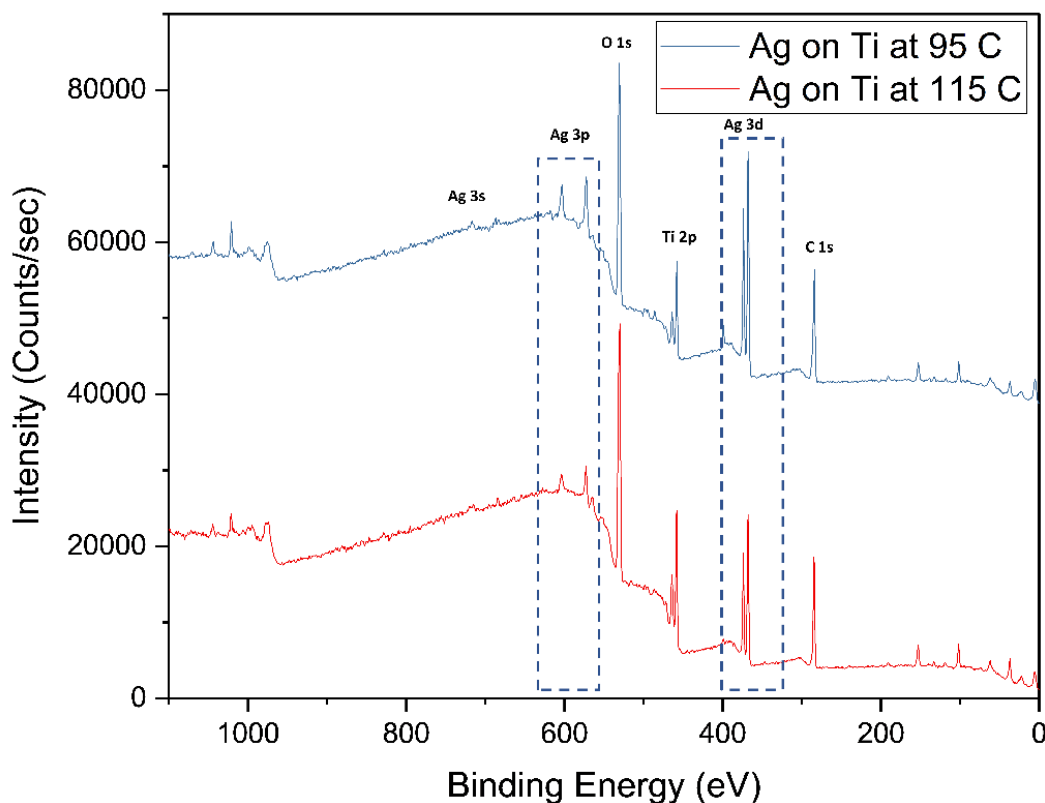


Figure 38: XPS of a) Ti  b) (3 s/5 s precursor pulse/purge, 2 s/10 s reducing agent pulse/purge), at 115 °C and 500 mtorr.

PDMS is an example of an inert polymer which has been used as maxillofacial prosthesis. Besides, fabrication of metal-polymer conductors is getting more attention nowadays. The XPS spectrum of Ag nanocoating on PDMS is displayed in Figure 39.
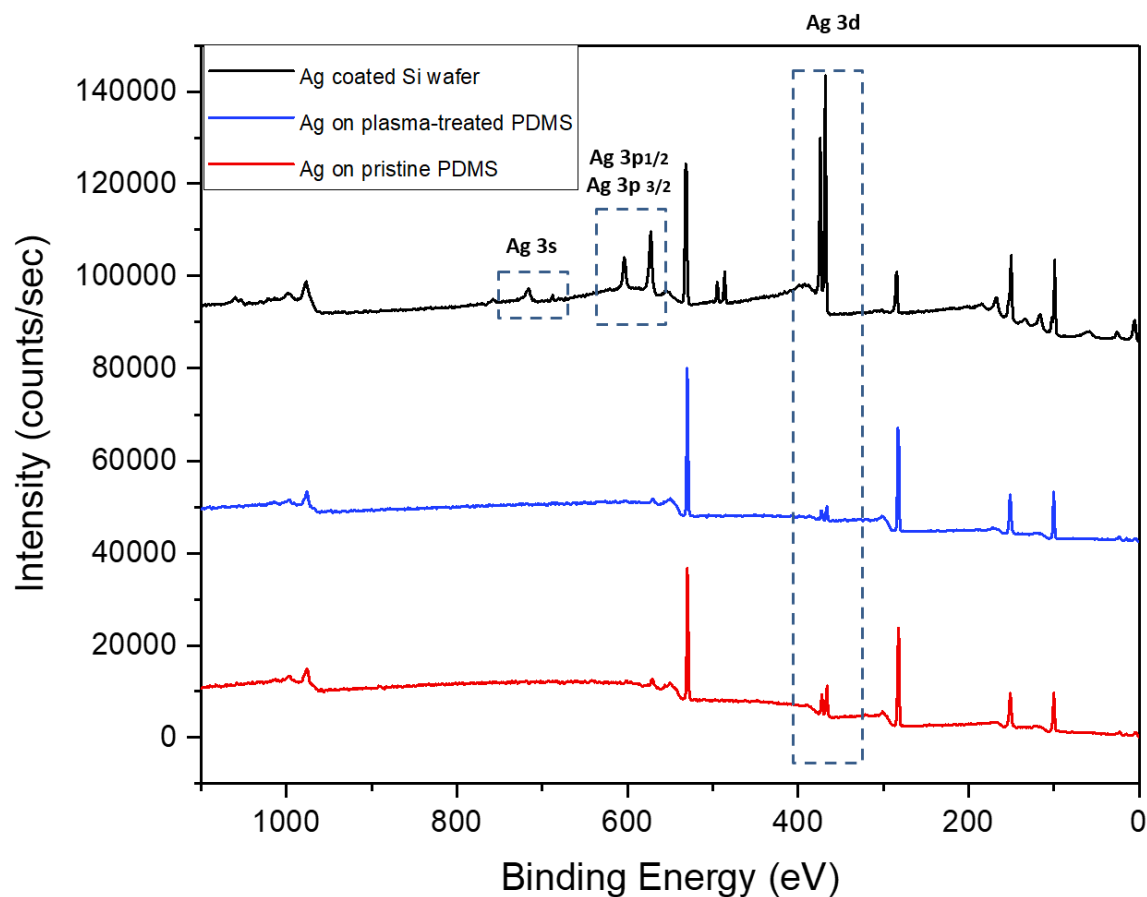


Figure 39: XPS spectra showing surface chemical composition after silver ALD on pristine PDMS and plasma-treated PDMS for 1300 cycles at 115 ˚C.

Results of silver deposition on pristine PDMS and plasma treated PDMS showed that for 1300 Ag ALD cycles, there is no significant difference between pristine and plasma treated PDMS, so the rest of Ag ALDs were applied on pristine PDMS. At lower cycle counts, Ag ALD did not show silver growth on PDMS surface. Upon increasing the number of cycles, distinct Ag peaks were observed on PDMS specimens that were coated with Ag ALD. Presence of 200

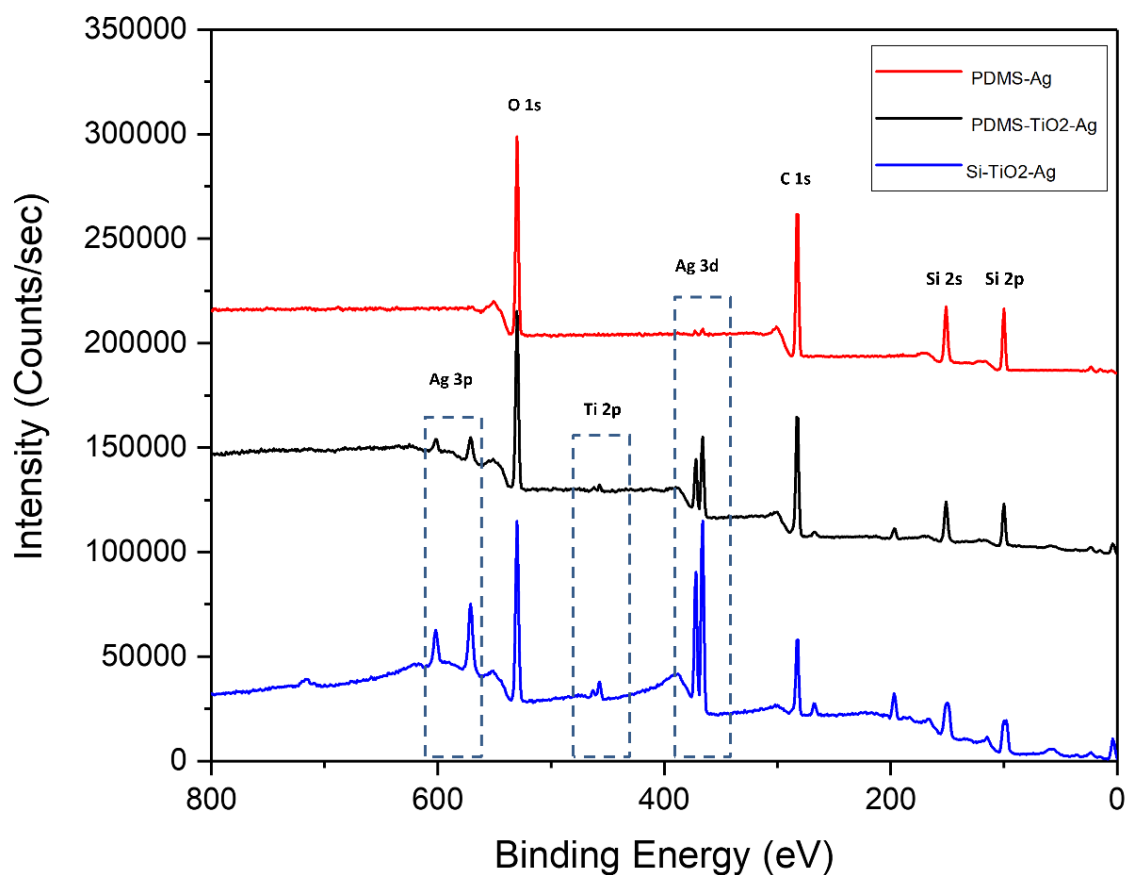cycles TiO$_2$ ALD interlayer helped with nucleation and growth of silver on the PDMS (Figure 40).



Figure 40: XPS spectra showing surface chemical composition after silver ALD on pristine PDMS and the role of TiO$_2$ interlayer on silver growth on PDMS (processing conditions: 1300 cycles at 115 ˚C).

# Sarah Hashemi Astaneh

| | |
|---|---|
| Education | Ph.D., Chemical engineering<br>University of Illinois at Chicago, USA<br>December 2020<br><br>M.Sc., Polymer engineering<br>Amirkabir University of Technology, Iran<br>December 2010<br><br>B.Sc., Polymer engineering<br>Amirkabir University of Technology, Iran<br>August 2008 |
| Publications | Hashemi Astaneh, S., Faverani, L., Sukotjo, C., Takoudis, C.G., Atomic layer deposition on dental materials: processing conditions and surface functionalization to improve physical, chemical, and clinical properties- A Review, Acta Biomaterialia, 121, 103-118 (2021)<br><br>Hashemi Astaneh, S., Jursich, G., Sukotjo, Takoudis, C.G., Surface and subsurface film growth of titanium dioxide on polydimethylsiloxane by atomic layer deposition, Applied Surface Science, 493, 779-786 (2019)<br><br>Rao, S., Hashemi Astaneh, S., Villanueva, J., Silva, F., Christos Takoudis, C.G., Bijukumar, D., Júlio CM Souza, J., Mathew, T.M., Physicochemical and in-vitro biological analysis of bio-functionalized titanium samples in a protein-rich medium, Journal of the mechanical behavior of biomedical materials, 96, 152-164 (2019)<br><br>Hashemi Astaneh, S., Sukotjo, C., Takoudis, C.G., Feinerman, A., Simple masking method for selective atomic layer deposition of thin films, Journal of Vacuum Science & Technology B, 38, 025001 (2020)<br><br>Hashemi Astaneh, S., Sukotjo, C., Takoudis, C.G., Functionalization of collagen with particulated silver thin film via atomic layer deposition, to be submitted. |